A coupled ice sheet model for the Global Resolved Energy Balance model for global simulations on time-scales of 100 kyr

Zhiang Xie

Doctor of Philosophy

A thesis submitted for the degree of *Doctor of Philosophy* at

Monash University in 2022

(*School of Earth, Atmosphere and Environment, Science Faculty*)

Copyright notice

Abstract

We introduce a newly developed global ice sheet model coupled to the Globally Resolved Energy Balance (GREB) climate model for the simulation of global ice sheet evolution on time scales of 100 kyr or longer (GREB-ISM v1.0). Ice sheets and ice shelves are simulated on a global grid, fully interacting with the climate simulation of surface temperature, precipitation, albedo, land-sea mask, topography and sea level. Thus, it is a fully coupled atmosphere, ocean, land and ice sheet model. We test the model in ice sheet stand-alone and fully coupled simulations. The ice sheet model dynamics behave similarly to other hybrid SIA (Shallow Ice Approximation) and SSA (Shallow Shelf Approximation) models, but the West Antarctic Ice Sheet accumulates too much ice using present-day boundary conditions. The coupled model simulations produce global equilibrium ice sheet volumes and calving rates like observed for present day boundary conditions. We designed a series of idealised experiments driven by oscillating solar radiation forcing on periods of 20 kyr, 50 kyr and 100 kyr in the Northern Hemisphere. These simulations show clear interactions between the climate system and ice sheets, resulting in slow build-up and fast decay of ice-covered areas and global ice volume. The results also show that Northern Hemisphere ice sheets respond more strongly to time scales longer than 100 kyr. The coupling to the atmosphere and sea level leads to climate interactions between the Northern and Southern Hemispheres.

Using a series of sensitivity experiments with the GREB-ISM v1.0, we further quantify the importance of several climate-ice sheet feedbacks and analyse the associated physical mechanisms. The result indicates that the inclusion of ice sheets will delay the response to the external forcing and facilitate the climate cooling in the high latitude and altitude areas in the Northern Hemisphere, but with a small amount of warming elsewhere, particularly in shoreline grids because of land-sea transition. The albedo feedback is a major positive feedback in favour of ice sheet build-up, whereas

precipitation is the greatest negative feedback that inhibits the growth of ice sheets. The surface lifting due to the topography feedback changes surface mass balance, causing the development of the ice sheets in the North Hemisphere. The sea level feedback influences ice sheets by shifting their location and altering the land-sea mask. As for surface temperature, the albedo feedback triggers a global surface temperature cooling with maximum at high latitude and altitude areas. Due to the lapse rate in the troposphere, the regions where ice sheets are developing and shrinking experience the greatest surface temperature cooling and warming, respectively. As a result, the topography and ice latent heat feedback significantly cools the land area at high latitudes while warms the low latitudes. On the other hand, the precipitation feedback leads to surface temperature warming at high latitudes and cooling at low latitudes. Last but not least, the sea level feedback leads to a dipole surface temperature response owing to the ice sheet shifting, as well as scattered shoreline grids warming due to the sea-land conversion.

In summary, the GREB-ISM is a useful tool to understand the feedbacks and interaction in ice-age cycle. The model can run global simulations of 100 kyr per day on a desktop computer, allowing the simulation of the whole Quaternary period (2.6 Myrs) within one month.

New page (standard thesis only)

Declaration

This thesis is an original work of my research and contains no material which has been accepted for the award of any other degree or diploma at any university or equivalent institution and that, to the best of my knowledge and belief, this thesis contains no material previously published or written by another person, except where due reference is made in the text of the thesis.

Signature:

Print Name: ZHIANG XIE

Date: 22 June 2022

Publications during enrolment

- **Xie, Z.,** D. Dommenget, F. S. McCormack, and A. N. Mackintosh, 2022: GREB-ISM v1.0: A coupled ice sheet model for the Globally Resolved Energy Balance model for global simulations on timescales of 100 kyr. Geosci. Model Dev., 15, 3691–3719, https://doi.org/10.5194/gmd-15-3691-2022.
- R. J. Nicholls, Z., Meinshausen, M., Lewis, J., Gieseke, R., Dommenget, D., Dorheim, K., Fan, C. S., Fuglestvedt, J. S., Gasser, T., Goluke, U., Goodwin, P., Hartin, C., P. Hope, A., Kriegler, E., J. Leach, N., Marchegiani, D., A. McBride, L., Quilcaille, Y., Rogelj, J., J. Salawitch, R., Samset, B. H., Sandstad, M., N. Shiklomanov, A., B. Skeie, R., J. Smith, C., Smith, S., Tanaka, K., Tsutsui, J. and **Xie, Z.**. 2020. Reduced Complexity Model Intercomparison Project Phase 1: Introduction and evaluation of global-mean temperature response, Geosci. Model Dev. [J]. 13(11), 5175–5190, doi:10.5194/gmd-13-5175-2020

Acknowledgements

I had never thought that I would be in Australia to pursue my PhD until I received the offer from Monash. At this moment, I want to say I am glad to choose Monash and have a precious 3.5 years PhD study.

I first want to thank my main supervisor Dietmar. Before coming to Monash, I did not have any numerical model development experience. But with help from Dietmar, I have built up a simple Earth system model at the end. During the progress, I gradually understood how to step by step test the model, how to reduce model biases and the most importantly, when to stop developing. I learned many good habits for scientists from Dietmar, such as research dairy, website developing for research and also integrating the research into the teaching. He really sets a good example for me! And he always gives me frank advice both for my research and career. Many of them are super useful. Anyway, I learned a lot from him and really appreciate his patience and help to me.

I also want to thank my dear friends and other two supervisors. After coming to Australia, the precious friendship is the best medicine for homesick. Me and my wife are always welcome to join the colourful events and had a lot of fun. There are too many people I want to thank to list all of them here. Their accompany is the best experience of my Australia life. And also, as my supervisors, Andrew and Felicity gave a lot of suggestions and support. I had zero idea about ice sheet before coming to Monash. With their help, I have more confidence on my ice sheet model and also know much more about ice sheet dynamics.

Last but not least, I want to thank my family. Due to my study, my wife did not go for any jobs and went abroad with me without any hesitation. We always had relaxed talk and funny games to release all stress after my intense study. Where she is, where my family is. And also, my mom gave me a lot of support. She always believes her son's ability and supports all of my decisions, which encourages me a lot, especially during the time I was struggled with slow progress.

At the end, I end up with an ancient Chinese saying to summarize my subtle feeling on my PhD study:

When looking at it, it seems very deep; when digging into it, it seems very hard; I used to think it is still in a long distance ahead, but suddenly I realized I had passed it.   -- Analects

仰之弥高，钻之弥坚。瞻之在前，忽焉在后。-- 《论语》

Outline

Chapter 1 Introduction

1.1 Ice-age cycle

Understanding ice-age cycles in the Quaternary period requires an interdisciplinary research approach including the fields of astronomy, geology, physical geography, oceanography and atmospheric science. Geological proxy data show that the sea level and surface temperature significantly oscillated with a preferred time scale of about 100 kyr during the last million years (Fig 1.1 A, C), indicating that large ice sheets and glaciers formed and retreated many times over this period in response to climate forcing (Imbrie et al., 1984; Shackelton, 2000; Short et al., 1991). These oscillations in the late Quaternary are known as the ice-age cycles.

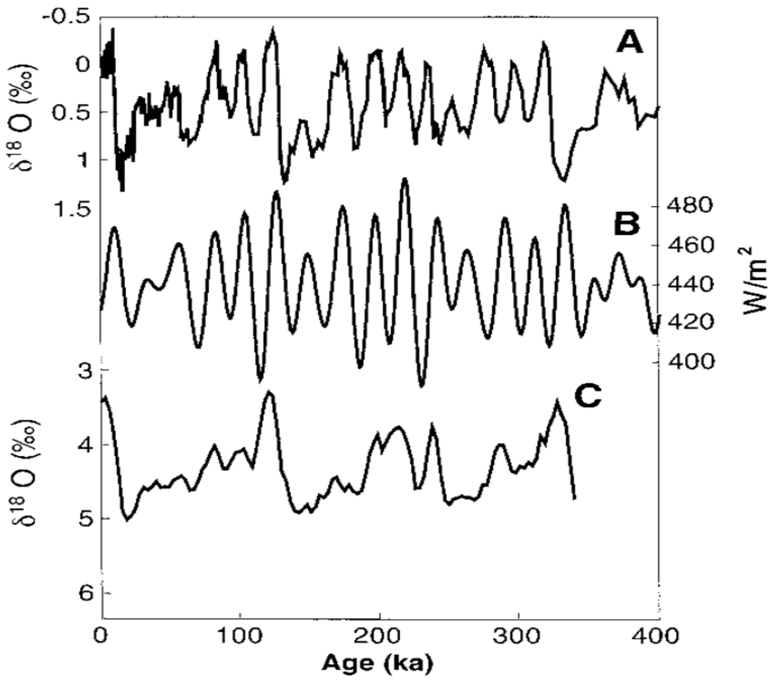

Fig. 1.1 (A) Vostok air δ18O record (air temperature) of Petit et al. (1999), published time scale. (B) The “classic” Milankovitch forcing, June insolation at 65°N. (C) Benthic δ 18O record of core V19-30 (sea level, Sundquist et al., 1985), published time scale. (Shackelton 2000, Fig 1).

By investigating ice-age cycles, researchers have identified many climate processes that generate long-term climate variability. Variations in Earth’s orbit and resulting changes in solar forcing have been widely accepted as a major driver of ice age cycles (Abe-Ouchi et al., 2013; Imbrie et al., 1984; Milankovitch, 1941; Short et al., 1991; Tabor et al., 2015; Wunsch, 2004). The Earth's axis and variations in orbital parameters, such as precession, eccentricity and obliquity, can effectively regulate the incoming solar radiation received at the Earth surface, and the season length for both hemispheres, leading to global temperature oscillations on time scales of 20 to 100 kyr (Fig 1.1 B, Huybers, 2011; Short et al., 1991). Additionally, greenhouse gases, especially CO_2, are a critical forcing during the late Quaternary (Shackelton, 2000). Before the industrial revolution, atmospheric CO_2 varied as an internal climate feedback originating from the ocean, biosphere or lithosphere (Bauska et al., 2018; Hogg, 2008). This carbon cycle of the earth system significantly changes the surface energy budget and affects climate variability.

The formation of large ice sheets is another important element of climate variability over the last million years (Bintanja and Van De Wal, 2008; Ganopolski and Brovkin, 2017). During ice ages, Northern Hemisphere ice sheets can cover a significant portion of the North American and European continents (Manabe and Broccoli, 1985; Mix et al., 2001), modifying climate through changes in the albedo of snow, low surface temperature, surface elevation and sea level (Bintanja and Van De Wal, 2008; Felzer et al., 1996; Hock, 2005; Manabe and Broccoli, 1985; Mix et al., 2001; Overpeck et al., 2006).

In addition, there are many other factors that potentially affected the ice age climate system such as deep ocean temperatures, ocean and atmospheric circulation changes, vegetation cover and atmospheric dust content. The interactions between these climate elements led to a complex picture of the Quaternary, and the details of these interactions still remain unclear.

1.2 Modelling of paleoclimate

In order to understand the physical basis of climate – ice sheet interactions during ice-age cycle, we usually perform numerical experiments with state-of-the-art ice sheet and climate models. Yet a fully coupled high resolution climate-ice sheet model is usually not feasible because of computational reason (Berends et al., 2018; Fyke et al., 2011), so we must have alternative methods to run the simulation. One common method is called the direct asynchronous method. In this framework, climate model runs to steady state using the boundary conditions from an ice sheet model. The ice sheet model is then driven by the climate model output, and run until its own steady state is reached. The repetition of the above procedure enables us to generate a long-term simulation in a relatively short computational time (Deconto and Pollard, 2003). Another technique is to perform an indirect asynchronous method, in which the ice sheet is forced by a reconstructed climate forcing. The climate forcing here could be the interpolation of several GCM snapshots in accordance with a temporally varying index (Greve, 1997; Niu et al., 2019). It could also be a combination of "climate matrix" based on parameters like orbital forcing values (Berends et al., 2018; Pollard, 2010; Pollard et al., 2013). Furthermore, statistical algorithms like the Gaussian process emulator has also been applied to mimic and accelerate climate-ice sheet coupling processes (Van Breedam et al., 2021).

Another high potential strategy for the climate-ice sheet coupling is a simple Earth system model, that is, by dynamically coupling the ice sheet model with a simplified climate model with low resolution and strong parameterization approach (Fyke et al., 2011; Ganopolski et al., 2010; Tigchelaar et al., 2019). This method is very close to the fully coupled simulation and thus shows much more details on the climate-ice sheet interaction. By using an Earth system model of intermediate complexity, Ganopolski and Brovkin (2017) explored the interactions between the carbon cycle, Northern Hemispheric ice sheets and climate over the last 400, 000 years. They suggested that the CO_2 evolution is sensitive to the model parameterizations. Similarly, Tigchelaar et al. (2019) evaluated the time evolution of the Antarctica ice sheet in last 400 kyr by coupling ice sheet model with low resolution climate model. And they pointed out that Antarctica ice sheet evolution in the late Quaternary is related to nonlinear interaction among atmospheric, oceanic and sea level forcing, instead of a single factor.

Those simple Earth system models are usually focusing on one hemisphere rather than global scale. However, it is necessary to use globally coupled model to better understand the paleoclimate in the Earth system. One question that one hemisphere modelling cannot address is why symmetric orbit forcing, such as precession and obliquity, can contribute to global cooling or warming. The insolation at 65°N is usually used to represent the strength of orbital forcing in the ice-age cycles (Calov and Ganopolski, 2005; Imbrie, 1982; Imbrie et al., 1984). In fact, when the insolation at 65°N reaches its minimum, the South Hemisphere also enters glacial period, even though insolation at South Hemisphere usually reaches its maximum (Bentley, 1999; Shackelton, 2000). This phenomenon indicates a strong interaction between two hemispheres. So, modelling the North or South Hemisphere alone is insufficient. Additionally, the formation and retreat of massive ice sheets in both hemispheres are the major causes of the sea level change (Lambeck et al., 2014). Some previous studies have already noticed that the sea level change may also feedback to the ice sheet evolution by changing grounding line position (Gomez et al., 2020; Schoof, 2007a; Tigchelaar et al., 2019). But due to one hemisphere coupling, the sea level change is usually taken as external forcing in simulation. Overall, a globally coupled Earth system model is required to further explore the ice sheet-climate interaction.

1.3 The Globally Resolved Energy Balance (GREB) model

The GREB model is developed and fully described in Dommenget and Flöter (2011), with the additional introduction of a new hydrological cycle model in Stassen et al. (2019). The model has three layers (atmosphere, surface and sub-surface ocean) with a global, horizontal grid spacing of 3.75° x 3.75° (96 x 48 points). The GREB model simulates four prognostic variables: surface (T_{surf}), atmospheric (T_{atmos}) and subsurface ocean temperature (T_{ocean}), and surface humidity (q_{air}):

$$\gamma_{surf}\frac{dT_{surf}}{dt} = F_{solar} + F_{thermal} + F_{latent} + F_{sense} + F_{ocean} + F_{correct} \tag{1.1}$$

$$\gamma_{atmos}\frac{dT_{atmos}}{dt} = -F_{sense} + Fa_{thermal} + Q_{latent} + \gamma_{atmos}(\kappa_a \cdot \nabla^2 T_{atmos} - \vec{u} \cdot \nabla T_{atmos}) \tag{1.2}$$

$$\frac{dT_{ocean}}{dt} = \frac{1}{\Delta t}\Delta To_{entrain} - \frac{1}{\gamma_{ocean}-\gamma_{surf}}Fo_{sense} + Fo_{correct} \tag{1.3}$$

$$\frac{dq_{air}}{dt} = \Delta q_{eva} + \Delta q_{precip} + \kappa_a \cdot \nabla^2 q_{air} - \vec{u} \cdot \nabla q_{air} + \Delta q_{correct} \quad (1.4)$$

where γ_{surf}, γ_{atmos}, γ_{ocean} are heat capacity of surface, atmosphere and deep ocean, F_{solar}, $F_{thermal}$, F_{latent}, F_{sense}, F_{ocean}, $Fa_{thermal}$, Q_{latent} are heat flux terms, including solar radiation, longwave radiation on surface, surface latent heat, sensible heat, land-sea heat difference, net longwave radiation for air and latent heat due to precipitation. κ_a and $\vec{u}$ are circulation parameters, representing air diffusion rate and wind velocity at 850hPa, respectively. $\Delta To_{entrain}$ represents ocean temperature tendency due to entertainment. Δq_{eva}, Δq_{precip} are humidity tendency due to evaporation and precipitation. There are three flux correction terms, $F_{correct}$, $Fo_{correct}$ and $\Delta q_{correct}$.

The main physical processes that control the surface temperature tendencies are: solar (short-wave) and thermal (long-wave) radiation, the hydrological cycle (including evaporation, moisture transport and precipitation), horizontal transport of heat, and heat uptake in the subsurface ocean. GREB further simulates a number of diagnostic variables, such as precipitation snow/ice cover and sea ice, resulting from the simulation of the prognostic variables.

Atmospheric circulation (mean winds) and cloud cover are seasonally prescribed boundary conditions, and prescribed flux corrections ($F_{correct}$, $Fo_{correct}$ and $\Delta q_{correct}$) are used to keep the GREB model close to the observed mean climate. State-independent flux corrections of surface temperatures or other variables allow a climate model to be close to the observed or any other state, while still being able to fully respond to external forcing or internal variability (Dommenget and Rezny, 2018; Irvine et al., 2013; Schneider, 1996). The flux correction terms are estimated by balancing the tendency equation (1.1)-(1.4) for observed boundary conditions to result into the observed T_{surf}, T_{ocean} and q_{air} for each calendar month (see for Dommenget and Flöter 2011 details).

Since the GREB model does not simulate the atmospheric or ocean circulation, it is conceptually very different from Coupled General Circulation Model (CGCM) simulations. The model does simulate important climate feedbacks such as the water vapour and ice-albedo feedback, but an important limitation of the GREB model is that the response to external forcing or model parameter perturbations do not involve circulation or cloud feedbacks. The GREB does not have any internal (natural) variability since daily weather systems are not simulated. Subsequently, the control climate or response to external forcing can be estimated from one single year, assuming an equilibrium has been reached. The primary advantage of the GREB model in the context of this study is its simplicity, speed, and low computational cost. The simulation of one year of global climate with the GREB model can be done about 1sec (about 100,000 simulated years per day on a desktop computer), and model simplicity allows the user to straightforwardly investigate cause and effect in coupled simulations. As an intermediate complexity model, the GREB v1.0 joined the Reduced Complexity Model Intercomparison Project (RCMIP, Nicholls et al., 2020), which aims to provide a computationally efficient model tools for climate science. As a Reduced Complexity Model, GREB shows a comparable modelling performance as complex model in climate change scenarios, such as double CO_2 scenario, which provides a relatively reliable tool for long-term simulation.

1.4 Thesis design

The project aims at developing a simple ice sheet scheme that is fully coupled to the GREB model and use this fully coupled Earth system model, GREB-ISM, to simulate global ice age cycles on time scales longer than 100,000 yrs. Based on the GREB-ISM, we will be able to understand the details of the climate-ice sheet feedbacks in paleoclimate changes. Following are two main goals in the project:

- Develop an ice sheet model and coupled it with the GREB in order to obtain a simple Earth system model used for million years simulation.
- Understand the physical processes within the climate-ice sheet feedback during the ice-age cycle.

The output of the project will improve the GREB model and enable the model to investigate the interaction between ice sheet and climate system in time scale of up to a million years.

The thesis chapter has been divided into 6 chapters.

The Chapter 1 gives an overall introduction about the whole thesis, including the ice-age cycle, progress of paleoclimate modelling, the Global Resolved Energy Balance model (GREB) and the chapter organization.

The Chapter 2 describes our newly developed ice sheet model. This chapter begins with a brief overview of ice sheet dynamics, followed by an explanation of the model grid and glacier mask. Mass balance, momentum balance, and energy balance are used to explain the dynamic core of the new model. We finally conclude with a summary of the model structure and a brief discussion.

The climate-ice sheet coupling strategy is summarized in the Chapter 3. In this chapter, we demonstrate the information exchange between the ice sheet model and the GREB, as well as the modifications made to the GREB to accommodate the ice sheet model coupling requirements.

To verify the newly developed ice sheet model and the coupled Earth system model (GREB-ISM), we conduct a series of benchmark experiments in the Chapter 4. We first evaluate the stand-alone ice sheet model based on its numerical performance, modelling of actual ice sheets and transition simulation in past 200, 000 yrs. Later, the coupled GREB-ISM is tested by modelling the present-day ice sheets and climate as well as a series of experiments with idealized solar forcing.

The GREB-ISM is applied in the Chapter 5 to explore the climate-ice sheet feedbacks. In this chapter, several sensitivity experiments are used to evaluate five distinct climatic feedbacks, namely albedo feedback, topography feedback, ice latent heat feedback, precipitation feedback and sea level feedback. We will quantify the importance of each feedback and investigate its underlying physical mechanism.

Last but not least, we provide a brief overview and discussion of the entire thesis in the Chapter 6.

Chapter 2 Ice sheet model development

2.1 Introduction

Ice sheets are ice masses of continental size on solid land, together with ice shelf floating in bays nourished by the inflow from surrounding ice sheets (Greve and Blatter, 2009). Ice sheets usually accumulate by snowfall and disappear due to melting and calving. However, in the ice age, ice sheet can be extended and cover a vast of land domain (Manabe and Broccoli, 1985; Mix et al., 2001). And thus the ice age climate is profoundly influenced by the albedo of snow, low surface temperature, surface elevation and sea level change (Felzer et al., 1996; Hock, 2005; Manabe and Broccoli, 1985; Mix et al., 2001; Overpeck et al., 2006).

Mass balance is basically the sum of accumulation (snowfall) and ablation (melting and calving) (Anonymous, 1969). An energy-balance melt model is a physically based approach, which calculate the melting energy and ice thickness change according to the surface energy balance during fusion (Hock, 2005). Another popular empirical method is Temperature-index melt models like PDD model (positive degree day model, Hock 2003), which is widely used in the existing ice sheet models (Bueler and Brown, 2009; Winkelmann et al., 2011). Calving is defined as the component of ablation consisting of the breaking off of discrete pieces of ice from a glacier margin into lake or sea water, producing icebergs, or onto land in the case of dry calving. Calving is a very complex process and very hard to measure (Levermann et al., 2012; Winkelmann et al., 2011).

When mass accumulates on ice sheet, uneven mass distribution leads to an ice flow to advert mass. Rood (1987) pointed out that many traditional advection schemes applied in chemical transport model always suffer issues like strong diffusion, non-monotonic or high computational expense. However, some finite volume schemes were developed, some of which are positive defined (no negative value), monotonic, mass conservative and relatively low computational expense and was widely applied in atmospheric and chemical transport model (Allen et al., 1991; Carpenter et al., 1990; Colella and Woodward, 1984; Lin et al., 1994; Lin and Rood, 1996, 1997). Since the requirement of ice sheet model advection scheme is similar with chemical transport model (mass conservation, monotone and positive defined), Flux-Form Semi-Lagrangian Transport (FFSL, Lin and Rood, 1996) scheme in geocoordinate is a good option for ice sheet modeling and thus applied in our model.

Another two important processes regulating ice temperature are diffusion and heat production due to internal friction (Greve and Blatter, 2009). When deformation of ice sheet occurs in ice sheet, heat will be generated because of internal friction, which is proportional to strain rate of ice. And also, the heat in different layers will redistribute by diffusion process (mostly vertical diffusion) so that there is no dramatic temperature gradient.

To accelerate and simplify the ice sheet modelling, we applied Shallow Ice Approximation (SIA, Hutter, 1983) for grounded ice sheets and Shallow Shelf Approximation (SSA, Macayeal, 1989) for floating ice shelves. Both of them are approximations to Stokes flow. SIA assumes that the gravitational driving stress entirely balances the basal shear stress of grounded ice (Pattyn, 2003). For long-term simulation, SIA is a computationally efficient approximation and widely applied in grounded ice sheet modelling (Larour et al., 2012; Pollard and Deconto, 2012; Winkelmann et al., 2011). However, the SIA fails to capture the ice shelf stress balance, in which lateral shear becomes dominant. In this case, the Shallow Shelf Approximation is a more proper solution (Macayeal, 1989). Different from SIA, SSA is a two-dimension stress balance model ignoring the vertical shear (Larour et al., 2012).

Overall, the ice sheet model is a global thermomechanical ice flow model that comprises momentum balance, mass balance, and energy balance modules with the prognostic variables: thickness and temperature, and diagnostic velocities. Our aim is to develop an ice sheet model which is able to be globally coupled with climate model for million years simulation. To achieve this goal, our ice sheet model is based on the large-scale ice sheet approximation and a spherical coordinate with coarse horizontal and vertical resolution (3.75^o x 3.75^o, 4 vertical layers). The processes we include in the new ice sheet model is summarised in Fig 2.1. For the numerical schemes, a short summary is listed in Table 2.1.

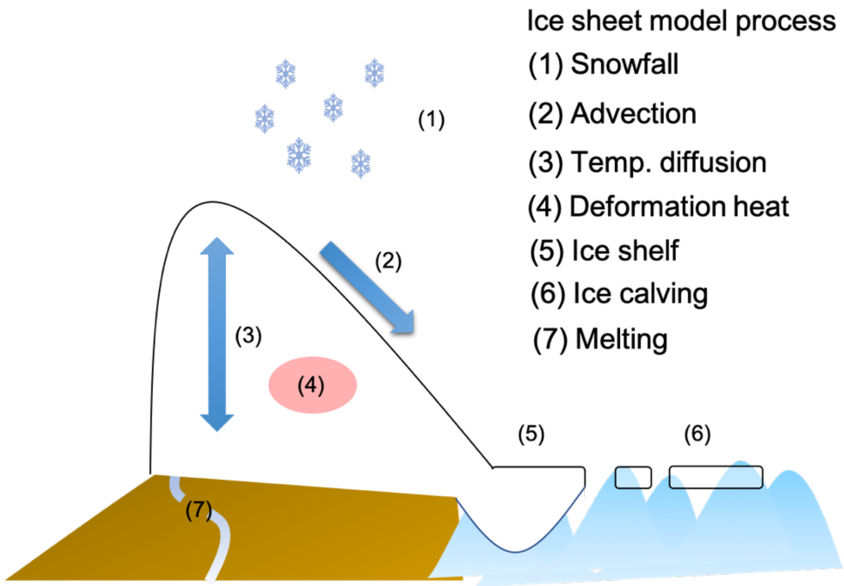

Fig 2.1 The simulated physical processes in the new ice sheet model.

This chapter will describe the ice sheet model, including the model grid, dynamical methods used, parameterizations and approximations made. We will first define the model grids in section 2.2 and then explain how ice sheet and ice shelf grids are identified in section 2.3. In section 2.4, the surface mass balance scheme is presented, including snowfall rate, melting and calving. Following that, the momentum balance and energy balance are discussed in section 2.5 and 2.6, respectively. At the end, we give a brief discussion on the new ice sheet model in section 2.7. The explanation and values of the symbols in this chapter can be found in Symbols and Parameters List section at the end of thesis.

Table 2.1: Processes and their relevant numeric scheme for the ice sheet model.

Processes	Time step	Contribute to	Scheme / Physical basis
Mass balance	half day (GREB)	ice thickness	energy balance
Advection	one year	ice thickness	finite volume (FFSL, Lin and Rood 1996)
Vertical diffusion	one year	ice temperature	finite difference

Vertical advection	one year	ice temperature	finite difference
Deformation heat	one year	ice temperature	on vertical sheer of horizontal velocity

2.2 Model grid

The ice sheet model uses the same horizontal grid as the GREB model. The Arakawa C scheme (Pollard and Deconto, 2012) is adopted for the simulation of velocities, with the ice thickness and temperature specified at the centre of the grid, and zonal and meridional velocities are specified at the grid boundary midpoint. For the vertical coordinates, we apply a terrain-following coordinate, ξ, in the ice sheet model, where

$$\xi = \frac{z - \frac{H}{2}}{\frac{H}{2}} \tag{2.1}$$

in which z is vertical coordinate for ice sheet (z=0 represents ice sheet base) and H is ice thickness.

We chose the number of layers to be 4, to be close to the minimal number of layers which can still resolve the vertical velocity in the ice sheets: the surface layer ($\xi = 1$), two Gaussian nodes ($\xi = \pm\frac{1}{\sqrt{3}}$, nodes for 2 points Gaussian quadrature, Hildebrand 1987) and the base layer ($\xi = -1$). The vertical integration in the model is based on Gaussian-Jacobi quadrature (F. B. Hildebrand, 1966), where temperature vertical distribution is estimated by a polynomial curve fitting according to the four layers, which is expressed by:

$$T(\xi) = c_0 + c_1\xi + c_2\xi^2 + c_3\xi^3 \tag{2.2}$$

where T is the temperature, c_i ($i = 0,1,2,3$) are regression coefficients derived from the temperatures at the above four vertical nodes at each time step. The pressure melting point is set if the temperature surpasses that threshold. The global, horizontal model grid has cyclic boundary conditions. For the grid points at the poles, we assume the poleward neighbour is the point at the same latitude, but shifted by 180°, following the approach in Allen et al. (1991). To avoid numerical instability in the polar regions, a zonal wave filter is applied from 76.875°S to the South Pole (Lin and Rood, 1997; Suarez and Takacs, 1995).

2.3 Glacier mask

The GREB-ISM ice sheet evolution depends on whether the ice is grounded (land), floating (ice shelves) or if we have thin ice over the ocean (sea ice). The ice thickness, *H*, is used for both sea ice and ice sheet. For very thin ice cover, the gravity driven ice flow is negligible and thus it does not follow ice sheet dynamics (e.g., snow or sea ice). To distinguish large ice mass from snow or sea ice, *H* must be above 10 m (Fyke et al., 2011). In detail (ρ_i and ρ_o are ice and ocean density, b is bed rock height):

- ***Grounded ice (land) points***: ice sheet is grounded on bedrock, satisfying the condition (Larour et al. 2012):

  $$b + \frac{\rho_i}{\rho_o} H > 0.$$

- ***Floating ice (ice shelves) points***: ice thickness $H \geq 10\text{m}$ and does not reach the bedrock, satisfying the floating condition: $b + \frac{\rho_i}{\rho_o} H \leq 0.$
- ***Ocean points***: all other points. The ocean points here include sea ice grid ($H \geq 0$) as well.

The definition of this glacier mask does implicitly define groundling lines of glaciers by shifting points from grounded ice to floating ice according to the ice thickness, bed topography and global sea level (see also Section 3.3.8 for the sea level impact on the bed elevation).

2.4 Mass balance

The ice surface elevation, calculated from the mass balance equation, is the primary input from the ice sheet model to the GREB model, calculated for all global grid points. The mass balance equation is:

$$\frac{\partial H}{\partial t} = s - a - \nabla \cdot (\vec{V}_m H) \tag{2.3}$$

where s, a and $\vec{V}_m$ are ice accumulation (snowfall), ice ablation and vertical mean of ice flow horizontal velocity.

where the accumulation of snow (s), ablation (melting) of ice (a), and ice transport ($\nabla \cdot (\vec{V}_m H)$) control the mass balance. The surface mass balance terms (s, a) are calculated at the same time step as GREB (half day) and thus we have seasonal ice thickness change. The ice transport term is calculated with an annual time step (Section 3.2.4).

The methods used to calculate the terms on the right-hand side depend on whether ice is grounded (ice sheet), floating (ice shelves), or sea ice. The mass balance for sea ice is described in Section 3.5. For the ice sheet and shelves, the two local surface forcing terms for the ice mass balance from equation (2.3) are the source (accumulation) and sink (ablation) terms. The accumulation is due to snowfall:

$$s = \frac{\rho_o}{\rho_i} r \cdot p \tag{2.4}$$

with the snowfall ratio, ***r***:

$$r = \begin{cases} 1, T_{atmos} < T_m \; and \; T_{surf} < T_m - 2^oC \\ \frac{1}{2}\left(1 - \frac{T_{surf} - T_m}{2^oC}\right), T_{atmos} < T_m \; and \; T_m - 2^oC < T_{surf} < T_m + 2^oC \\ 0, otherwise \end{cases} \tag{2.5}$$

where T_m is melting point.

The ice ablation rate is due to surface melting by positive surface heat flux:

$$a = -\frac{F_{ice}}{\rho_i L_m} \tag{2.6}$$

with the latent heat flux for melting ice, F_{ice}:

$$F_{ice} = \begin{cases} -F_{surf} & \text{partial melting:} \quad F_{surf} \leq Fmax_{melt} \\ -\frac{\rho_i L_m H}{\Delta t} & \text{complete melting:} \; F_{surf} > Fmax_{melt} \\ 0 & \text{no melting:} \qquad F_{surf} < 0 \end{cases} \tag{2.7}$$

where L_m is latent heat flux of fusion.

Here, the maximum heat flux for complete ice melting is $Fmax_{melt} = \rho_i L_m \frac{H}{\Delta t}$. The surface heat flux, F_{surf} only considers the net surface heat flux beyond the freezing point:

$$F_{surf} = \gamma_{surf} \frac{T_{se} - T_m}{\Delta t} \tag{2.8}$$

and the estimated surface temperature without ice fusion is:

$$T_{se} = T_0 + \Delta t \frac{F_{net}}{\gamma_{surf}} \tag{2.9}$$

where F_{net} is defined as equation (1.1) right hand side.

We currently do not explicitly include an ocean basal melting scheme in our model. On the one hand, our ice shelf viscosity is tuned to fit the current day ice shelf thickness, which partially contains basal melting effects (see section 2.5). On the other hand, including a basal melting scheme (Martin et al., 2011) does not contribute to a significant model improvement in our model simulations (see section 4.3.3).

The snow accumulation and melting, as described above, control all land ice and snow cover, and therefore also simulate the seasonal cycle of snow and ice cover over land. Fig 2.2 illustrates the seasonal cycle of ice cover in both hemispheres as simulated by the GREB-ISM model with present day boundary conditions. The ice cover change for ocean points comes from sea ice changes, which is described in Section 3.5. The overall snow cover (land) distribution and seasonal cycle resemble observations (Robinson et al., 2012). Similarly, the mean sea ice extent and seasonal cycle are comparable with the observed (Rayner et al., 2003), with some overestimation of sea ice extent around Antarctica in summer.

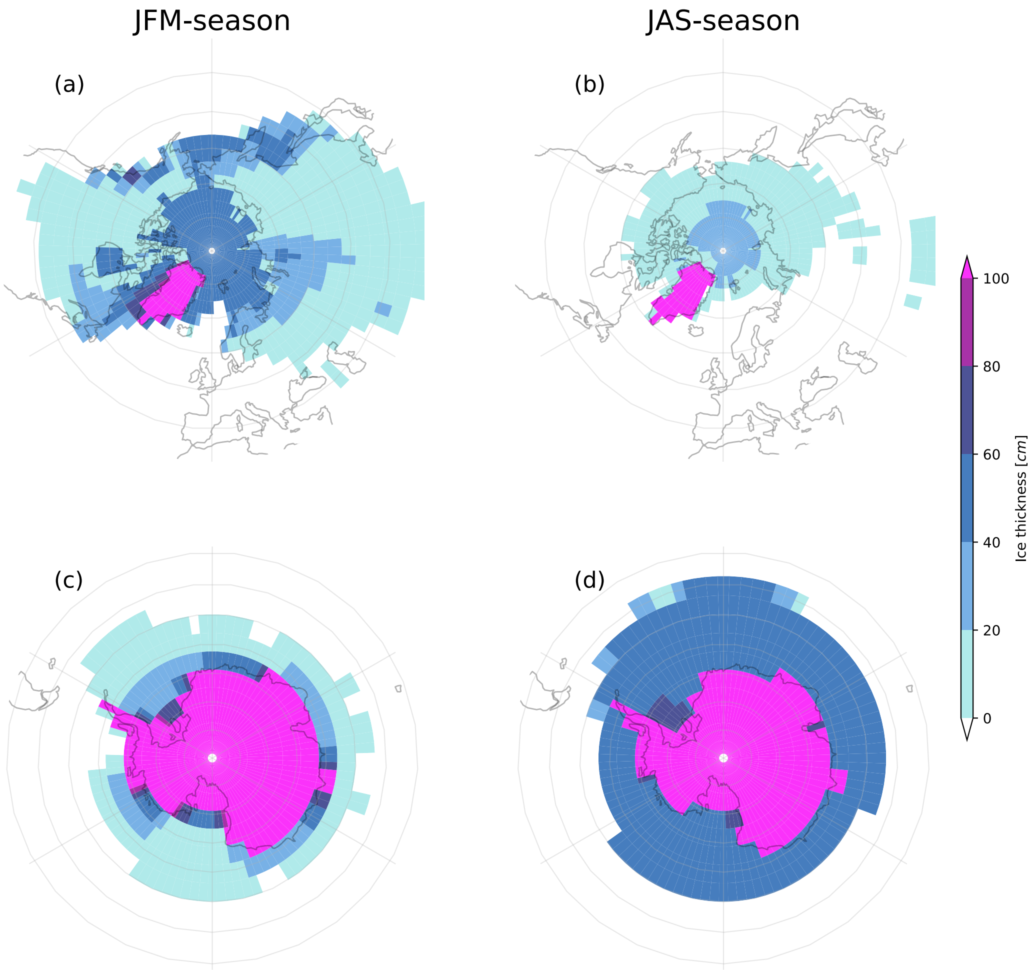

Figure 2.2 GREB-ISM seasonal ice thickness (cm) during January-February-March (left) and July-August-September (right) from the coupled dynamic equilibrium experiment equilibrium state (200 kyr). The scale is chosen to highlight seasonal ice cover.

Calving

A boundary condition for the mass transport equations is required at the ice front: here, ice from the ice sheet can be freely advected to the attached ocean grid and become sea ice (see section 3.5 for the dynamics of sea ice). In this way, calving is diagnosed as transport from ground (land) or floating ice (shelves) onto ocean points.

2.5 Momentum balance

Ice flow on grounded ice points is solved based on the shallow ice approximation (SIA; Hutter 1983; Morland 1984) for momentum balance:

$$\vec{V} = \vec{V}_b - 2\rho_i g \nabla z_{topo} \int_{z_b}^{z} A \exp\left(\frac{-Q}{RT}\right) \sigma_e^{n-1} (H - z') dz' \quad (2.10)$$

$$\vec{V}_m = \frac{1}{z - z_b} \int_{z_b}^{z} \vec{V}\, dz' \quad (2.11)$$

Where z_{topo} and z_b are surface topography and ice sheet bottom layer, A, Q, R, σ_e are ice sheet softness parameter, activate energy, universal gas constant and effective stress.

and the shallow shelf approximation (SSA; Macayeal 1989) on floating ice points (solved in geo-coordinate latitude ϕ and longitude λ):

$$\frac{\partial}{r_e \cos\phi\, \partial\lambda}\left(\eta_{SSA} \mathrm{H}\left(4 \frac{\partial \mathrm{V}_x}{r_e \cos\phi\, \partial\lambda} + 2 \frac{\partial \mathrm{V}_y}{r_e\, \partial\phi}\right)\right) + \frac{\partial}{r_e \cos\phi\, \partial\phi}\left(\eta_{SSA} \mathrm{H}\left(\frac{\partial \mathrm{V}_x}{r_e\, \partial\phi} + \frac{\partial \mathrm{V}_y}{r_e \cos\phi\, \partial\lambda}\right) \cos\phi\right) = \rho_i g H \frac{\partial z_{topo}}{r_e \cos\phi\, \partial\lambda} \quad (2.12)$$

$$\frac{\partial}{r_e \cos\phi\, \partial\phi}\left(\eta_{SSA} \mathrm{H}\left(4 \frac{\partial \mathrm{V}_y}{r_e\, \partial\phi} + 2 \frac{\partial \mathrm{V}_x}{r_e \cos\phi\, \partial\lambda}\right) \cos\phi\right) + \frac{\partial}{r_e cos\phi\, \partial\lambda}\left(\eta_{SSA} H\left(\frac{\partial \mathrm{V}_x}{r_e\, \partial\phi} + \frac{\partial \mathrm{V}_y}{r_e cos\phi\, \partial\lambda}\right)\right) = \rho_i g H \frac{\partial z_{topo}}{r_e\, \partial\phi} \quad (2.13)$$

where r_e is Earth radius, V_x, V_y are ice surface velocity zonal and meridian component for ice shelf, η_{SSA} is constant ice viscosity for ice shelf.

The viscosity (η_{SSA}, 2×10^{14} Pa s) in our model is larger than in other models (Bueler and Brown, 2009). This high viscosity is tuned by adjusting ice shelf thickness to observation, which may be impacted by uncertainties in the observations, other model fields, or in physical processes such as ice shelf basal melting effects.

Vertical velocities (w) are recovered through incompressibility:

$$w = -\int_{z_b}^{z} \nabla \cdot \vec{V}\, dz \quad (2.14)$$

The deformation of ice under stress is described by Glen's flow law (Glen, 1953, 1954, 1955):

$$\eta = \frac{1}{2EA\sigma_e^{n-1}}, \qquad A = A_0 \exp\left(\frac{-Q}{RT'}\right) \tag{2.15}$$

where A_0 is softness parameter in isotherm case, T' is the temperature corrected for the dependence of melting point on pressure:

$$T' = T - \beta\,(H - z) \tag{2.16}$$

In our model, the viscosity η_{SSA} (2×10^{14} Pa s) has been set as a constant value to match with the observed ice surface velocity and calving in the stand-alone dynamic equilibrium experiment (section 4.3.3). Each of Eqs (2.10)-(2.14) above are expressed in z-coordinates, but are transformed into ξ-coordinates for the model integration. Boundary conditions for the mechanical model are required at the ice sheet surface, base, and at the ice shelf-ocean front. A stress-free ice surface is assumed:

$$\boldsymbol{\sigma} \cdot \boldsymbol{n} = \boldsymbol{0} \tag{2.17}$$

where $\boldsymbol{n}$ is the normal unit vector at the ice surface.

At the base, the horizontal ice velocities follow the viscous-type sliding law defined in Greve (1997):

$$\vec{V}_b = -C_{sl} H ||\nabla z_{topo}||^2 \nabla z_{topo}, \quad z = z_b \tag{2.18}$$

The slide law coefficient for basal velocity C_{sl} is as in Greve (1997). In section 4.3.3 we discuss to what extent variations in C_{sl} could improve the simulations.

In GREB-ISM current version, we do not set a specific transition zone for grounded ice and floating ice, but these two types of ice are connected through boundary condition at interface. As a result, for stress conditions, the grounded ice (SIA scheme) provides the boundary condition for horizontal velocities of ice shelf (SSA scheme). On the other hand, at the interface with the open ocean points follow Greve and Blatter (2009), which in our model is expressed as:

$$4\frac{\partial}{r_e\cos\phi\,\partial\lambda}\left(\eta_{SSA}H\frac{\partial v_x}{r_e\cos\phi\,\partial\lambda}\right)+2\frac{\partial}{r_e\cos\phi\,\partial\lambda}\left(\eta_{SSA}H\frac{\partial v_y}{r_e\,\partial\phi}\right)=\rho_i gH\frac{\partial z_{topo}}{r_e\cos\phi\,\partial\lambda} \tag{2.19}$$

$$4\frac{\partial}{r_e\cos\phi\,\partial\phi}\left(\eta_{SSA}H\frac{\partial v_y}{a\,\partial\phi}\cos\phi\right)+2\frac{\partial}{r_e\cos\phi\,\partial\phi}\left(\eta_{SSA}H\frac{\partial v_x}{r_e cos\phi\,\partial\lambda}\cos\phi\right)=\rho_i gH\frac{\partial z_{topo}}{r_e\,\partial\phi} \tag{2.20}$$

2.6 Energy balance

The ice temperature (energy) balance:

$$\frac{\partial T}{\partial t}=-\vec{V}\cdot\nabla T-w\frac{\partial}{\partial z}T+\frac{\partial}{\partial z}\frac{\kappa}{\rho_i C_p}\frac{\partial}{\partial z}T+\frac{1}{\rho_i C_p}\left(\sigma_{xz},\sigma_{yz}\right)\cdot\frac{\partial\vec{V}}{\partial z} \tag{2.21}$$

The ice temperature balance at the surface is constrained by T_{surf} as computed in the GREB-ISM model (see section 3.2):

$$T=T_{surf},\quad z=z_{topo} \tag{2.22}$$

The geothermal heat flux is an important boundary condition for ice sheet. Previous studies show that the model with uniform geothermal heat flux is still able to reproduce the ice sheet evolution in the paleoclimate (Abe-Ouchi et al., 2007; Tigchelaar et al., 2019). For consistency, we therefore assume a globally constant bottom layer geothermal flux ($G, 4.2\times10^{-2}$ W m^{-2}) as in Huybrechts et al. (1996) and Payne et al. (2000):

$$\frac{\partial T}{\partial z} = -\frac{\rho_i C_p G}{\kappa}, \quad z = z_b \tag{2.23}$$

where κ, C_p are ice sheet diffusion coefficient and specific heat capacity for ice.

2.7 Summary and discussion

This chapter describes the construction of the newly developed ice sheet model. The new ice sheet model is based on global spherical grids with dimensions of 3.75° x 3.75° and 4 vertical layers. The model grids are divided into grounded ice, floating ice and ocean grid based on the ice thickness and floating criterion. The dynamic core of model uses the Shallow Ice Approximation (SIA, Hutter 1983) for ice sheets and Shallow Shelf Approximation (Macayeal, 1989) for ice shelves. The surface mass balance scheme of the new ice sheet model is based on the surface energy balance and snowfall rate. The dynamic core has a one-year time step, while the surface mass balance has a half-day time step (same as the GREB). The new model is capable of simulating the seasonal variation of surface ice and the response to the ice sheet topography.

It is worth noting that the ice sheet dynamic core and surface mass balance schemes have different time steps. Because snowfall and ice fusion in the mass balance scheme directly feedback to the surface energy balance, the time step of the mass balance scheme is set to the same as that in the GREB. The ice sheet dynamic, on the other hand, tolerates a much longer time scale than the rest of the climate system, hence the time step is set significantly longer. In current version, the model time step is not adaptive and the numerical stability issue at high latitudes are solved by using wave filtering. However, some models have applied time adaptive scheme to stably accelerate the modelling, such as Parallel Ice Sheet Model (Bueler and Brown, 2009; Winkelmann et al., 2011). This is a good technique and it is worthwhile to be further explored in the future.

One may argue that the resolution of the new model is too low to resolve the evolution of some ice sheet dynamics. For instance, there are many studies indicated that 4 km is a threshold to better capture the grounding line dynamics and idealized ice sheet evolution (Cornford et al., 2020; Leguy et al., 2021). However, we aim at simulating the time evolution of global-scale ice sheets on time scales of 100 kyr. For these kinds of problem, one has to make compromises to achieve feasible speed on the computing system. Past studies that addressed similar time scales to the ones we are interested in, also use coarser resolution models (Abe-Ouchi et al., 2007; Ganopolski et al., 2010; Willeit and Ganopolski, 2018). And as a result, the high resolution such as 4 km is not yet feasible on these timescales (Fyke et al., 2011). Another alternative way to improve the simulation in a low-resolution model is using sub-grid schemes. For instance, the sub-grid grounding line parameterization (Schoof, 2007b) has yet to be incorporated into the model, which is believed to improve the accuracy of ice sheet modelling in a lower resolution (Leguy et al., 2021).

Chapter 3 Model coupling

3.1 Introduction

Numerical modelling of the climate-ice sheet coupled system is an important way to investigate the effect of ice sheets on the ice age. In the early stage, climate models only simulated the atmosphere and ocean, and ice sheet variations were included as external forcing (Bush, 2004; Gates, 1976; Manabe and Broccoli, 1985; Webb et al., 1998). Most studies with numerical simulations focused on a specific period, like the last glacial maximum, and specific regions, like the Northern Hemisphere (Bush, 2004; Webb et al., 1998) due to limitations in computational resources. Ice sheet modelling at continental scale in response to orbital forcing requires the simulation of long (>10 kyr) periods, due to the relatively slow ice sheet adjustment time to climate forcing. Numerical studies of at large spatial and temporal scales therefore often use decoupled simulations with surface temperature and precipitation taken as boundary conditions for ice sheet models (Greve, 1997; Huybrechts, 2002; Payne et al., 2000). Fortunately, thanks to computer and model developments, progressively more studies apply coupled climate-ice sheet simulations on time-scale of 100 kyr to 1 Myrs (Abe-Ouchi et al., 2013; Ganopolski et al., 2010; Tigchelaar et al., 2019; Willeit et al., 2019). However, as far as we know, there are currently no global, million year, coupled climate-ice sheet simulations available.

In this chapter, we introduce a fully climate-ice sheet coupled Earth system model as a tool for paleo-climate research. The model is capable of simulating global, coupled ice-climate simulations of 100 kyr within 24 hrs on a desktop computer. It is designed for studies of global interactions between ice sheets and climate on time scales of 100 kyr to 1 Myrs. The starting point for this development is the Globally Resolved Energy Balance (GREB v1.0) climate model, which simulates the fast climate feedbacks relevant for the climate response to external forcing, such as CO_2 concentration or variations in solar radiation, on time scales of up to 500 yr (Dommenget and Flöter, 2011; Stassen et al., 2019). We introduce a new ice sheet model (ISM) into the GREB model, defining the new GREB-ISM model.

Of course, the introduction of an ice sheet model requires a number of changes to the original GREB model. First, the surface energy balance needs to be changed after considering ice sheet model. On the one hand, during the melting season, the ice latent heat term takes effect and cools the surface (Hock, 2005). On the other hand, because the surface heat capacity of the marine ice sheet and sea ice differs from that of the sea and ocean, a change in surface heat capacity is also necessary. The albedo of the surface is dramatically altered when the ice cover changes (Fyke et al., 2018; Ryan et al., 2019). The original GREB treats surface albedo as a function of surface temperature to mimic the ice cover change. After coupling with the ISM, the ice thickness can now be directly incorporated into surface albedo scheme. Another important effect of the ice sheet is the change in topography as a result of its growth (Edwards et al., 2014; Hakuba et al., 2012). The surface elevation must be updated during ice sheet development, and the sensible heat flux must be rectified due to the lapse rate-induced drop in air temperature. Additionally, since global ice sheet modelling allows for the evaluation of global ice volume, we can now include sea level variability in our simulation, which causes a shift in land-sea distribution and, as a result, climate change. Besides these, the precipitation scheme used in the original GREB assumes the linear relation between precipitation and local variables, which shows a quite large bias at high latitudes (Stassen et al., 2019). As a result, we devise a new precipitation method at high latitudes to better estimate snowfall rate here. To complete ice mass life cycle, the ice mass calved from ice sheet boundary is assumed to enter into ocean grid and creates sea ice. This assumption necessitates an adjustment to the sea ice scheme to account for the change in sea ice thickness. And last but not least, the original GREB meridian transport is not strong enough to reproduce the realistic temperature gradient at different latitudes. So, we need to fix this issue.

The overall coupling strategy can be depicted by Fig 3.1. The GREB provides input to the ISM in the form of surface temperature, surface energy flux, precipitation, and air temperature, while the

ISM gives information to the GREB in the form of ice latent heat and ice thickness tendency. In both components, variables such as surface elevation, land-sea mask, albedo, and sea level are employed.

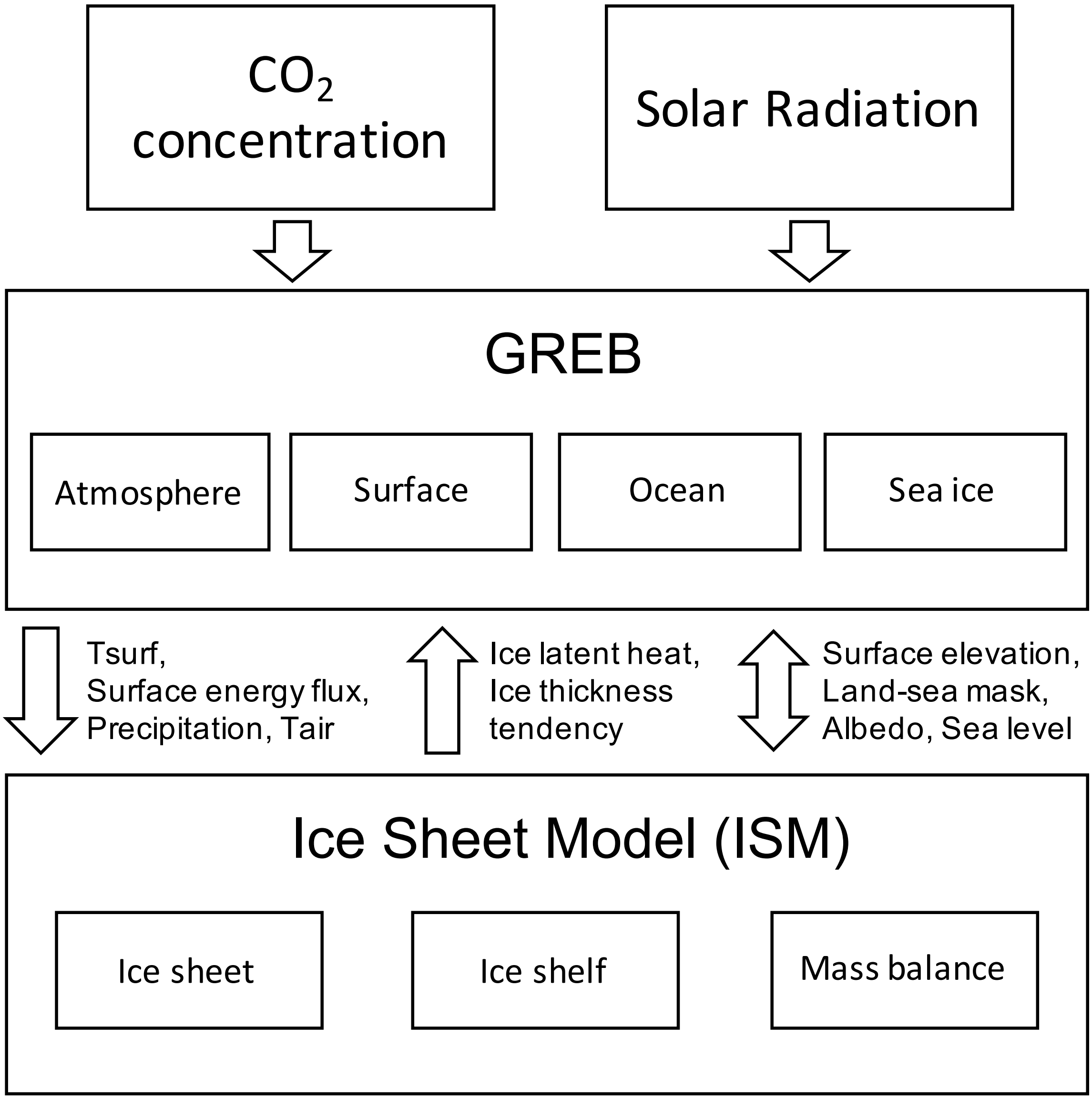

Figure 3.1 Schematic illustrating the coupled GREB-ISM.

In the following sections, we will go through the details of how we changed the processes mentioned above. Sections 3.2 and 3.3 will detail the changes made to the surface mass balance equation and heat capacity. In section 3.4, we focus on the new precipitation scheme. In section 3.5, the new sea ice scheme will be discussed. The revised albedo scheme for the new coupled model will be presented in Section 3.6. The topography and its related surface sensible heat flux change are depicted in sections 3.7 and 3.8. The sea level and land-sea mask change, which is mentioned in section 3.9, is another important development. In section 3.10, the modification of heat meridian transport is described. Finally, in section 3.11, we summarised the entire chapter.

3.2 Energy exchange between GREB and ice sheet / sea ice

The introduction of a prognostic ice sheet model introduces the additional heat flux term, F_{ice} for the T_{surf} tendency eq. (1.1), resulting in the new equation:

$$\gamma_{surf}\frac{dT_{surf}}{dt} = F_{solar} + F_{thermal} + F_{latent} + F_{sense} + F_{ice} + F_{ocean} + F_{correct} \quad (3.1)$$

The calculations of F_{ice} are described in the mass balance section 2.4 and the sea ice section 3.5. The effect of F_{ice} can best be illustrated by a simple response experiment, in which we add a 10 m ice cover and evaluate how surface temperature responds to it (Fig 3.2). In this response experiment 10 m of ice cover is introduced over a large region of Europe (Fig 3.2d, black box) at the start of the simulation and then the fully-coupled GREB-ISM model is run for 4 years to respond to this change.

The introduction of the ice cover forces surface temperature below the freezing point at all locations, as long as the ice sheet is present (Fig 3.2a-c). The atmospheric heat fluxes and sea ice dynamics force the sea ice to melt, which it does faster over the ocean points due to horizontal sea ice transport. Over land the ice cover melts after the first year and allows surface temperature to go back to the control run values. The atmospheric heat and moisture transport cause cooling in adjacent regions (Fig 3.2d).

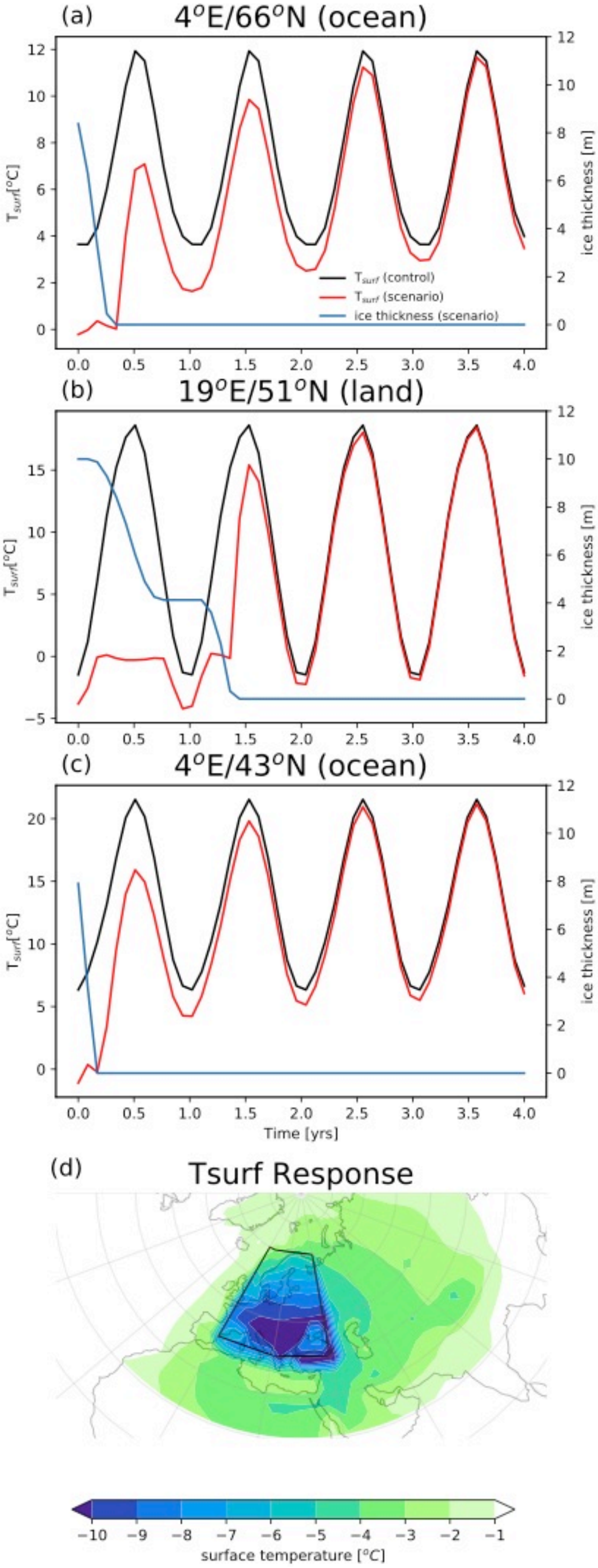

Figure 3.3 GREB-ISM response to adding a 10 m ice sheet in surface temperature (units: °C) and ice thickness (units: m). (a), (b) and (c) are the temperature and ice thickness evolution at three different locations. The black, red and blue curve represent control run surface temperature (without

adding 10 m ice), scenario run surface temperature (with adding 10 m ice) and scenario run ice thickness. (d) shows the temperature difference (units: ^{o}C) between scenario and control at the end of the first simulation year. The black outlined region in (d) mark the area in which the initial 10 m ice sheet is added.

3.3 Surface heat capacity

The surface layer effective heat capacity (γ_{surf}) in the GREB model is equal to the heat capacity of a water column of the mixed layer depth over ice free ocean points and equivalent to 2 m soil for all other points (e.g. land and ice covered). Thus, the formation of sea ice changes the heat capacity from that of the mixed layer depth to a 2 m soil column. This is unchanged from the original GREB model.

3.4 Precipitation correction

The hydrological cycle model in GREB developed in Stassen et al. (2019) simulates precipitation as a function of the simulated atmospheric humidity (q_{air}), the observed mean and standard deviation of the vertical air motion (ω_{mean} , ω_{SD}):

$$\Delta\, q_{precip_{S2019}} = r_{precip} \cdot q_{air} \cdot (c_{rq} \cdot rq + c_{\omega} \cdot \omega_{mean} + c_{\omega SD} \cdot \omega_{SD}) \tag{3.2}$$

This model aimed at a realistic simulation of precipitation with a focus on the regions of greatest precipitation, i.e. the tropical oceans. While the precipitation model is very good in these regions (Stassen et al., 2019), it only has limited skills over higher latitude land regions, which are most important for the ice sheet mass balance of the GREB-ISM.

To allow the ice sheet mass balance to receive unbiased mean precipitation forcing under present day conditions, we introduced a land precipitation correction in the GREB-ISM model. The new precipitation equation with flux correction is expressed as:

$$\Delta q_{precip} = \Delta q_{precip_{S2019}} + q_{zonal} \cdot p_{correct} \tag{3.3}$$

where $q_{zonal} \cdot p_{correct}$ is the flux correction of the equation. The flux corrections are only active over land and are a function of calendar month. They are estimated in a way that the simulated Δq_{precip} matches the precipitation observation for every calendar month of the year.

Here, we note that the $\Delta q_{precip_{S2019}}$ model assumes that precipitation is proportional to the local humidity (q_{air}). Stassen et al. (2019) demonstrate that this assumption is less appropriate in higher latitude land regions, as there is no clear relationship between the local q_{air} and Δq_{precip}. Due to lack of a clear local relationship, we relaxed this constraint and assumed that the precipitation over land is a function of the zonal mean humidity, reflecting the mostly zonal structure of the atmospheric circulation. Therefore we set the correction term to be proportional to the zonal mean q_{air} defining q_{zonal}. Within 30^{o} of the poles q_{zonal} is estimated as the mean from the pole to 60^{o}.

With this approach the precipitation over higher latitude land responds to cooling or warming similarly to other regions (e.g. oceans for lower latitudes). Additionally, Δq_{precip} in equation (1.4) is also proportional to the precipitation here. We will discuss the precipitation response of the GREB-ISM further below in the context of the response experiments.

3.5 Sea ice

Sea ice is a diagnostic variable in the original GREB model but is now changed to be a prognostic variable in GREB-ISM. Over land and ice shelf points, ice thicknesses (H) follow the dynamics described in the ice sheet model Section 2.4. Over ocean points we use the same prognostic variable (H), but the sea ice thickness dynamics follow a different tendency equation, namely:

$$\frac{\partial H}{\partial t} = \Delta H_{seaice} - \kappa_{si}\nabla^2 H \quad (3.4)$$

with the local sea ice growth:

$$\Delta H_{seaice} = \frac{\boldsymbol{F_{ice}}}{\boldsymbol{\rho_i L_m}} \quad (3.5)$$

and where the latent heat of ice fusion F_{surf} is defined by eqs. (2.7)-(2.9):

$F_{ice} = -F_{surf}$	ice grows:	$T_{se} < T_{sm}, F_{surf} < 0\ and\ H < 0.5\ m$
F_{ice} from equation (11)	ice melts:	$\mathrm{T_{se}} > \mathrm{T_{sm}}, \mathrm{F_{surf}} > 0$
$F_{ice} = 0$	no change:	otherwise

(3.6)

The sea ice growth threshold of 0.5 m reflects the fact that sea ice is a very good insulator and subsequently does not transfer atmospheric heat fluxes very well once a certain ice thickness is reached. This in practice limits the growth of sea ice by atmospheric heat flux to less than 0.5 m typically. In this case $F_{ice} = 0$ and it will no longer grow the sea ice, but only cool T_{surf}. (Eqs (28)).

Sea ice transport is estimated by isotropic diffusion ($\kappa_{si}\nabla^2 H$). This approximates the effect of turbulent winds and ocean currents transporting sea ice, leading to fast decay of sea ice near open ocean. The diffusion coefficient κ_{si} was chosen to roughly lead to a sea ice decaying time scale of about one month.

3.6 Albedo coupled to ice sheet

The surface albedo (α_{surf}) in the original GREB model was diagnosed as function of T_{surf}, but is now diagnosed as a function of the ice thickness (H):

α_{surf} = 0.1 H= 0.0

α_{surf} = 0.1 +17.5 m^{-1}· H $H \in$ [0.0, 0.02 m] (3.7)

α_{surf} = 0.45 H> 0.02 m

The albedo in GREB-ISM does not relate to vegetation and soil type and so on. But it does relate to the climatology cloud cover.

The linear relation between ice thickness and albedo in the GREB-ISM model was estimated from the assumption that for the observed Northern Hemispheric seasonal cycle of snow/ice cover over land the overall albedo matches the mean overall albedo of the original GREB model.

3.7 Topography coupled to ice sheet

The land topography (z_{topo}) in the original GREB model is a fixed boundary condition that influences a number of processes: thermal radiation, hydrological cycle and the transport of heat and moisture by advection and diffusion. For the GREB-ISM the land topography is now a function of the bed topography and ice sheet height:

$$z_{topo} = b + H, \quad \text{for grounded ice} \tag{3.8}$$
$$z_{topo} = \left(1 - \frac{\rho_i}{\rho_o}\right) H \ , \quad \text{for floating ice}$$

The GREB-ISM does not simulate any glacial isostatic adjustment.

3.8 Sensible heat flux between surface and atmosphere

The variable land topography (z_{topo}) should affect the sensible heat flux between T_{surf} and T_{atmos}, which was not simulated in the original GREB model. Here it needs to be considered that the GREB model does not resolve the vertical structure of the atmosphere, as it only has one atmospheric layer. However, in the real world T_{atmos} decreases with surface elevation, following a moist adiabatic lapse rate. We therefore change the sensible heat flux between T_{surf} and T_{atmos}, which was approximated in the original GREB model by Newtonian coupling between T_{surf} and T_{atmos}. In the GREB-ISM model this is now replaced with a Newtonian coupling between T_{surf} and an adjusted T_{atmos}:

$$F_{sense} = ct_{sense}\left(T_{atmos} + \Gamma \cdot z_{topo} - T_{surf}\right) \tag{3.9}$$

Here we choose a globally constant moist adiabatic lapse rate $\Gamma = -6\ \mathrm{K\ km^{-1}}$. The effect of this sensible heat flux is illustrated with a simple response experiment, see Fig 3.3. For this experiment we increase z_{topo} by 1000 m over the centre of Asia, and show the response of the annual mean T_{surf} and precipitation relative to a control simulation with no changes in z_{topo} (Fig 3.3). T_{surf} decreases in response to the topographic perturbation, approximately linearly to the moist adiabatic lapse rate. The higher topography also affects the hydrological cycle, reducing the precipitation locally and also remotely through transport of relatively reduced atmospheric humidity.

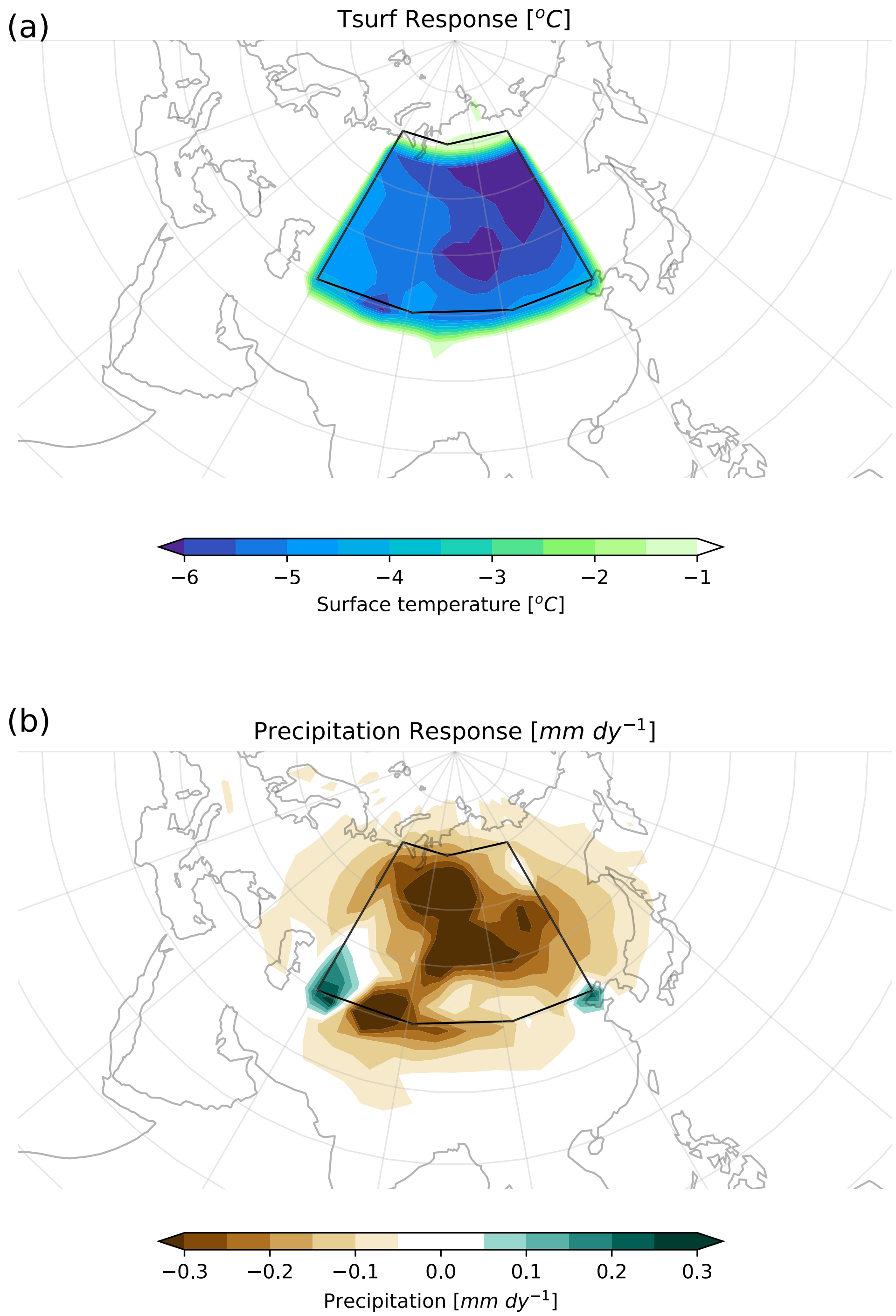

Figure 3.3 GREB-ISM response to a lifting of the topography by 1000 m for surface temperature (a,

units: ^{o}C) and precipitation (b, units: mm dy^{-1}). The response is defined as the scenario run (1000 m topography lifting) minus control run (no lifting) at the end of the first simulation year. The box represents the lifted region.

3.9 Sea level and land-sea mask

A sea level subroutine is added in GREB-ISM. Only grounded ice thickness impacts the global sea level. Consequently, the sea level change slv is defined by:

$$\mathrm{slv} = \frac{\int_{grounded}(\mathrm{H}\text{-}\mathrm{H_{ref}})dA}{\mathrm{A_{ocean}}} \tag{3.10}$$

where H_{ref} is the reference ice thickness, A_{ocean} is total area of ocean grid and $\int_{\mathrm{grounded}} dA$ is an integration over all grounded ice points. slv will be added to bed topography b, which eventually impacts the land-sea mask. The sea level and land-sea mask are updated every model year.

The soil moisture, which is a boundary condition for estimating surface evaporation is initially set to observed values over land and then changes if land-sea distribution alters. If the sea level lowers and an ocean point turns into a land point ($b > 0$) then the land point has a soil moisture value of 0.3 (equivalent to the mean value for land points in Dommenget and Flöter 2011). In turn, if the sea level rises and a land point turns into an ocean point ($b < 0$), then the soil moisture value is set to 1.0.

3.10 Meridional heat transport

The study by Dommenget et al. (2019) showed that the GREB model, without flux corrections for T_{surf}, has a high latitude climate that is too cold and a tropical climate that is too warm, indicating that the meridional heat transport is too weak. The meridional heat transport in the GREB model results from the atmospheric heat transport by the mean advection due to the mean horizontal wind field and by isotropic diffusion. The latter depends on the diffusion coefficient $\kappa_a = 8 \times 10^5$ m^2 s^{-1} in the GREB model. This value is not strongly constrained by observations and may effectively be different by an order of magnitude. Since the meridional heat transport may play an important role in the global ice age cycle, we enhance this diffusion coefficient by a factor of 5. This reduces the mean T_{surf} bias in higher latitudes and the tropics in the GREB model without flux corrections, while at the same time does not increase biases in other locations, indicating it is a better approximation of the isotropic diffusion.

3.11 Summary and discussion

In this chapter, we discussed the coupling strategy for the GREB-ISM. An additional heat flux term is added to the surface energy balance equation to represent the ice latent heat. Then, surface albedo, surface elevation, sensible heat and sea ice are expressed in terms of ice thickness. As a result of ice sheet modelling, sea level and land-sea mask change are incorporated into the model. The surface heat capacity of ice is set to the same value as that of the land grid. Last but not least, precipitation and meridional heat transfer are changed to fit the new ice sheet model.

One of the major changes in the GREB is to set surface albedo as a function of ice thickness. This change leads to a higher complexity of the albedo change. For example, in the coupled GREB-ISM, the surface albedo during the melting season is not only related to the contemporaneous surface temperature, but also connected with the total snow accumulation during the snowing season. In the section 5.4.3, we will see this change can amplify the climate feedback by accumulating the signal through different seasons.

Another important change is to introduce the lapse rate for surface air temperature. In the original GREB, the air temperature and surface temperature are very close to each other. However, in the GREB-ISM, the air temperature is treated as the air potential temperature rather than the surface temperature. And thus, the topography change impacts on surface temperature and air temperature differently. When the ice sheet surface elevation raises, the surface temperature tends to decrease significantly while the air temperature barely changes, leading to a relatively large temperature difference between surface temperature and air temperature.

However, some of our current model settings are quite primary. The most significant constraint is the absence of changes in atmospheric and oceanic circulation. To illustrate effect from the general circulation, the GREB-ISM current version uses diffusion and advection with today's circulation. This setting is unable to capture the large-scale stationary wave pattern shift caused by paleoclimate topography changes (Felzer et al., 1996; Herrington and Poulsen, 2012). As for the oceanic circulation, we do not include the effect from the oceanic circulation such as Atlantic Meridional Overturning Circulation (AMOC), which is also regarded as an important role in causing long-term fluctuation during paleoclimate (Kapsch et al., 2021; Risebrobakken et al., 2007; Zhang et al., 2014). All of those factors need to be considered in the future model development.

Apart from the coupling with climate system, some previous studies also argued that the interaction between ice sheet and liposphere, like glacial isostatic adjustment (GIA) process (Abe-Ouchi et al., 2013; Han et al., 2021), might be important. However, the recent research indicates that the impact of the process is highly related to the lapse rate value (supporting information, Han et al. 2021). To simplify the physical process and exclude the extra uncertainty in our model, we do not include the GIA process in our simulation. Of course, this is an interesting topic which we can further explore in the future.

Chapter 4 Model benchmark experiment

4.1 Introduction

Our main target is to develop a model tool for paleoclimate simulation, which is a climate-ice sheet coupled Earth system model. To achieve this goal, we develop a new global ice sheet model. As a result, it is necessary to verify the numerical performance of the new ice sheet model before coupling with the climate model. So, we will use several standard benchmark experiments to test our ice sheet model and then run standalone ice sheet model simulation under given climate forcing. After that, the new coupled Earth system model GREB-ISM will be tested by simulating current climate equilibrium and some idealized paleoclimate forcing experiments.

For ice sheet model, an early project, European Ice Sheet Modelling Initiative (EISMINT) model intercomparison project (Huybrechts et al., 1996; Payne et al., 2000), designed a series of standard benchmark experiments with idealized situation. In order to test dynamic and thermodynamic part of ice sheet model individually, EISMINT phase I (EISMINT I) experiments provide several standard experiments and model results under given horizontal resolution and boundary condition (Huybrechts et al., 1996). Furthermore, EISMINT phase II (EISMINT II) is an improved model comparison project, which further examines the whole ice sheet model including dynamic and thermodynamic model components. The experiments in EISMINT are widely used to test and compare numerical performance of large-scale ice sheet models (Bueler et al., 2007; Pattyn, 2003). Recently, there are more ice sheet model comparison projects available, such as the Ice Sheet Model Intercomparison Project for CMIP6 (ISMIP6, Nowicki et al., 2016) and the Marine Ice Sheet Model Intercomparison Project (MISMIP, Cornford et al., 2020; Pattyn et al., 2012, 2013). However, those model comparison projects are usually designed for complex ice sheet/shelf model with high resolution. Considering the ISM is fairly simple and low resolution, we decide to use EISMINT experiments to verify its numerical performance.

Besides these, the ice sheet model also needs to be further verified by reproducing current day ice sheets, such as Greenland Ice Sheet (Greve, 1997; Larour et al., 2012) and Antarctica Ice Sheet (Martin et al., 2011). The ISM is not designed to represent every physical feature of an ice sheet because it is a simple ice sheet model with a low resolution coupled with an Earth system model. Instead, the ice thickness is the most important feature because the most of exchange variable between ice sheets and climate component are related to the ice thickness. Consequently, our test experiments here will mainly focus on the total ice mass balance, including ice thickness and ice flow transportation. The ISM is expected to reproduce a similar ice thickness distribution and reasonable boundary mass calving as today's observation.

Concerning the modelling of the ice age cycle, we should include some typical events in our model simulations. Approximately 127, 000 years ago, the Earth experienced a warm era known as the Eemian or Last Interglacial (Fyke et al., 2011; Ganopolski and Brovkin, 2017; Johnsen et al., 1997; Otto-Bliesner et al., 2017). During this time, the sea level was believed to have been higher than it is now, and the ice sheets in both hemispheres retreated from their current positions (Nicholl et al., 2012; Parry et al., 2011). However, around 21,000 years ago, the climate on Earth was extremely cold, which is known as the Last Glacial Maximum (Kageyama et al., 2017, 2021). Back then, the Northern Hemisphere was covered in vast ice sheets, and the sea level dropped dramatically (Clark et al., 2009; Fairbanks, 1989; Lambeck et al., 2014; Velichko et al., 1997). As two typical events, it is necessary for the paleoclimate ice sheet model to reproduce them, as well as their relevant retreat and creation processes.

When the ISM is coupled with the GREB, the coupled GREB-ISM is required to reproduce realistic ice thickness as well as climate variables such as surface temperature and precipitation. The Pre-Industrial or Late Holocene simulation is one of usual test experiments for new developed climate-ice sheet coupled model (Fyke et al., 2011; Roche et al., 2014). During this time period, there was a lot of observation data that was relatively reliable, which makes it a great reference for model verification. Aside from this, the coupled Earth system models were also tested by simulating the typical events such as the Emian and LGM (Fyke et al., 2011), as well as last 130 kyr (Ganopolski et al., 2010). Those experiments are designed to test if the coupled model can capture the climate variability in transition simulations. However, the current version of the GREB-ISM cannot reproduce the whole transition climate variability because the atmospheric and oceanic general circulation change are still missing. In order to assess if the GREB-ISM can capture the main climatic change features during the ice-age cycle, we run a series of transition experiments driven by an idealized North Hemisphere solar forcing with typical periods during the ice age cycle (20, 50 and 100 kyr, Huybers, 2011).

Overall, besides introduction, this chapter will be divided into four main parts: data, standalone ice sheet model experiments, coupled climate-ice sheet model experiments and summary. In section 4.2, we will first introduce data used in the experiments. The section 4.3 includes all benchmark experiments for standalone ice sheet model. The numerical scheme of our ice sheet model will be tested by using benchmark experiments from EISMINT I (section 4.3.1) and EISMINT II (section 4.3.2). Then, the stand-alone ice sheet model will be evaluated by simulating the current ice sheets (section 4.3.3) and time evolution of ice sheets in past 200 kyrs ice-age cycle (section 4.3.4). The coupled GREB-ISM will be tested in section 4.4. The current ice sheets and climate state are simulated to further examine the numeric stability and accuracy of the coupled GREB-ISM in section 4.4.1. Following this, we show several transition experiments driven by solar insolation of varied frequency in section 4.4.2, which are used to evaluate the coupled model's performance in long-term integrations. At the end, we will give a brief summary for our results.

4.2 Data

Input values for most climatology for the GREB model, such as surface temperature, atmospheric humidity, horizontal winds and vertical air motion, are taken from the ERA-Interim dataset (Dee et al., 2011). Soil moisture is from NCEP reanalysis data from 1950-2008 (Kalnay et al., 1996), cloud cover climatology from the ISCCP project (Rossow and Schiffer, 1991) and ocean mixed layer depth climatology from Lorbacher et al. (2006). Precipitation data is from Global Precipitation Climatology

Project (GPCP, Adler et al. 2003) and for Antarctica we use the dataset from NCEP-DOE (Behrangi et al., 2020; Kanamitsu et al., 2002).

The modern observed bed topography and ice thickness data for Greenland and Antarctica are obtained from BedMachine (Morlighem et al., 2017, 2020), Greve (1997) and Martin et al. (2011). Ice surface velocity data come from Making Earth System Data Records for Use in Research Environments (MEaSUREs) Program (Joughin, 2017; Joughin et al., 2010; Mouginot et al., 2012; Rignot et al., 2011, 2017). In this study, the bed topography refers to all different types of ice basis. Fig 4.1 shows the global map in the GREB model resolution of the bed topography and observed ice thickness. Ice sheet calving rates are taken from Bigg (1999) for Greenland and Liu et al. (2015) for Antarctica. For paleoclimate proxies, the Greenland Ice Core Project (GRIP) (Greve, 1997; Johnsen et al., 1997) are used to impose surface air temperature anomalies for the last 250 kyr. $d^{18}O$ proxy from sea sediment (Imbrie et al., 1984) is used as a proxy for global sea level change for the last 250 kyr. The surface temperature and precipitation during Last Glacial Maximum (LGM) for a forced transition experiment is obtained from CMIP6.PMIP.AWI.AWI-ESM-1-1-LR datasets (Shi et al., 2020) from the Paleoclimate Modelling Intercomparison Project (PMIP4, Kageyama et al., 2017).

For convenience of data comparison, we interpolated all high-resolution data into GREB-ISM resolution.

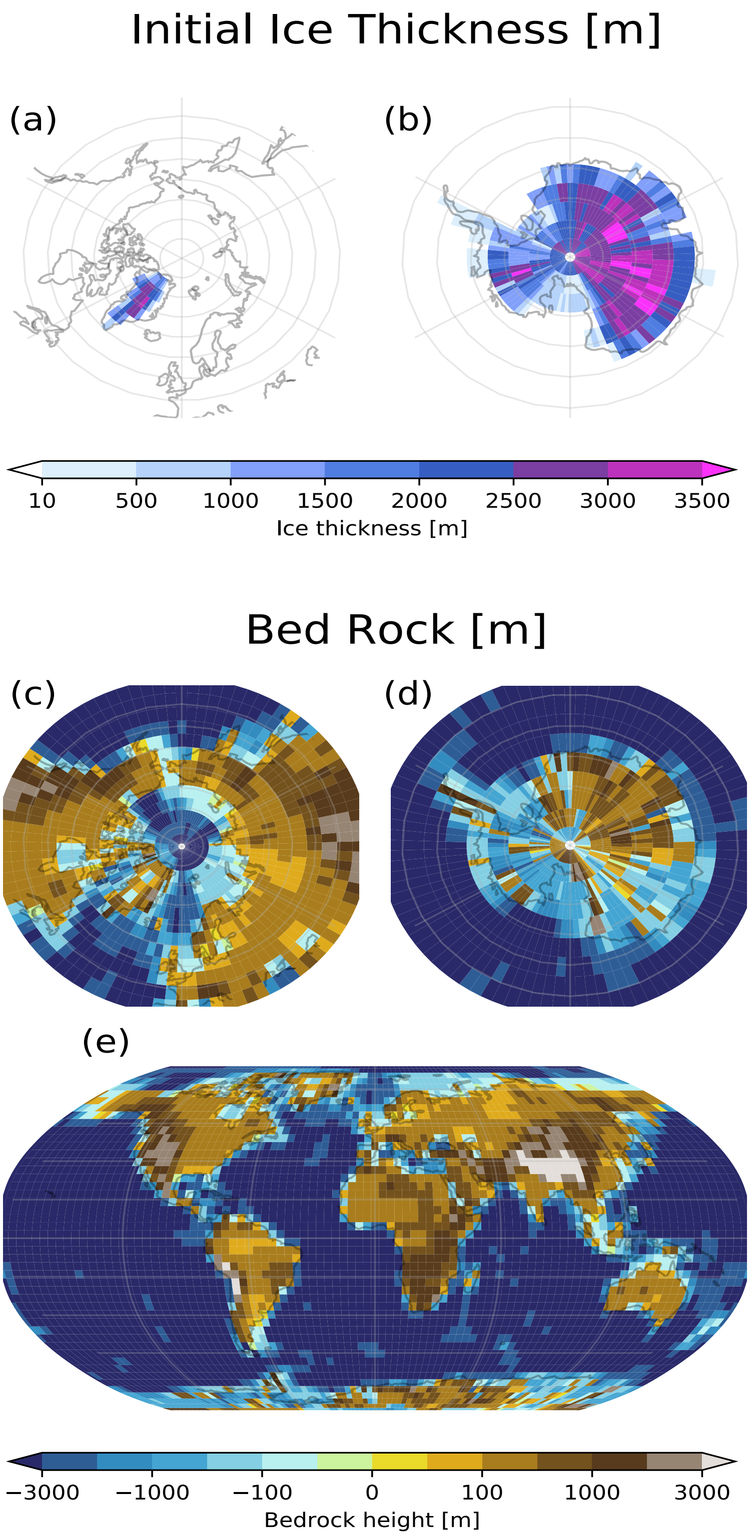

Figure 4.1 Initial ice thickness (a,b) and bed rock (c-e) in GREB-ISM. Ice thickness less than 10 m is not shown.

4.3 Model benchmark: Ice sheet model stand-alone simulations

We start our evaluation of the new ice sheet model GREB-ISM with stand-alone ice sheet model simulations forced with idealized or observed boundary conditions. These simulations focus on the ice sheet simulation only. Sections 4.3.1 and 4.3.2 use standard experiments from the European Ice Sheet Modelling Initiative (EISMINT) model intercomparison Phase I (Huybrechts et al., 1996) and II (Payne et al., 2000), which test the ice sheet model response to idealised mass and temperature forcing within a given horizontal resolution, with the ice mechanics decoupled from the thermodynamics in EISMINT I and coupled in EISMINT II. In section 4.3.3, we discuss a simulation on the global GREB-ISM grid forced with observed boundary conditions to estimate the dynamically-forced equilibrium of the ice sheet model. Finally, we discuss an idealised time-varying ice sheet response experiment, forced with temperature and precipitation similar to Niu et al., (2019) over the past 250 kyr.

4.3.1 EISMINT I

All simulations in EISMINT I (Huybrechts et al. 1996, H96 hereafter) are based on a regional grid in Cartesian coordinates that have higher resolutions than the GREB model grid (~50 km). For a better comparison of the numerical schemes we changed the GREB-ISM grid (3.75˚ x 3.75˚) for these experiments to a model grid with 96 points in the zonal and 144 points in the meridional direction (3.75˚ x 1.25˚). Only the first 15 points in the meridional direction are used for the ice sheet simulation. The ice sheet divide in these simulations is the south pole. The length of the meridional grid is not calculated based on Earth radius. Instead constant value of 50 km is used. The simulations are integrated for 200 kyr, but near equilibrium is reached after about 50 kyr.

The mass balance S and surface temperature T_{surf} forcings are given as:

Fixed margin experiment:
$$\begin{cases} S = 0.3\ \mathrm{m\,yr^{-1}} \\ T_{surf} = T_{min} + S_T d^3 \end{cases} \tag{4.1}$$

Moving margin experiment:
$$\begin{cases} S = \min\{S_{max}, S_b(R_{el} - d)\} \\ T_{surf} = (270\ \mathrm{K} - S_H H) \end{cases} \tag{4.2}$$

The parameters in equations (4.1)-(4.2) are listed in Table 4.1.

Table 4.1: Variables (upper) and parameters (below) list for EISMINT experiments.

variable name	symbol	unit
Distance from the divide	d	km
Ice thickness	H	m
Surface mass balance	S	m
Surface temperature	T_{surf}	K

			EISMINT I		EISMINT II		
Parameter	symbol	unit	fixed margin	Moving margin	experiment A	experiment B	experiment C
Melting distance	R_{el}	km	/	450	450	450	425
Mass balance gradient coefficient	S_b	$m\ yr^{-1}\ km^{-1}$	/	0.01	0.01	0.01	0.01
Surface temperaturer lapse rate	S_H	$K\ m^{-1}$	/	0.01	/	/	/
Surface mass balance	S_{max}	$m\ yr^{-1}$	/	0.5	0.5	0.5	0.25
Surface temperature gradient coefficient	S_T		$8 \times 10^{-8} K\ km^{-3}$	/	$1.67 \times 10^{-2}\ K\ km^{-1}$	$1.67 \times 10^{-2}\ K\ km^{-1}$	$1.67 \times 10^{-2}\ K\ km^{-1}$
Surface temperature miminum	T_{min}	K	239	/	238.15	233.15	238.15

Table 4.2 shows the comparison between the new ice sheet model GREB-ISM and model results from H96. The GREB-ISM simulations of the ice thickness at divide, and mass flux at midpoint are mostly similar to those found in H96 for both the fixed and moving margin experiments. The ice mass flux in the GREB-ISM is larger than in H96 for the moving margin experiment. An additional experiment (not shown) with the GREB-ISM in Cartesian coordinates as used in EISMINT I simulation finds the ice mass flux close to H96, suggesting this result may be mesh shape depending.

Table 4.2: EISMINT I steady state experiment result comparison between GREB-ISM and the model ensemble from H96 for fixed-margin (F) and moving-margin (M) experiments.

Experiment	ice thickness at divide m	Mass flux at midpoint 10^2 $\mathrm{m^2a^{-1}}$	Basal temperature at divide ^{o}C
EISMINT I (F)	3384.4 ± 39.4	794.99 ± 5.67	-8.97 ± 0.71
GREB-ISM (F)	3399.06	750.14	-11.74
EISMINT I (M)	2978.0 ± 19.3	999.38 ± 23.55	-13.34 ± 0.56
GREB-ISM (M)	2916.025	1234.40	-14.93

The transition experiments with oscillating forcing of temperature and mass balance with periods of 20 kyr and 40 kyr are presented in Fig 4.2. The GREB-ISM ice thickness simulation is similar to those of H96 for both fixed and moving margin experiments (Fig 4.2). In both experiments, the basal temperature at the divide is about one to two degrees colder than in the H96 simulations, which is related to the coarse vertical resolution. This mismatch disappears if we increase the vertical resolution to 10 layers (not shown).

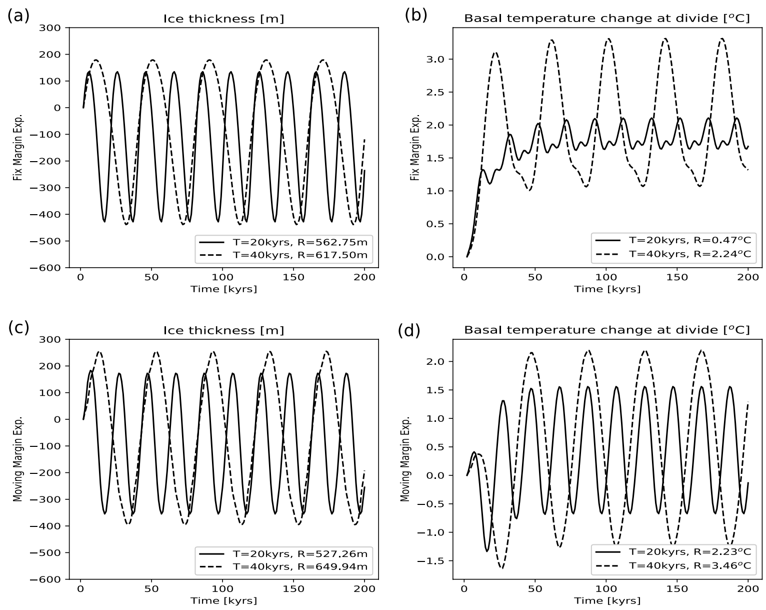

Figure 4.2 Time evolution of ice thickness (a, c, unit: m) and homologous basal temperature (b, d, unit: K) in the EISMINT I fixed (a, b) and moving (c, d) margin experiments with GREB-ISM with 20/40 kyr period forcing. R marks the range (maximum minus minimum in the last 50 kyr) of the simulated variables.

4.3.2 EISMINT II

EISMINT II experiments (Payne et al. 2000, P2000 here after) involve coupling between the mechanical and thermodynamical components of the ice sheet model. These experiments are designed to test how the ice sheet temperature variations interact with the ice sheet transport. The GREB-ISM model grid used is similar as in EISMINT I, but the number of points in the meridional direction is increased from 15 to 31 and the length of the meridional grid is set to 25 km. All experiments are integrated for 200 kyr. The boundary conditions for the first experiment (***A***) are:

$$\begin{cases} S = min\{S_{max}, S_b(R_{el} - d)\} \\ \mathrm{T_{surf}} = T_{min} + S_T d \end{cases} \tag{4.3}$$

with the parameters given in Table 4.1. The results of experiment A are summarised in Table 4.3.

Table 4.3: Results for basic glaciological quantities in EISMINT II experiments after 200 kyr. Differences are defined as current experiment minus experiment A. Percentage changes are relative to experiment A. The results of P2000 are shown in the form of "mean $\pm$ range". See text for details.

Model (Exp. label)	volume 10^6 km^3	area 10^6 km^3	Melt fraction	Divide thickness m	Divide basal temperature K
GREB-ISM (A)	2.065	0.932	0.466	3829.77	254.038
P2000	2.128 ±0.145	1.034 ±0.086	0.719 ±0.290	3688.342 ±96.740	255.605 ±2.929
Model (Exp. label)	**volume change %**	**area change %**	**Melt fraction change %**	**Divide thickness change %**	**Divide basal temperature difference K**
GREB-ISM (B)	-4.066	/	38.642	-5.821	4.576
P2000 (B)	-2.589 ±1.002	/	11.836 ±18.669	-4.927 ±1.316	4.623 ±0.518
GREB-ISM (C)	-25.907	-17.079	-100	-12.137	3.856
P2000 (C)	-28.505 ±1.204	-19.515 ±3.554	-27.806 ±31.371	-12.928 ±1.501	3.707 ±0.615

The final GREB-ISM values for ice volume, area, divide thickness and basal temperature at the ice sheet divide are all within the range of the models in P2000, indicating a fairly good agreement. The basal melt fraction is underestimated by the GREB-ISM by about 30%, which is related to a cold bias at the bed of the ice sheet.

Experiment B and C in EISMINT II are designed for testing the model sensitivity to various boundary conditions. $\mathrm{T_{min}}$ in experiment B is set as 5 K cooler than in experiment A, to evaluate the sensitivity of the model to the mean ice temperature. Table 4.3 depicts the difference between experiment B and A. The GREB-ISM shows, in general, similar changes in ice volume, ice divide thickness, and ice divide basal temperature as in P2000. However, the basal melt fraction change shows a significant discrepancy, which is related to the cold bias of the basal temperature in experiment A.

For experiment C, S_{max} and R_{el} are set as 0.25 m yr^{-1} and 425 km respectively to evaluate the impact of different mass balances. The results of experiment C are shown in Table 4.3. For the changes in ice volume, area, divide thickness and divide basal temperature, the response difference between Experiment C and A in GREB-ISM is equivalent to results from P2000. The changes in melt fraction in the GREB-ISM deviate from those of P2000, which is again likely to be related to the cold bias in basal temperatures in the GREB-ISM in experiment A.

Overall, the model reproduces the total ice thickness and ice cover well in the idealised experiments of EISMINT I and II. Although there is a bias in the basal temperature estimation in GREB-ISM, this issue does not have a significant impact on the ice thickness and cover area, which suggests the model is appropriate for global climate and ice evolution simulations.

4.3.3 Globally forced dynamical equilibrium

We now focus on simulating the observed global ice sheets forced with present-day boundary conditions. Although we cannot assume that observed Greenland and Antarctic Ice Sheets are in equilibrium with present day forcing, the dynamic equilibrium simulation should produce a global ice sheet distribution similar to the current observations.

Ice surface temperature and precipitation forcings in the experiment are set to the climatologies derived from ERA-interim, NCEP-DOE and GPCP data. GREB-ISM is run for 200 kyr, initialized with observed ice thickness. Figures 4.2-4.5 show results from this simulation and Table 4.4 compares the simulation values of total ice volume boundary calving with observed values from the literature. The model reaches an equilibrium after about 50 kyr for both the Northern and Southern Hemispheres. Greenland ice thicknesses and calving rates show only small differences compared with the initial values. They are also within the estimated calving values from observation (Bigg, 1999). The trends in Antarctica are larger, in particular over West Antarctica. Here we see a significant increase in ice volume and calving (Fig 4.3d and 4.5d). The West Antarctic ice sheet thickness increase is inconsistent with the observed values, suggesting a model limitation.

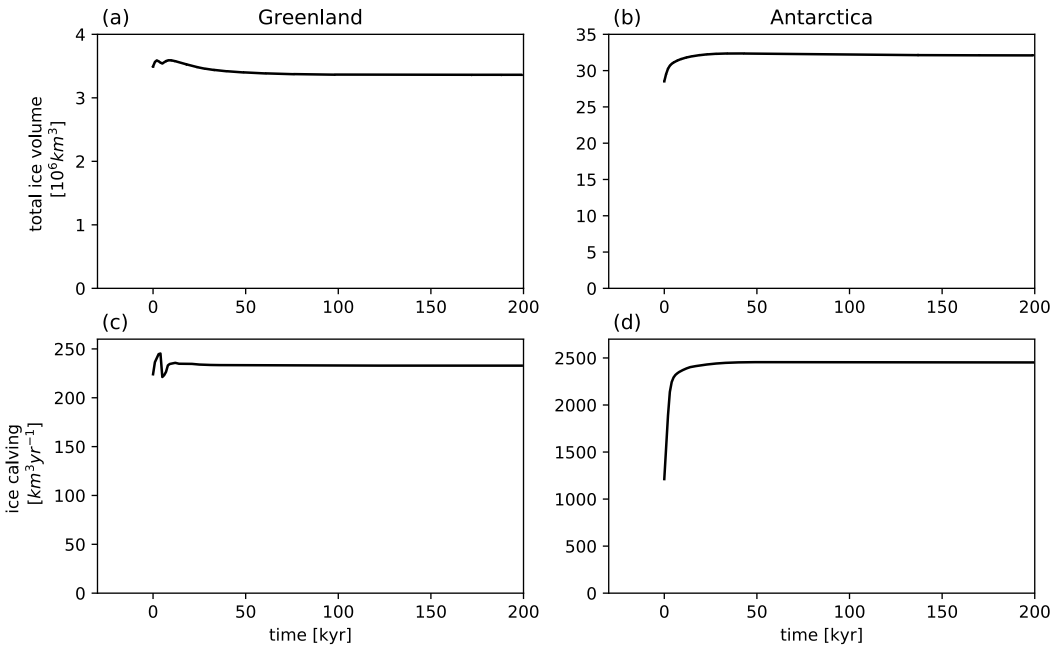

Figure 4.3 Time evolution of total ice volume (a, b, units: 10^6 km^3) and ice calving (c, d, units: km^3 yr^{-1}) in Greenland (a, c) and Antarctica (b, d) from the forced stand-alone dynamic equilibrium experiment.

Table 4.4: Ice volume and boundary calving from the forced dynamic equilibrium experiment and observation.

Experiment(region)	total ice volume $10^6 km^3$	boundary calving 10^{12} kg

Observation (Greenland)	2.83 (Greve, 1997) 3.12 (Morlighem et al., 2017, 2020)	170 - 270 (Bigg et al., 1999)
GREB ISM (Greenland)	3.36	211.91
Observation (Antarctica)	25.6 (Martin et al., 2011) 26.8 (Morlighem et al., 2017, 2020)	1781 $\pm$ 64 (Liu et al., 2015)
GREB ISM (Antarctica)	32.09	2231.69

We could not find the specific limitation that is causing West Antarctic Ice Sheet bias. The precipitation forcing does play a role in controlling the West Antarctic Ice Sheet, but we could not find any reasonable precipitation forcing that would result in significantly improved simulations of the West Antarctic Ice Sheet. The parameterization of the floating ice for ice shelves (SSA) also impacts the simulation of West Antarctic Ice Sheet. The ice shelf can grow and become grounded as an ice sheet with lower viscosity. However, again we could not find any reasonable value for the ice viscosity (η_{SSA}) that would significantly reduce this bias. We further tested different sliding law coefficient C_{sl}, ranging from $6x10^3$ yr^{-1} to $6x10^5$ yr^{-1}. The result indicates that the varying coefficient values do not bring a fundamental simulation improvement. Similarly, a basal melting scheme (Martin et al., 2011) with different strength has also been tested, but improvement could not be found.

The simulated ice surface velocity for Antarctica and Greenland shows a reasonable pattern, capturing the main features of the transport (Fig 4.4) and the mean values. For Antarctica the ice mean flow is 109 m/yr, faster than the observation (80 m/yr) from MEaSUREs data (Mouginot et al., 2012; Rignot et al., 2011, 2017), and slower in the interior and faster near the boundaries. The largest velocities (more than 1000 m yr^{-1}) appear in ice shelf regions (Ross and Filchner-Ronne Ice Shelf), which is due to the presence of the floating ice for ice shelves (SSA). Similarly, Greenland ice velocities are also in good agreement with observations (Joughin, 2017; Joughin et al., 2010) in terms of pattern and mean flow magnitude (57 m/yr simulated and 56 m/yr observed).

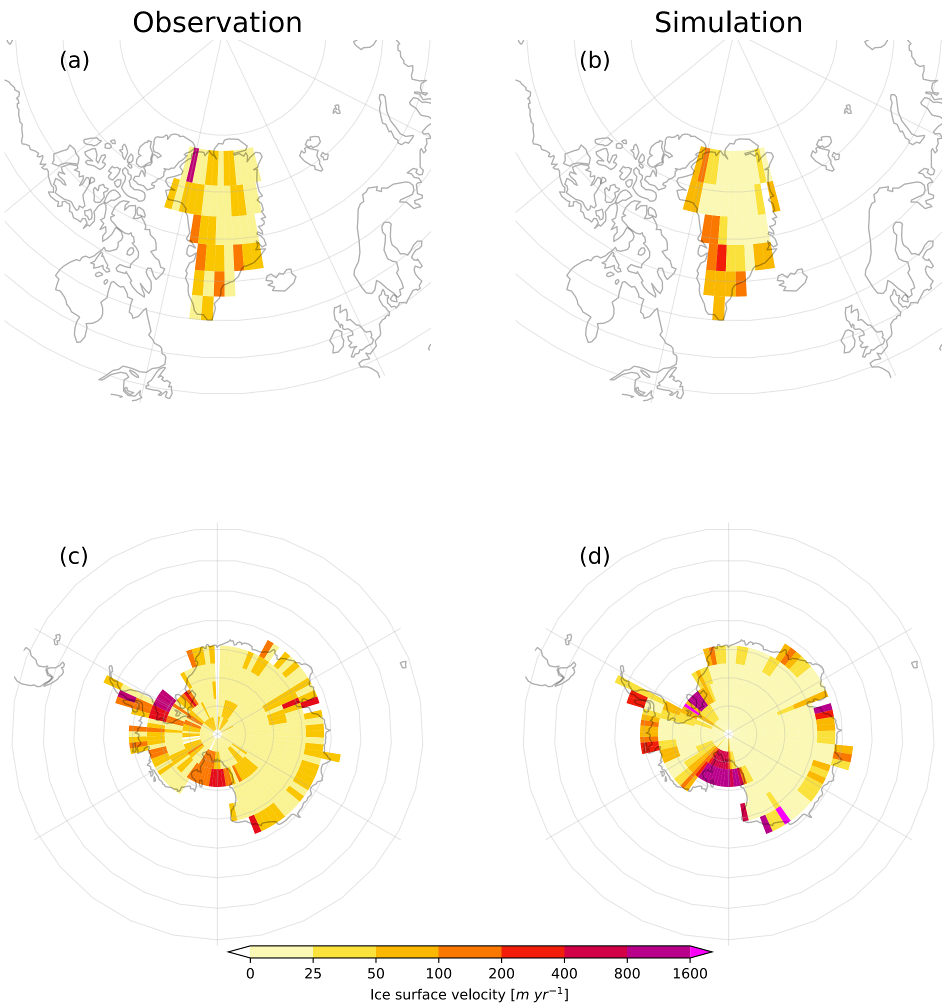

Figure 4.4 Comparison of ice surface velocity (unit: m yr^{-1}) from observations (left) and the GREB-ISM forced stand-alone dynamic equilibrium experiment at equilibrium state (right).

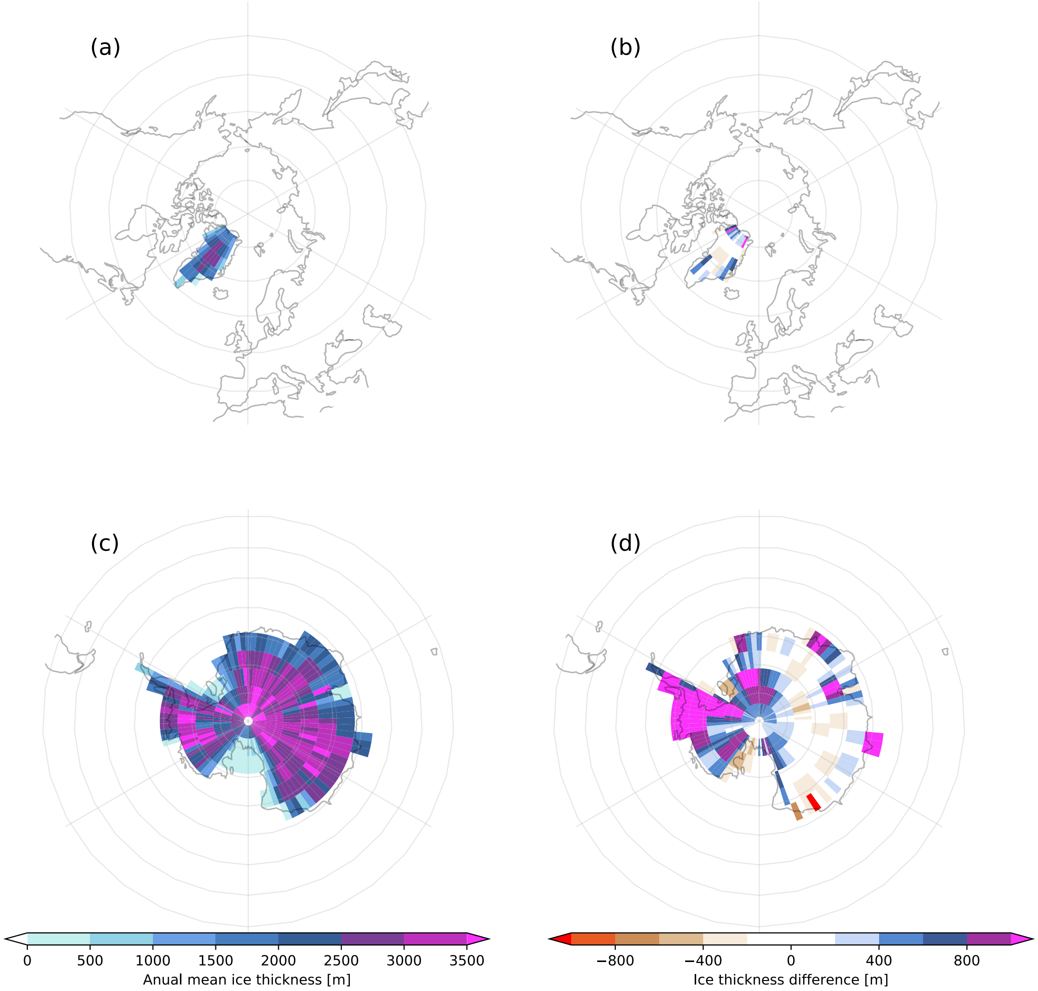

Figure 4.5 Results from the GREB-ISM forced stand-alone dynamic equilibrium simulation at equilibrium state: Annual mean ice thickness (a, c) and the ice thickness difference (b, d) between GREB-ISM simulation and the observation in Greenland (a, b) and Antarctica (c, d). The ice thickness observation is derived from Bedmachine dataset (Morlighem et al., 2017, 2020).

4.3.4 Transition experiment

We next evaluate the capability of the global ice sheet model to respond to realistic changes in the boundary conditions. We therefore design an experiment, in which we force the GREB-ISM with surface temperature and precipitation forcing over the past 250 kyr, similar to the one discussed in

Niu et al., (2019) for the North Hemisphere, but extend to the whole globe to evaluate the response of the ice sheet on a global scale. The surface temperature and precipitation forcing for this experiment are:

$$\begin{cases} \mathrm{T_{surf}}(\lambda, \phi, \mathrm{t}) = \mathrm{T_{today}}(\lambda, \phi, t_{day}) + (\mathrm{T_{LGM}}(\lambda, \phi, t_{day}) - \mathrm{T_{today}}(\lambda, \phi, t_{day}))\frac{\delta^{18}O(t)-\delta^{18}O_{PD}}{\delta^{18}O_{LGM}-\delta^{18}O_{PD}} \\ S(\lambda, \phi, \mathrm{t}) = \min\left[\mathrm{S_{today}}(\lambda, \phi, t_{day}) + (\mathrm{S_{LGM}}(\lambda, \phi, t_{day}) - \mathrm{S_{today}}(\lambda, \phi, t_{day}))\frac{\delta^{18}O(t)-\delta^{18}O_{PD}}{\delta^{18}O_{LGM}-\delta^{18}O_{PD}}, 0\right] \end{cases} \tag{4.4}$$

The surface temperature ($\mathrm{T_{surf}}$) and ice mass balance (S) are present-day regional and seasonally varying climatologies ($\mathrm{T_{today}}$, $\mathrm{S_{today}}$) plus a seasonally changing (t_{day}) forcing pattern for $\mathrm{T_{surf}}$ and S that varies according to $\delta^{18}O$ proxy data derived from the Greenland Ice Core Project (GRIP) dataset (Greve, 1997). $\delta^{18}O_{PD}$ and $\delta^{18}O_{LGM}$ represent $\delta^{18}O$ at present day and Last glacial Maximum (LGM) respectively. The LGM reference climate forcing pattern $\mathrm{T_{LGM}}(\lambda, \phi, t_{day})$ is taken from the AWI Earth System Model (AWI-ESM), which results from a CGCM simulation forced by insolation, greenhouse gas and ice sheet. The main feature of this forcing pattern (not shown) is a much colder climate (more than 10 ºC) from North America to Central Asia and Antarctica, where large ice sheet developed or surrounded (Kageyama et al., 2017). The simulation is integrated between -250 kyr to present and initialized with present-day observed ice thickness. We are trying to test the model with idealized simulation, so the external forcing data is roughly chosen, which is one of limitation for our experiment.

The time series in Fig 4.6 depicts the sea level change in this simulation from -200 kyr BP compared with a $\delta^{18}O$ proxy timeseries from ocean sediments (Imbrie et al., 1984). The two curves show similar time series variations with a correlation of -0.67. This indicates that qualitatively the GREB-ISM ice sheet shows similar overall global ice sheet variations to those observed over the past 200 kyr. The GREB-ISM sea level varies by about 120 m, which is exact observations suggested sea level changes (Fairbanks, 1989; Lambeck et al., 2014), indicating that the simulated ice sheet volume variations are similar to the observed. The sea level is also 20 m lower than present day due to the excess West Antarctic Ice Sheet volume that we also observed in the dynamical equilibrium simulation.

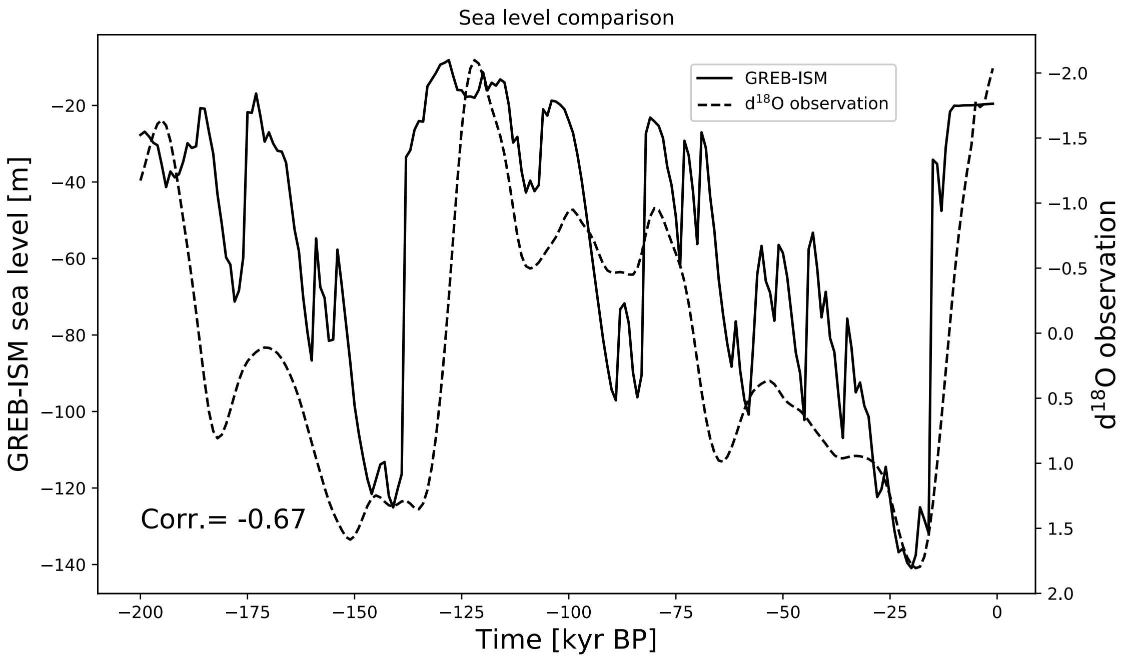

Figure 4.6 Time series of simulated sea level (left axis; units: m) from the stand-alone transition experiment and $d^{18}O$ proxy data (right axis, the axis has been inverted).

There are several significant extremes in the past 200 kyr simulation, which correspond to the Last Interglacial (LIG; -127 kyr), Last Glacial Maximum (LGM; -21 kyr) and present day. The ice sheet thicknesses for these three time periods are shown in Fig 4.7. During the LIG, only the Greenland Ice Sheet thickness exceeded 400 m in the Northern Hemisphere and the Antarctic Ice Sheet thickness is similar to present day. During the LGM large European (e.g. Fennoscandia) and North American (Laurentide) ice sheets are reproduced with thousands of meters ice thickness, which is also what we expected according to previous studies (Clark et al., 2009; Velichko et al., 1997). However, the ice sheets cannot extend over the main European continent, probably because some relevant processes missed in our simulation, such as atmospheric or oceanic circulation, which is one limitation for the model in current version.

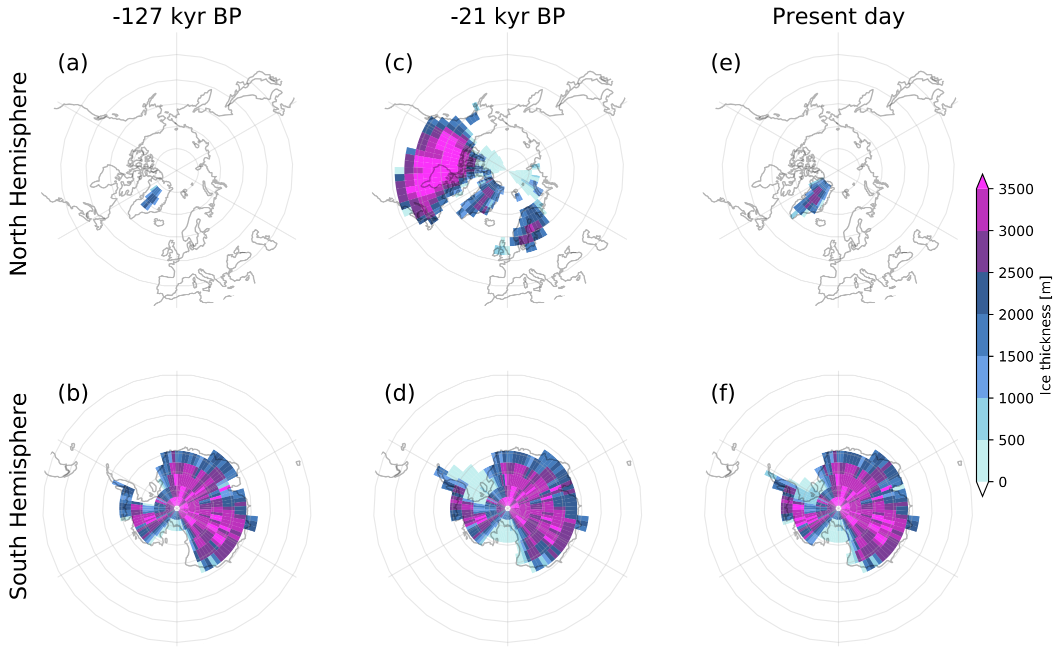

Figure 4.7 Global ice thickness (unit: m) distribution in the Last Interglacial (left), the Last Glacial Maximum (middle) and present day (right) from the stand-alone transition experiment.

The estimate of ice sheet volume in Greenland and Antarctica for the Last Interglacial, Last Glacial Maximum and Late Holocene from GREB-ISM and from Fyke et al., (2011) are presented in Table 4.5. Overall, our simulation of the Greenland Ice Sheet is similar to Fyke et al., (2011) but with larger time variations. However, the simulation of Antarctica ice thickness shows very little to no variations between these three periods. The difference between the GREB-ISM model and Fyke et al., (2011) in Antarctica ice sheet may be due to different experimental setup. Fyke et al., (2011) varied and changed the ice shelf parameterization periods during their simulation, which was not done in our experiments. In summary, the results of this experiment indicate that the GREB-ISM ice sheet model does have realistic responses to time varying boundary conditions.

Table 4.5: Annual mean ice volume in the stand-alone transition experiment for different time periods from GREB-ISM simulation and from Fyke et al. (2011).

Scenario	GREB-ISM Greenland 10^6 km^3	Fyke et al. (2011) Greenland 10^6 km^3	GREB-ISM Antarctica 10^6 km^3	Fyke et al. (2011) Antarctica 10^6 km^3
LIG	1.04	2.19	29.97	31.2
LGM	5.47	3.69	31.28	40.4
Late Holocene	3.40	3.47	32.52	30.9

4.4 Model benchmark: GREB-ISM coupled simulations

We now focus on the fully coupled GREB-ISM model, in which the ice sheet and other climate variables are interacting in both directions. In the following sections, two sets of experiments are presented. First a dynamic equilibrium experiment is conducted, which is similar to the experiment discussed in Section 4.3.3, but now fully coupled with fixed boundary conditions. Second, a set of experiments with shortwave radiation oscillating on periods of 20 kyr, 50 kyr and 100 kyr for the Northern Hemisphere are conducted, to mimic time scale of Milanković cycle. Those two experiments are designed to evaluate how coupling influences the model's behaviour and to what extent the ice sheet responds to periodic solar forcing. The discussion of these experiments will focus on the introduction of the GREB-ISM model. A more detailed analysis of the ice sheet dynamics coupled with climate dynamics is left for future studies.

4.4.1 Dynamic equilibrium for present day conditions

In this experiment, the GREB-ISM model is fully coupled and forced with the fixed boundary conditions of present-day 340 ppm CO_2 concentration and solar radiation. T_{surf} and land precipitation are flux corrected to the mean present-day values. However, those flux corrected variables can respond to changes in the climate system, since the flux correction terms are state-independent (see Section 1.3). The simulation is 200 kyr long and results are shown in Fig 4.8 and 4.9.

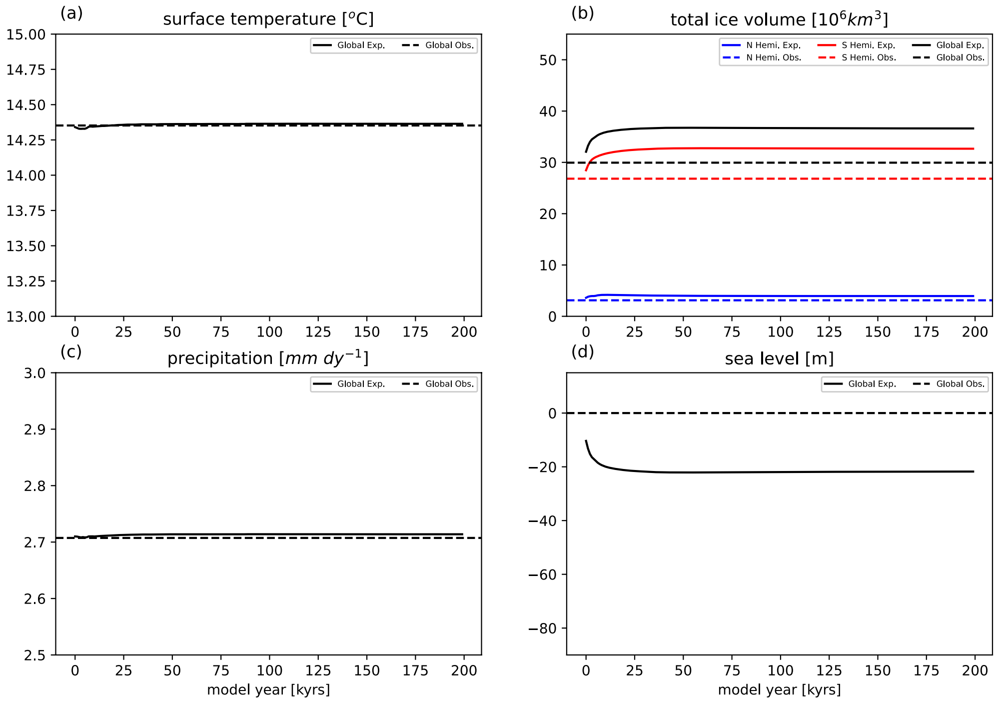

Figure 4.8 Results from the fully coupled dynamic equilibrium experiment: Evolution of global annual mean surface temperature (a, units: $^{\text{o}}$C), total ice volume (b, units: 10^6 km^3), annual mean precipitation (c, units: mm dy^{-1}) and sea level change (d, units: m). The dash line are modern observation references.

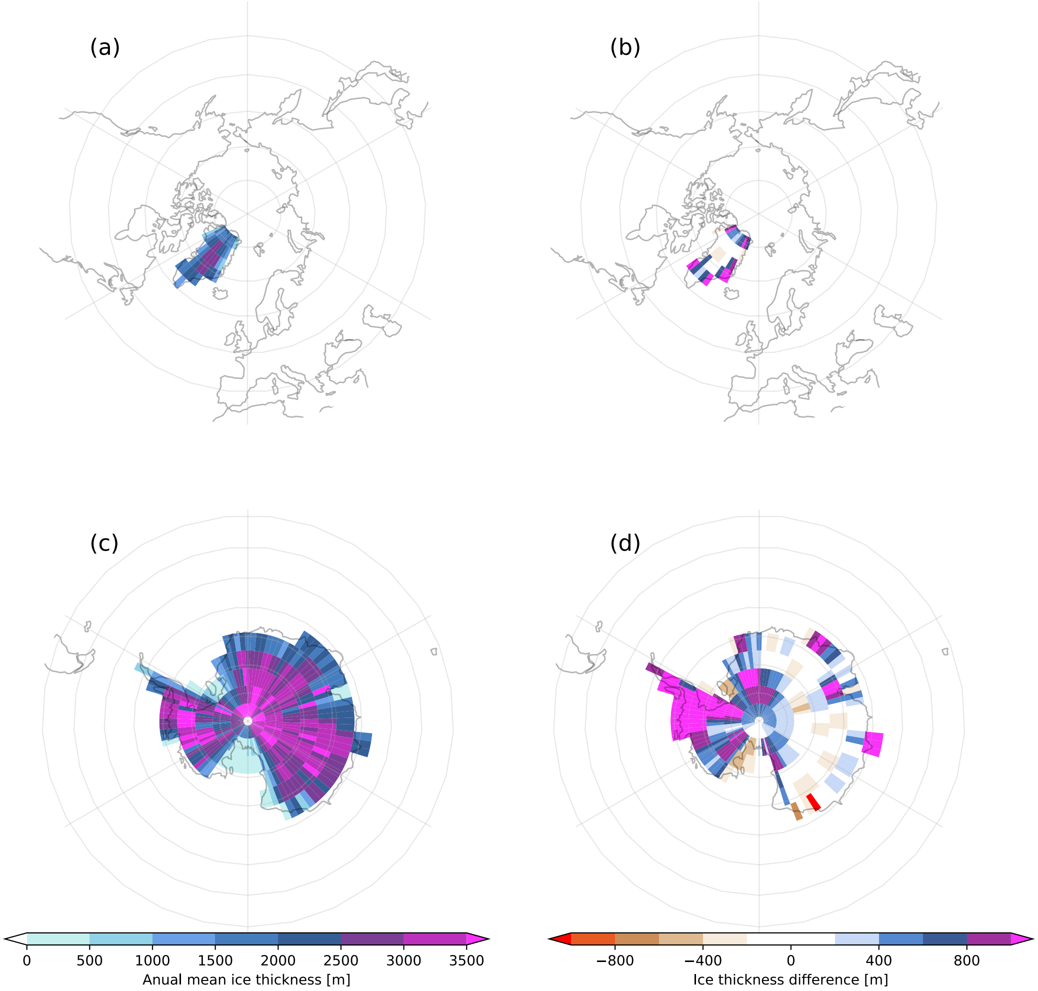

Figure 4.9 Same as Fig 4.5 but for the coupled dynamic equilibrium experiment.

T_{surf} and precipitation show no long-term drift and are close to the observation (Fig 4.8a, c). Both reach equilibrium after about 50 kyr. The global ice volume difference is mainly contributed by ice thickness difference in Southern Hemisphere (Fig 4.8b), which is similar to the one in the forced experiment discussed in section 4.3.3 (Figs 4.3 and 4.5). As the ice volume increases, the sea level shows a clear decrease tendency and reach equilibrium after 50 kyr as well. The ice thickness spatial pattern in coupled experiment is comparable to the stand-alone experiment (Figs 4.7 and 4.5). Overall, this control run simulation shows that the coupled GREB-ISM system converges towards an equilibrium state close to the observed one. The simulated trends appear to be mostly due to the anomalous growth of the West Antarctic Ice Sheet.

4.4.2 Shortwave radiation oscillation experiment

In the following experiments we use the same set up as in the previous section, but allow the Northern Hemisphere shortwave radiation, sw, to oscillate, taking the form:

$$\mathrm{sw(t)} = \left(1 + \mathrm{A}_{sw} \cdot \sin\left(2\pi \frac{\mathrm{t}}{\mathrm{pd}}\right)\right) \cdot \mathrm{sw}_{\mathrm{present}} \tag{4.5}$$

where A_{sw} is the amplitude of the *sw* oscillations, which increases from 0 at 13° N to 0.1 at 35° N and maintains 0.1 northward of 35° N. The oscillation period, *pd*, is set to 20 kyr, 50 kyr and 100 kyr in three individual simulations. The *sw* oscillation is relative to the present-day solar radiation, $\mathrm{sw}_{\mathrm{present}}$. The shortwave maximum amplitude is about 20 W m^{-2} at 65° N in the annual mean (Fig 4.10a-c) and varies with latitudes and seasons (not shown). The 20 kyr, 50 kyr and 100 kyr oscillation periods are simulated for 210, 325 and 350 kyr. The time series for selected climate variables are shown in Fig 4.10. The results are shown in reference to the final year of the control run, which is the coupled dynamical equilibrium simulation in section 4.3.3.

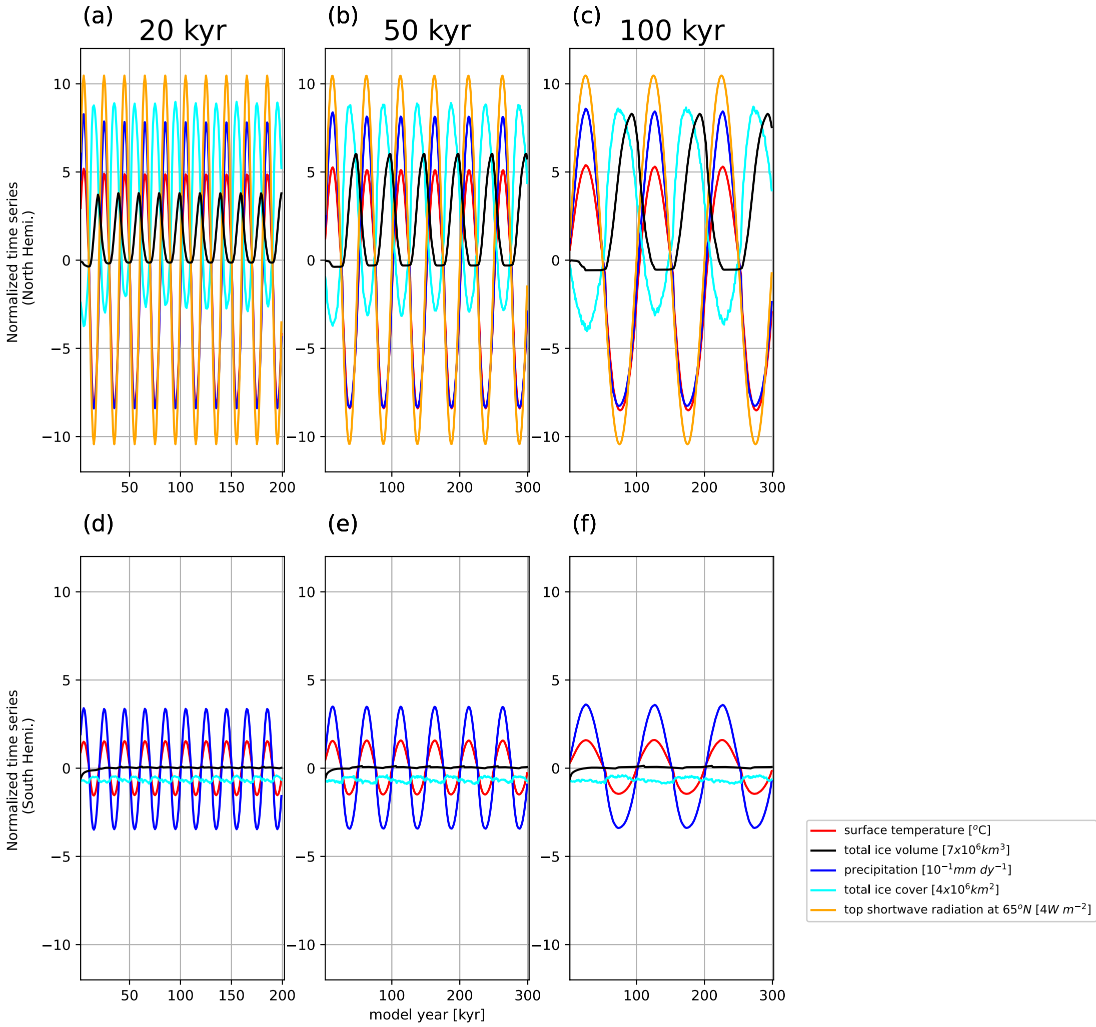

Figure 4.10 Time evolution of change in total ice volume (black, unit: $7 \times 10^6 \mathrm{km}^3$), surface temperature (red, unit: $^{\mathrm{o}}\mathrm{C}$), precipitation (blue, unit: $10^{-1}\mathrm{mm\ dy}^{-1}$), ice cover area (cyan, unit: $4 \times 10^6 \mathrm{km}^2$) and solar radiation at 65 $^{\mathrm{o}}$N (orange, unit: $4\mathrm{W\ m}^{-2}$) from the shortwave oscillation experiment in North (upper) and South (lower) Hemisphere with forcing period of 20 kyr (left), 50 kyr (middle) and 100 kyr (right). The control equilibrium state values from the coupled dynamic equilibrium experiment are removed to obtain changes.

To illustrate ice form and retreat in one cycle, we show results from the last forcing cycle of each simulation in Figs. 4.10-4.13. Starting with the 20 kyr oscillation run, there are a number of interesting aspects to point out (Figs 4.10a, d, 4.11a, d and 4.13a-d). First, at the initial half cycle, the ice volume is slightly lower than the reference state, indicating a warming period leads to deglaciation (Figs 4.10a-c). Then, after the second cycle, the ice volume is always larger than in the control simulation and the cycles are very similar to each other. If we focus on the last cycle of the simulations (Figs 4.11-4.13), we note that T_{surf} and precipitation are mostly in phase with each other and with the shortwave radiation forcing. The Northern Hemispheric T_{surf} oscillation amplitude is about +/- 6 ºC and the mean value is clearly below zero (the control run value). This is despite the fact that the mean shortwave radiation is the same as in the control run. This suggests that the oscillating shortwave radiation has a mean cooling effect. This overall cooling is related to the overall increase in the mean ice sheet volume and extent.

It is beyond this study to fully explore how this effect arises, but it is likely to be related to the ice-albedo effect. In the control run the Northern Hemispheric summer mean ice cover is nearly zero, and with increasing SW forcing, does not decrease much further. However, it can increase substantially for decreased SW forcing, leading to a mean ice cover in the oscillation run that is much larger than in the control. Subsequently, the Northern Hemispheric albedo is also much higher than in the control leading to a cooler Northern Hemispheric T_{surf}.

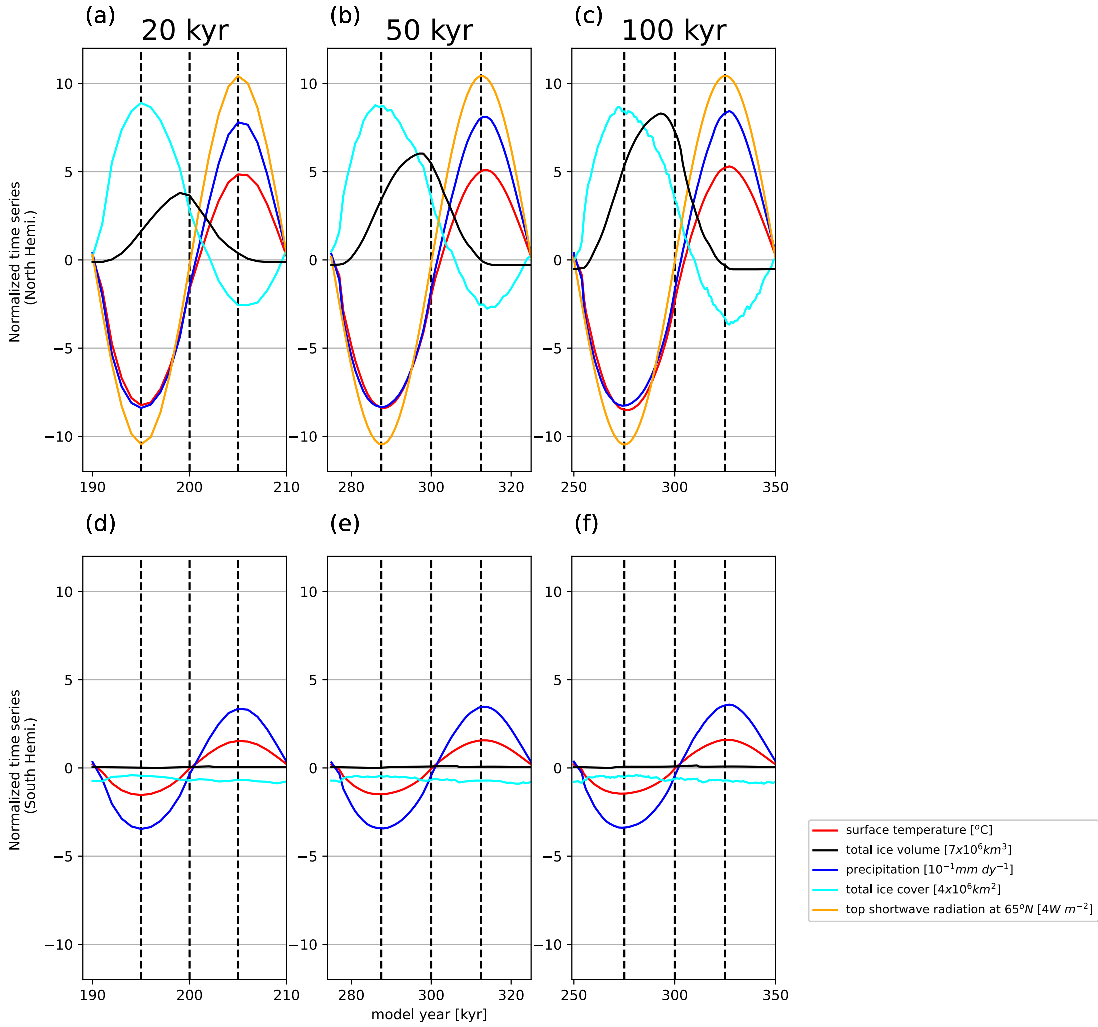

Figure 4.11 Same as Fig 4.10 but only for the last cycle of each run. The vertical dash lines represent the solar forcing sine function phases of -90^o, 0^o and 90^o.

The ice sheet response to the 20 kyr shortwave oscillation has a number of interesting aspects. As mentioned above, the mean ice sheet volume is larger than in the control run. Indeed, it is never smaller than in the control run, not even at the minimum (compare Fig 4.10a and 4.11a), with the exception of the first cycle. Ice covered regions and ice volume are out of phase. The ice-covered regions (including land snow and sea ice) grow first and are nearly 180° out-of-phase with the *sw* forcing. The ice sheet volume lags behind the ice-covered area and reaches its maximum nearly 90° (a quarter cycle) after the minimum in shortwave radiation (Fig 4.11a). This illustrates that the ice sheets have not had enough time to equilibrate with the *sw* forcing. Further, we can notice that the ice sheet growth and decay is asymmetric, with a slower build up and faster decay in ice volume, with the reverse pattern in ice sheet area. In the build-up phase the ice sheet extends over large regions at lower latitudes but has relatively thin ice (Fig 4.12b). In the decaying phase the ice sheets retreat to higher latitudes and the ice sheet is relatively thick (Fig 4.12d).

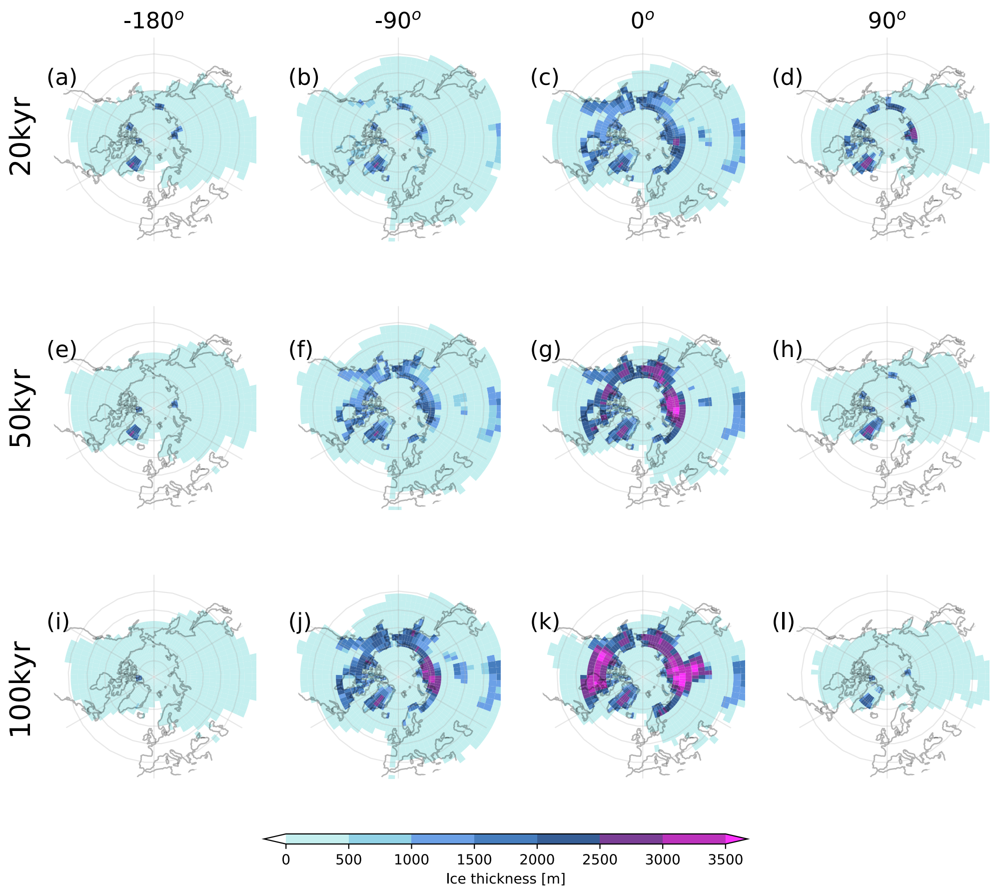

Figure 4.12 Ice thickness (unit: m) distribution in four phases for the forcing periods of 20 kyr (upper), 50 kyr (middle) and 100 kyr (lower) from the last cycle of the shortwave oscillation experiment. The corresponding -180^{o}, -90^{o}, 0^{o} and 90^{o} phase of the solar forcing phases are marked in the headings.

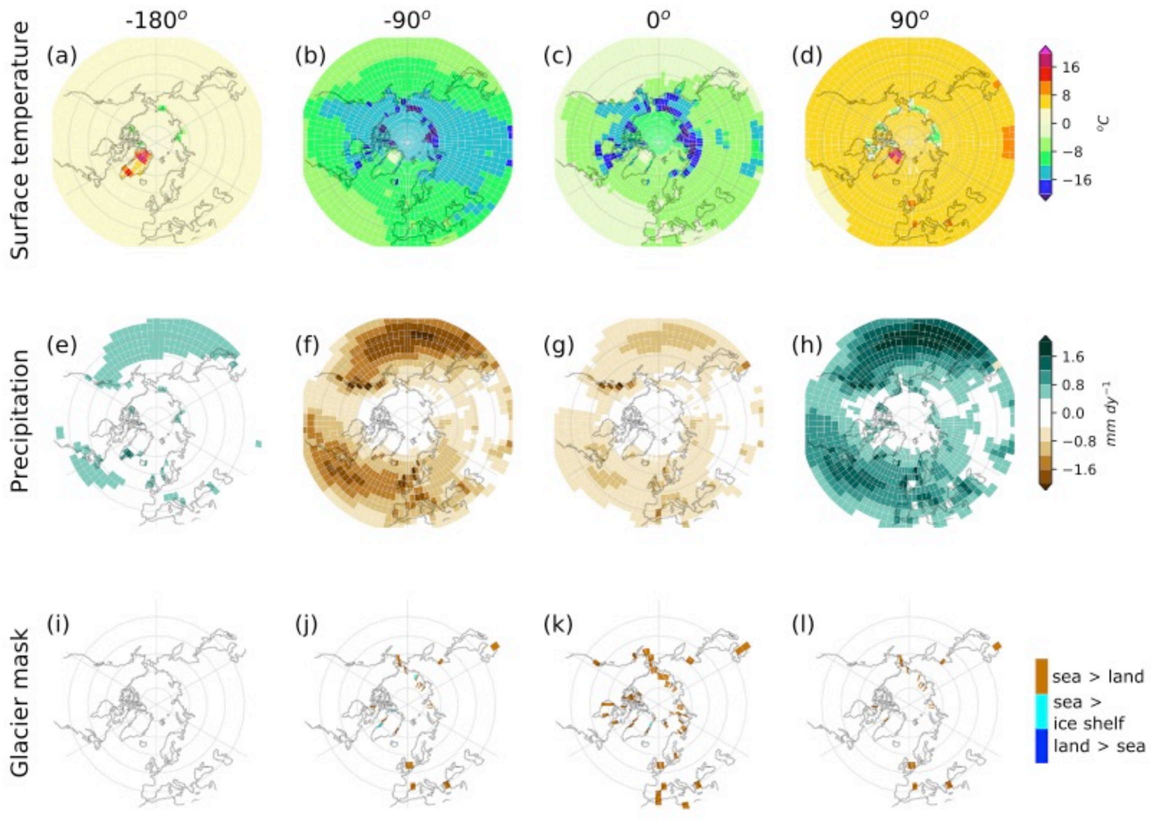

Figure 4.13 Surface temperature anomalies (upper; unit: °C), precipitation anomalies (middle; unit:mm dy^{-1}) and glacier mask change (lower; brown, cyan and blue represent from ocean to land, from ocean to ice shelf and from land to ocean respectively) in four phases during the last cycle of the 20 kyr shortwave oscillation experiment. The equilibrium state from coupled dynamic equilibrium experiment is removed to obtain anomalies. The corresponding -180^{o}, -90^{o}, 0^{o} and 90^{o} phase of the solar forcing phases are marked in the headings.

The Northern Hemispheric *sw* forcing also leads to a response in the Southern Hemisphere climate (Fig 4.11d). This is mainly due to the GREB-ISM atmospheric heat and moisture transport. It is also partly due to the change in global sea level induced by the Northern Hemispheric ice sheet changes. The Southern Hemisphere ice sheet changes are in-phase with the Northern Hemisphere climate. It is further noted that the amplitude of the Southern Hemisphere precipitation response relative to T_{surf} is bigger than in the Northern Hemisphere (compare Fig 4.11a and d; given the same scaling factors). This suggests that the moisture transport is more affected by the Northern Hemispheric climate change than the heat transport.

The longer 50 kyr and 100 kyr period runs show a number of changes relative to the 20 kyr run. First, the ice sheet volume amplitudes increase relative to the 20 kyr run, illustrating that the ice sheets are more sensitive to longer time period forcings (Fig 4.11a-c). Second, we see a shift of the maximum ice volume closer to the phase of the minimum of the *sw* forcing, suggesting that the ice sheets become closer to equilibrium with longer period *sw* forcing. However, even the 100 kyr oscillation run still shows a significant delay in the ice sheet volume extrema relative to the forcing extrema, indicating that the ice sheets are not yet in equilibrium with the forcings. This illustrates that the intrinsic time scales of the Northern Hemispheric ice sheets are longer than 100 kyr. It is further interesting to note that the ice sheets can extend over shallow oceanic regions, like the Hudson Bay, Bering Strait or Artic Sea in the Siberian sector (Fig 4.12g, k), but at the same time do not extend into deep ocean regions (compare Fig 4.1c with Fig 4.12g, k).

The increase in ice thickness response for the longer 50 kyr and 100 kyr period runs has, however, little impact on the amplitudes of the T_{surf}, precipitation and ice cover response in the Northern Hemisphere, which also occurs in the Southern Hemisphere (Fig 4.11e and f). For ice sheet in the Southern Hemisphere, the ice thickness is almost keeping constant, which indicates the Antarctica Ice Sheet in the GREB-ISM is not very sensitive to the solar forcing in Northern Hemisphere.

4.5 Summary and discussion

We evaluated the performance of the stand-alone ice sheet model in a series of idealized and realistic ice sheet model simulations. We conducted simulations following the EISMINT I and II idealized experiments and found that the GREB-ISM ice sheet model performs similarly to other models with some limitations in the simulation of internal ice temperature. In simulations with realistic climate forcing close to present-day, we found that the equilibrium Greenland and most of the East Antarctic ice thickness distribution is very similar to observed, but the West Antarctic Ice Sheet gains too much ice. The overall surface ice velocities and associated calving rates of this model are similar to those observed for both Greenland and East Antarctica.

We investigated the West Antarctic Ice Sheet thickness bias, by evaluating whether uncertainties in precipitation and the parameterisation of the ice shelf dynamics (basal melting and viscosity) could cause this bias. However, we found that this bias is unlikely to be caused by these limitations alone and it is likely to also result from other, so far unknown, limitations in the GREB-ISM model. A possible explanation could be the complexity of the topography and land-sea distribution of West Antarctica and Antarctic Peninsula, which is not well resolved in the current model resolution. So, the coarse grid resolution of this model is likely to play a role in this limitation (Cuzzone et al., 2019).

A time dependent-simulation with simplified surface temperature and precipitation forcing of the past 250 kyr illustrated that the GREB-ISM model can produce a realistic ice sheet response for Greenland, North American and Fennoscandian ice sheets, together with sea level variability. The results for the Antarctic Ice Sheet are less conclusive, but may be due to the simplified setup of the experiment.

We further conducted a series of coupled GREB-ISM simulations to evaluate the full interaction of all climate elements in the model. The coupled model simulations produce global equilibrium ice sheets and calving rates very similar to observed for present-day boundary conditions. Much of this success in creating a realistic global ice sheet is related to the fact that the GREB-ISM model works with flux correction of surface temperature and land precipitation. This leads to realistic mass balance estimates for the ice sheets even in a fully interactive coupled simulation.

When forced with idealized, oscillating solar radiation forcing on the Northern Hemisphere with different oscillation periods (20 kyr, 50 kyr and 100 kyr) the model responds with growth of large continental ice sheets and clear interactions with the climate system in the Northern and Southern Hemispheres. The simulations illustrated asymmetries in the build-up and decay of large ice sheets in response to periodic forcing, showing that the ice sheets are more sensitive to longer time scales forcings. These experiments illustrate the potential of this model for exploring such interactions in future studies.

Chapter 5 Climate – ice sheet feedback

5.1 Introduction

Ice sheets comprise an essential part of the Earth system and have a great impact on the paleoclimate (Kageyama et al., 2018). Ice sheets interact with the climate system through a series of feedbacks.

One of the most important feedback is the ice-albedo feedback. The formation and retreat of ice sheets significantly alters the surface albedo. In most of cases, snow/ice sheet surface albedo can reach more than 0.45 (Ryan et al., 2019), which is much higher than the global mean albedo of 0.3. As a result, adjacent surface temperature drops due to decreased absorption of shortwave radiation, leading to more snow-covered regions (Gardner and Sharp, 2010). Since the snow and ice albedo is much higher than those of land and ocean surface and is tightly related to the surface temperature change (Gardner and Sharp, 2010; Ryan et al., 2019; Zeitz et al., 2021), the albedo feedback is usually regarded as a most essential process influencing the climate change in ice age cycles (Budyko, 1969; Felzer et al., 1996; Fyke et al., 2018; Petit et al., 1999).

Additionally, ice sheets take effect within the climate system through modifying the surface topography, so called topography feedback. The topography feedback is a nonlinear one because it influences the snowfall rate and surface temperature simultaneously (Edwards et al., 2014; Hakuba et al., 2012). As an ice sheet grows, the elevated surface height lowers the surface temperature due to the lapse rate in the troposphere (Abe-Ouchi et al., 2007; Fyke et al., 2018). Meanwhile, the low surface temperature and short air column due to surface lifting reduces the snowfall rate (Kapsch et al., 2021). Of course, the large topography created by massive ice sheets also has a considerable influence on the general circulation by atmospheric processes like stationary wave (Felzer et al., 1996; Hakuba et al., 2012; Herrington and Poulsen, 2012). In paleoclimate simulation, those processes are believed to be connected with the temperature and precipitation change (Abe-Ouchi et al., 2007;

Hakuba et al., 2012), deglaciation (Abe-Ouchi et al., 2013; Kapsch et al., 2021) and hysteresis of equilibrium states (Abe-Ouchi et al., 2013).

Apart from albedo and topography feedbacks, the ice latent heat effect is also a critical feedback. When ice melts into water, the fusion process needs to consume a large amount of energy, which is the ice latent heat. By fixing surface temperatures as frozen temperature, the ice latent heat has a significant impact on surface thermodynamics (Hock, 2005). Meanwhile, the surface energy balance is impacted by the change in climatic state, which in turn affects the ice melting process (Ebrahimi and Marshall, 2016; Patel et al., 2021). In particular, the ice latent heat, as a medium between ice thickness and surface energy balance, is able to aggregate the signal from various seasons and thus exhibit a seasonal inertial effect. For instance, if there is additional snowfall accumulation that cannot be completely melted away before or during the summer, the seasonal evolution of surface albedo will change (Marshall and Miller, 2020). This seasonal inertial effect is also included in the ice latent heat feedback discussion.

As an important source of ice sheet surface mass balance, snowfall rate change is very critical, especially during the cold period. The precipitation feedback is frequently tied with the topography feedback. For example, a negative feedback mechanism is the decrease in precipitation owing to surface temperature drop, caused by the raised surface height of ice sheets (Fyke et al., 2018; Medley and Thomas, 2019). Another process links precipitation intensity to mountain slope, because steep topographical changes typically result in heavy precipitation (Fyke et al., 2018; Hakuba et al., 2012). Last but not least, changes in circulation owing to ice sheet topography are also thought to be related to changes in precipitation during the ice age cycle (Löfverström and Liakka, 2016).

The total ice volume on Earth during the paleoclimate is intimately tied to global sea level change, which in turn affects climate via changing land-sea distribution. Owing to absence of global coupled ice sheet model, the sea level is usually taken as external forcing in paleoclimate simulation (Pollard and DeConto, 2009; Tigchelaar et al., 2019). Actually, most of sea level change during the late Quaternary can be attributed to the Northern Hemisphere ice sheets change (Bentley, 1999). In addition, the sea level feedback is usually considered as an important feedback for ice shelf around

Antarctica Ice Sheet because the sea level change potentially causes the Marine Ice Sheet Instability (Schoof, 2007a). As a result, the sea level feedback discussion usually focused on how sea level change caused by the Northern Hemisphere Ice Sheet impact the Antarctica Ice Sheet (Gomez et al., 2020; Maris et al., 2015; Tigchelaar et al., 2019).

Of course, many other feedbacks are related to the climate-ice sheet interaction. Pollard et al. (2015) pointed out that Antarctic Ice Sheet potentially retreated because of hydrofracturing and ice cliff failure, caused by the ice shelf basal melting. And both Abe-Ouchi et al. (2013) and Han et al. (2021) suggested the feedbacks associated with the solid Earth deformation takes effect during the ice sheet evolution. Moreover, Willeit and Ganopolski (2018) discussed the strong influence from surface albedo, and concluded that the existence of dust on surface snow potentially causes a large uncertainty in model simulation.

So, in this chapter, we will focus on the albedo, topography, ice latent heat, precipitation and sea level feedbacks. And we will conduct a series of sensitivity experiment with our simple Earth system model, the GREB-ISM, to explore its effect and its associated physical processes. Our experiment design and related procedure will be explained in section 5.2. The findings of our sensitivity experiment will be summarised in section 5.3, along with a comparison of different feedbacks. The section 5.4 will go through each piece of feedback and explain what the physical process is. This chapter will be summarised in section 5.5.

5.2 Experiment design

5.2.1. Design of sensitivity experiments

We create five process switches in the GREB-ISM to examine the effect of each climate-ice sheet feedback, including albedo, ice latent heat, topography, precipitation, and sea level feedback (Table 5.1):

Table 5.1 Climate – ice sheet feedback and process switches.

Feedback	ON	OFF
Albedo (ALBD)	albedo changes due to ice thickness	albedo fixed as initial condition
Latent heat (HEAT)	Ice latent heat is negative when melting	ice latent heat set as zero
Topography (TOPO)	Topography change to ice thickness, which is related to surface sensible heat, precipitation and convection	Topography fixed as initial condition
Precipitation (PREP)	Snowfall based on local precipitation	Snowfall fixed as initial condition
Sea level (SLV)	Sea level change to ice thickness	Sea level set as zero

ALBD (albedo feedback) switch: The surface albedo of a snow/ice-covered zone is higher than that of an ice-free grid. As a result, in the GREB-ISM, the surface albedo is a function of ice thickness. If we turn off the ALBD switch, the surface albedo will be unaffected by ice thickness and will remain with only seasonal variations.

TOPO switch (topography feedback): In the GREB-ISM, surface elevation depends on bedrock elevation and ice thickness. As a result of the surface elevation raising, a large ice sheet causes changes in sensible heat, precipitation, and atmospheric transportation. When the TOPO switch is turned off, the model's surface elevation remains unchanged rather than updating when ice thickness changes.

HEAT switch (ice latent heat feedback): If the surface is covered with snow or ice during the melting season, a large amount of surface heat flux will be used as ice latent heat to melt the surface snow or ice, rather than warming the surface temperature directly (equation 3.1). In the melting season, this activity has a significant impact on the surface energy balance. If we turn off the HEAT switch in the GREB-ISM, the ice latent heat will be set to zero. As a result, all surface heat flux will have a direct impact on the change in surface temperature.

PREP switch (precipitation feedback): Precipitation turns to snow in the GREB-ISM when both the surface and air temperatures are below the freezing point. As a result, changes in precipitation during the snowy season will be directly reflected in snowfall rate. If we turn off the PREP switch, however, the snowfall rate will remain constant, regardless of local precipitation.

SLV switch (sea level feedback): The GREB-ISM, as a global Earth system model, may simulate sea level by dividing total grounded ice sheet volume change from reference stage by total ocean area. Sea level rise will change bedrock elevation, affecting land-sea distribution and surface height, and so indirectly influencing climate and ice sheet modification. This procedure is controlled by a SLV switch. The sea level will be set to constant 0 if the SLV switch is turned off, suggesting that there would be no global sea level change.

Based on those feedbacks, we design following experiments to evaluate the role of different feedback by turning on or off different processes.

NOISM experiment. This experiment uses the old version GREB 1.0 (Stassen et al., 2019) without ice sheet model to represent the climate system excluding ice sheets.

FULL experiment (all switches on). This experiment uses fully coupled GREB-ISM with all processes on, to investigate the fully coupled Earth system response to external forcing.

We also have five other experiments: NALBD, NHEAT, NTOPO, NPREP, and NSLV. Each N-X experiment represents the simulation with the GREB-ISM to illuminate the climate response without a specific feedback by turning off X but leaving all other switches on.

The most prevalent external forcing in paleoclimate is CO_2 and solar insolation. Both have the ability to alter the Earth's net radiation budget and thus induce global warming or cooling. They do, however, differ in terms of seasonality. CO_2 is thought to be a globally uniform greenhouse gas, meaning that it has an impact across all seasons and latitudes. The influence of solar insolation, on the other hand, is largely depending on latitude and season. The variation in solar insolation in the Northern Hemisphere summer, for example, has a significant impact on the North Pole. However, because the North Pole receives no solar radiation during the Northern Hemisphere winter, changes in solar radiation have no effect. This seasonality difference could influence the simulation. As a result, the focus of this chapter's experiments will be on understanding the climate-ice sheet feedback in the presence of CO_2 and solar insolation forcing.

A control simulation and a scenario simulation are included in each of our experiments. We first perform a 30 kyr control simulation with current CO_2 concentrations and solar radiation, then a 100 kyr scenario simulation. We have two scenarios: a CO_2 reduction scenario and a solar radiation reduction scenario. In the FULL experiment, we want our two scenarios to have the same surface temperature response strength to be able to build large-scale ice sheets. So, we have tested several possibilities and finally select the following settings: for CO_2 reduction scenario, the CO_2 concentration drops from 340 ppm in the control to 40 ppm in the scenario, but solar radiation remains constant. Similarly, in the solar radiation reduction experiment, solar radiation is reduced to 95% of current levels in the scenario, but CO_2 remains at the same level as in the control simulation.

5.2.2 Method

We define the temperature and ice thickness *response* to external forcing by using scenario equilibrium to minus control run. And thus, we evaluate the *feedback effect* by using response in full experiment minus the experiment with specific feedback switch off. The feedback is positive if the feedback effect shows the same sign as the response in the FULL experiment.

5.3 Climate and ice sheet feedback

5.3.1 Ice sheet coupling effect

In order to examine the overall ice sheet coupling effect, we compare the coupled GREB-ISM (FULL) with the original GREB (NOISM) simulation under external forcing. For the original GREB model, global surface temperature cools down after abrupt CO_2 or solar radiation reduction (global mean cooling of 8.0 ºC for CO_2 scenario and 7.4 ºC for solar radiation scenario, Fig 5.1a, b). As comparison, after ice sheet model coupled with the GREB (FULL), there is still global cooling pattern, but with a stronger cooling at Northern Hemisphere land area and slightly weaker cooling at tropical and Southern Hemisphere (global mean cooling of 8.4 ºC for CO_2 scenario and 8.8 ºC for solar radiation scenario, Fig 1c, d). In both scenarios, the scenario run in NOISM experiment reaches its equilibrium within the first thousand years, whereas the scenario run in FULL experiment takes more than 20 kyrs. So, including the ice sheet causes the system to have a longer response time and exhibit an inertial effect in a long-time scale. It is worth to noting that the ice sheet cover in the FULL experiment shows a large regional discrepancy from the forced simulation based on proxy data (Fig 4.7c). Apart from the difference from the given forcing, the missing of relevant physical processes is also a potential limitation in our modelling, which needs further exploration.

From difference between FULL and NOISM experiments, we can better understand the effect of ice sheet (Fig 5.1e, f). In FULL experiment, massive ice sheets form at North America, North Eurasia and Tibetan Plateau. Due to lapse rate in troposphere, the surface air temperature decreases on the top of those ice sheets, leading to more than 10 °C negative surface temperature anomalies. On the other hand, a series of shoreline grids show strong positive anomalies. This is because the large ice sheets formation induces global sea level drop, which converts a series of coastline ocean grids into land grids. As the land is drier than the ocean, as long as the ocean grid convers into land, the oceanic surface latent heat cooling abruptly vanishes and finally the surface temperature warms up.

Another interesting feature is the positive anomalies around Pacific Ocean and Southern Hemisphere (Fig 5.1e, f). This phenomenon is due to ice sheet blocking effect on air transportation. In the GREB-ISM and the GREB, the atmospheric heat and water vapor are redistributed by advection and diffusion process. The formation of large ice sheets at Northern Hemisphere high latitude reduces the local diffusion rate and thus hinders the warm and wet air in low latitude entering into polar area. As a result, the surface temperature cools down Arctic while warms up in the other places. And as the sea ice albedo feedback is able to enhance the temperature change, the maximum positive anomalies appear around the seasonal sea ice region (Fig 5.1e, f).

Meanwhile, the land areas in Northern Hemisphere middle latitudes also show negative anomalies. The process detail is not fully understood yet. Our first guess is that this phenomenon may be related to the different albedo scheme between the GREB-ISM and the GREB.

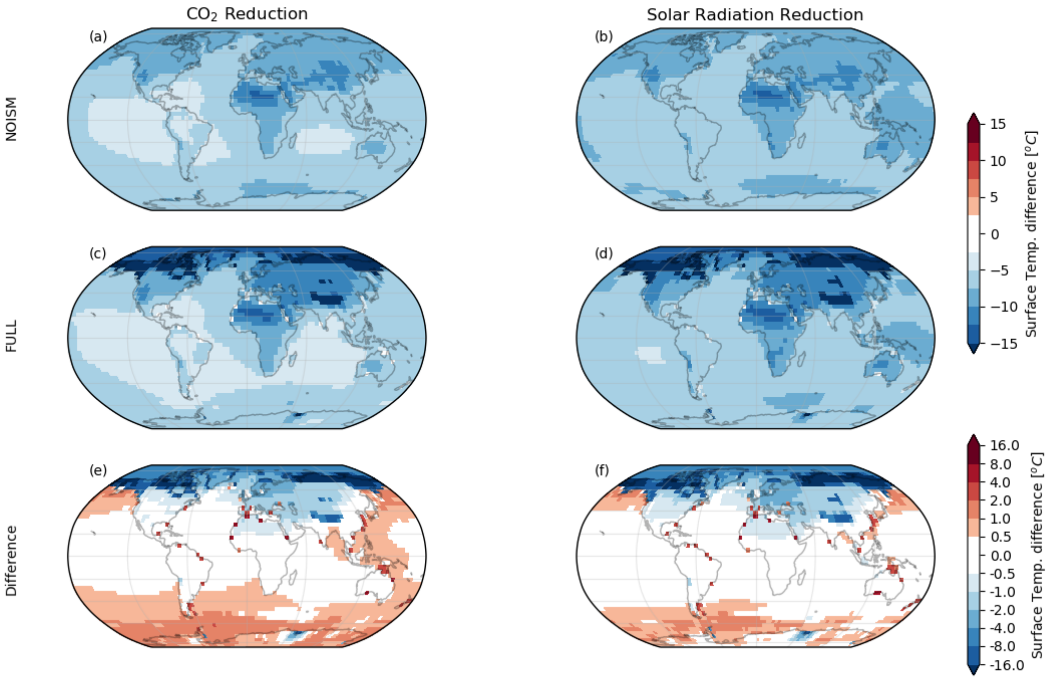

Fig 5.1 Temperature response (unit: °C) comparison between (a, b) NOISM experiment, (c, d) FULL experiment and (e, f) their difference (FULL – NOISM, values are plotted on a logarithmic scale) under (a, c, e) CO_2 reduction and (b, d, f) solar radiation reduction scenario. The temperature response is defined by using equilibrium ice thickness in scenario experiment (100 kyr) minus control experiment (30 kyr for FULL experiment, 50 yrs for NOISM experiment).

Fig 5.2 depicts the feature of ice sheet effect on zonal mean surface temperature. For CO_2 reduction scenario (Fig 5.2a), the zonal mean surface temperature in both experiments show a relatively weak cooling in Southern Hemisphere and strong cooling in Northern Hemisphere (Fig 5.2a). Interestingly, compared with NOISM experiment, the temperature cooling response in FULL experiment is significantly stronger to the north of 30 °N, with largest difference of 12.9 °C at 70 °N, but slightly weaker to the south of 30 °N. As for solar radiation reduction scenario, we can draw a similar conclusion (Fig 5.2b). This zonal temperature difference between FULL and NOISM is mostly owing to ice sheet formation in the Northern Hemisphere. The more land mass in Northern Hemisphere renders it easier to have large ice sheets. On the other hand, the large ice sheets hinder the diffusion between Northern Hemisphere polar region and lower latitude. Eventually, temperature cooling at south of 30 °N is slightly reduced. As for solar radiation reduction scenario, we have a similar conclusion but with generally stronger cooling effect in FULL experiment than its counterpart in CO_2 reduction scenario.

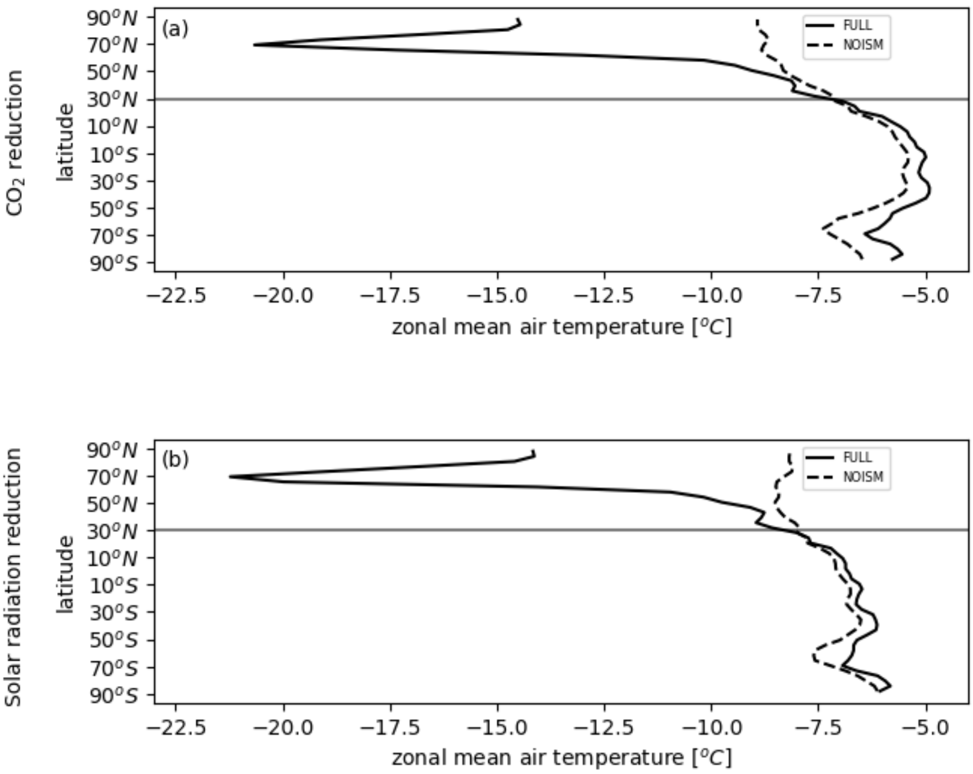

Fig 5.2 Zonal mean surface temperature response (unit: °C) comparison between (dash line) NOISM experiment and (solid line) FULL under (a) CO_2 reduction and (b) solar reduction scenario. The temperature response is defined by using equilibrium ice thickness in scenario experiment (100 kyr) minus control experiment (30 kyr for FULL experiment, 50 yrs for NOISM experiment). The gray line represents 30°N latitude.

Overall, ice sheet coupling processes result in significant local cooling on high latitudes in the Northern Hemisphere and modest warming of ocean grids in other locations. The ice sheet expansion area experiences the most substantial cooling due to topography, whereas some shoreline grids experience the most significant warming due to convertion from sea to land.

5.3.2 Sensitivity to different feedback processes

We then try to understand how each feedback influences the coupling process. In the FULL experiment (Fig 5.3a, b), the ice sheet response mainly concentrates on the Northern Hemisphere, where a vast area is covered by land. The ice thickness positive anomalies are mainly located around 60°N. However, the climate-ice sheet feedbacks can either enhance (through a positive feedback) or eliminate (via a negative feedback) this ice growth response to the external forcing. By evaluating the feedback effect, that is, the response of FULL experiment minus one switch off experiment, the intensity of each feedback can be quantified. The albedo feedback effect shows that most land grids to the north of 70°N have a positive ice thickness anomaly (more than 3 km), acting as the strongest positive feedback among all feedbacks (Fig 5.3c, d). In comparison to albedo feedback, ice latent heat feedback is likewise overall positive, although with less strength (Fig 5.3g, h). Topography feedback is also positive feedback, but it is less powerful than the two feedbacks mentioned before (Fig 5.3e, f). Apart from those positive feedbacks, precipitation feedback is the strongest negative feedback, which suppressed the ice sheets to build in a much larger size and height, and thus leads to a large negative ice thickness anomaly in the North Hemisphere (Fig 5.3i, j). The sea level feedback shows a much complex feature (Fig 5.3k, l). It converts a series of shoreline grids into land grids around Arctic, and thus provide a positive ice thickness anomaly at those converted grids. However, the sea level feedback also hinders formation of large ice sheet to the south of 65 °N.

For both CO_2 and solar radiation reduction scenarios, the NPREP experiment's zonal mean ice thickness is the largest in both hemispheres in scenario run (Fig 5.4a, c). Meanwhile, NALBD experiment has the least zonal mean ice thickness, followed by NHEAT and NTOPO. In comparison to the FULL experiment, the zonal mean ice thickness simulation in the NSLV experiment reveals a southerly shift. In the CO_2 reduction scenario, the simulation in the NSLV experiment is comparable to the results from the FULL experiment, however in the solar radiation reduction scenario, the simulation in the NSLV experiment is greater.

Considering the zonal mean feedback effect in CO_2 reduction scenarios (Fig 5.4b, d), an increase in zonal mean ice thickness maximum due to albedo, topography and ice latent heat feedbacks is about 1.6, 0.5 and 1.0 km, respectively. On the contract, precipitation feedback contributes to a maximum 2.7 km drop in zonal mean ice thickness. And precipitation feedback is the only feedback significantly changes the ice thickness in Southern Hemisphere. Last but not least, the sea level feedback basically moves the ice sheets north in aspect of zonal mean ice thickness.

The result shows that the albedo, topography and ice latent heat feedbacks are able to enhance the ice growth in the FULL experiment (through a positive feedback, Fig 5.3c-h), in which the albedo feedback creates the strongest and largest ice growth (Fig 5.3c, d). In contrast, the precipitation feedback largely eliminates the ice growth in the North Hemisphere, contributing as a negative feedback (Fig 5.3i, j). Furthermore, the sea level feedback effect is much more complicated (Fig 5.3k, l). It supports the ice accumulation in the polar Eurasian landmass but suppresses the ice growth at high latitudes as in Siberia. Additionally, the feedback effect difference between scenarios is most pronounced in the sea level feedback. Of course, simple combination of all above 5 feedbacks is not sufficient to reproduce the whole ice sheet-climate interaction, since those processes are highly nonlinear and it is also possible that we have missed some other feedbacks in our discussion.

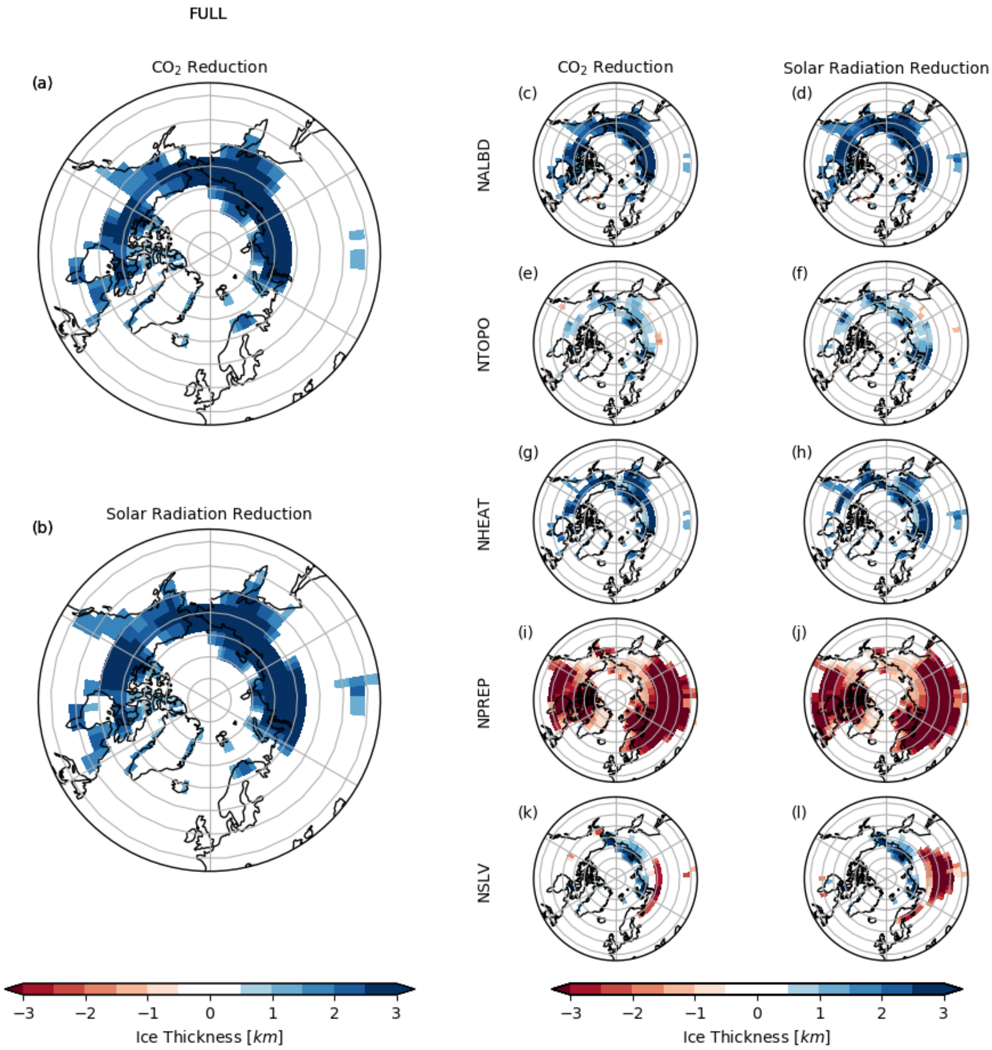

Fig 5.3 (a, b) Ice thickness response (unit: km) for FULL experiment and (c-l) feedback effect for individual feedback under (a, c, e, g, i, k) CO_2 reduction and (b, d, f, h, j, l) solar radiation reduction scenario. The ice thickness response is defined by using equilibrium ice thickness in scenario experiment (100 kyr) minus control experiment (30 kyr). The feedback effect is defined as the ice thickness response of the FULL experiment minus experiment without the specific feedback. "N-" represents experiment without specific feedback.

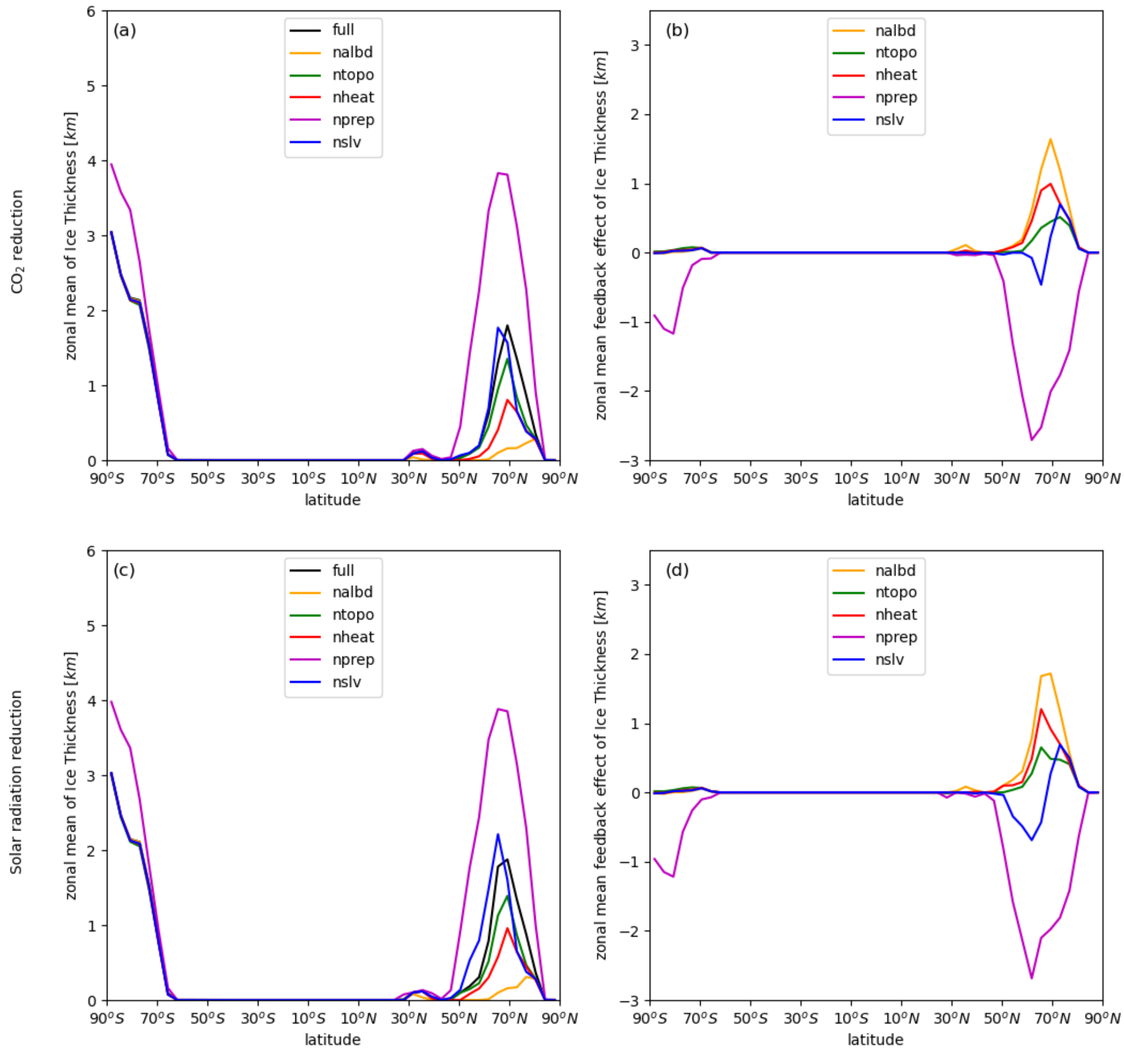

Fig 5.4 (a, c) Zonal mean ice thickness response (unit: km) and (b, d) zonal mean ice thickness feedback effect for individual feedback under (a, b) CO_2 reduction and (c, d) solar radiation reduction scenario.

In the FULL experiment, the surface temperature response to external forcing indicates a worldwide cooling effect, ranging from 0.5 °C near the tropics to more than 15 °C near the ice sheet growth zone (Fig 5.5a, b). When we look at the individual feedback effect, we see that it varies considerably. As a feedback directly impacts on the surface energy balance, the albedo feedback shows a global cooling effect (Fig 5.5c, d). As for topography feedback (Fig 5.5e, f), the Northern Hemisphere polar region is strongly cooled due to surface lifting, whereas the rest of the Northern Hemisphere is somewhat warmed because of weak meridional diffusion. Similarly, the ice latent heat feedback mostly cools the Northern Hemisphere ice growth areas (Fig 5.5g, h). The precipitation feedback is an overall negative feedback that has a strong warming effect north of 50ºN and a mild cooling effect south of 50ºN (Fig 5.6i, j). This is likely because the precipitation feedback prevents the building of larger ice sheets, and thus leads to improved global diffusion. The absence of large ice sheets in Northern Hemisphere heats the polar regions while cooling the low latitudes. The surface temperature anomalies caused by sea level feedback have a similar pattern to ice thickness change, showing that the temperature impact of sea level feedback is mostly related to local effect from ice sheets.

Interestingly, those feedbacks also have some commonalities. The first is a series of hotspots along the shore in albedo, topography, ice latent heat, and sea level feedback results (Fig 5.5c-h, k, l). Because of the global ice sheet growth in those feedbacks, the sea level drop renders a series of shoreline grids above sea level, and this conversion from sea to land results in a huge surface latent heat reduction. Finally, those shorelines have seen significant warming as a result of reduced heat loss owing to surface latent heat (section 5.4.5). When looking at the precipitation feedback effect (Fig 5.5i, j), we notice multiple scattered cold sites, indicating a reversal process. Another noticeable feature is the warming in the North Pacific in topography, ice latent heat and sea level feedback results (Fig 5.5e-h, k, l). For North Pacific, this is linked to the building of large ice sheets crossing Bering Strait, which heats the North Pacific by preventing cold, dry air from the North Pole from mixing with warm, moist air here. And then, the anomalies caused by air transportation are amplified by the sea ice cover in the North Pacific. So, we finally see the warming centre on the North Pacific.

The zonal mean surface temperature of all experiments reveals a warm tropic and cold poles pattern, with considerable difference near the North Pole (Fig 5.6a, c). When looking at zonal mean feedback effect (Fig 5.6b, d), the albedo feedback shows a global cooling effect. Another two feedbacks with a global effect are the topography and precipitation feedback. In contrast to topography feedback, which cools both the North and South Poles while heating the low latitudes, precipitation feedback warms the high latitudes while cooling the low latitudes. Apart from all above, the ice latent heat feedback is relatively regional and takes effect mainly on Northern Hemisphere polar region. In terms of sea ice feedback, the surface temperature anomalies are corresponding to the ice thickness anomalies, and show a large difference between two scenarios.

As a result of albedo, topography and ice latent heat feedbacks, the maximum decrease in zonal mean surface temperature is about 15, 9 and 7 ºC, respectively. On the other hand, precipitation feedback warms up zonal mean surface temperature with maximum of 13 ºC. Sea level feedback has a tendency to warm central Siberia and cool the shoreline grids surrounding the North Pole by shifting large ice sheets, but with a scalar difference in two scenarios.

Again, the result indicates that climate response due to CO_2 and solar insolation forcing is mostly enhanced by albedo feedback while mainly eliminated by precipitation feedback. Besides, ice latent heat and topography feedback are overall positive feedback for the process. Sea level feedback is a complicated feedback with different performance in different external forcing. Plus, by altering the rate of local diffusion, the massive ice sheets can have a global effect. Our results here agree with numerous earlier investigations, which established that albedo feedback has a dominating role in Northern Hemisphere climate change during paleoclimate (Abe-Ouchi et al., 2007; Budyko, 1969; Felzer et al., 1996). However, the difference between our study and their work is also obvious. First, those early studies only evaluate the effect from albedo feedback and topography feedback and few of them discussed the ice latent heat, precipitation and sea level feedbacks. Second, the topography feedback in those early studies also included the atmospheric circulation change like stationary wave pattern, which is absent in our research. In spite of those detailed difference, our conclusion is roughly same.

Feedback effect of total ice volume in Northern Hemisphere is used to quantify the strength of different climate-ice sheet feedback strength (Table 5.2). For CO_2 reduction scenario (solar radiation reduction), albedo feedback is the most major positive feedback, which contributes to 36.49 (43.36) $\times 10^6$ km^3 ice volume, following by ice latent heat feedback of 24.08 (26.68) $\times 10^6$ km^3 and topography feedback of 10.66 (14.49) $\times 10^6$ km^3. Precipitation feedback is a dominant negative feedback, preventing 104.31 (110.51) $\times 10^6$ km^3 of further ice growth in the FULL experiment. The major difference between two scenarios is in sea level feedback, which increases ice accumulation of 2.44 $\times 10^6$ km^3 in CO_2 reduction scenario but decrease total ice volume of 9.75 $\times 10^6$ km^3 in solar radiation reduction scenario.

Table 5.2 Total Northern Hemisphere ice volume (unit: 10^6 km^3) response in different experiments and their corresponding feedback effect. The feedback effect is defined as the ice volume response of the FULL experiment minus experiment without the specific feedback. "N-" represents experiment without specific feedback.

		FULL	NALBD	NTOPO	NHEAT	NPREP	NSLV
CO_2 reduction	Response	37.78	1.29	27.12	13.70	142.09	35.34
	Effect		36.49	10.66	24.08	-104.31	2.44
Solar radiation reduction	Response	45.92	2.56	31.43	19.24	156.43	55.67
	Effect		43.36	14.49	26.68	-110.51	-9.75

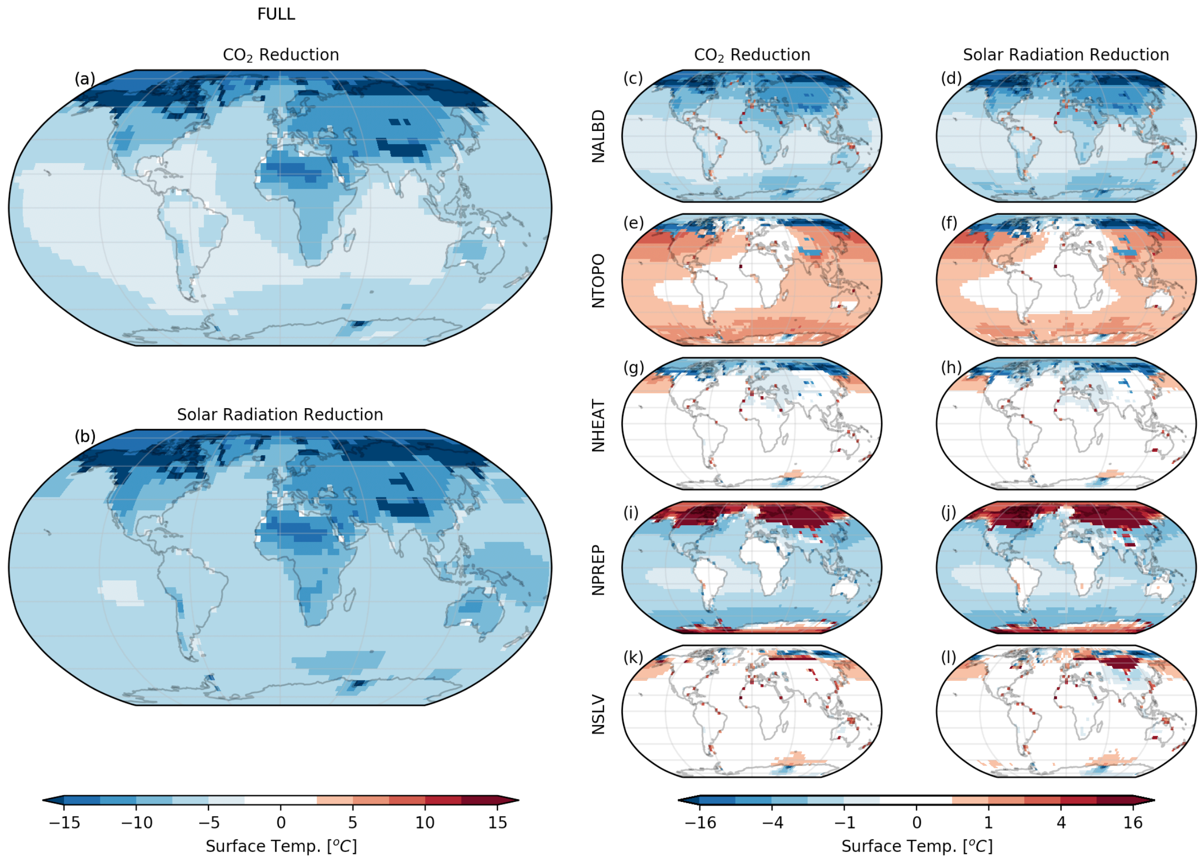

Fig 5.5 Same as Fig 5.3 but for surface temperature (unit: ^oC).

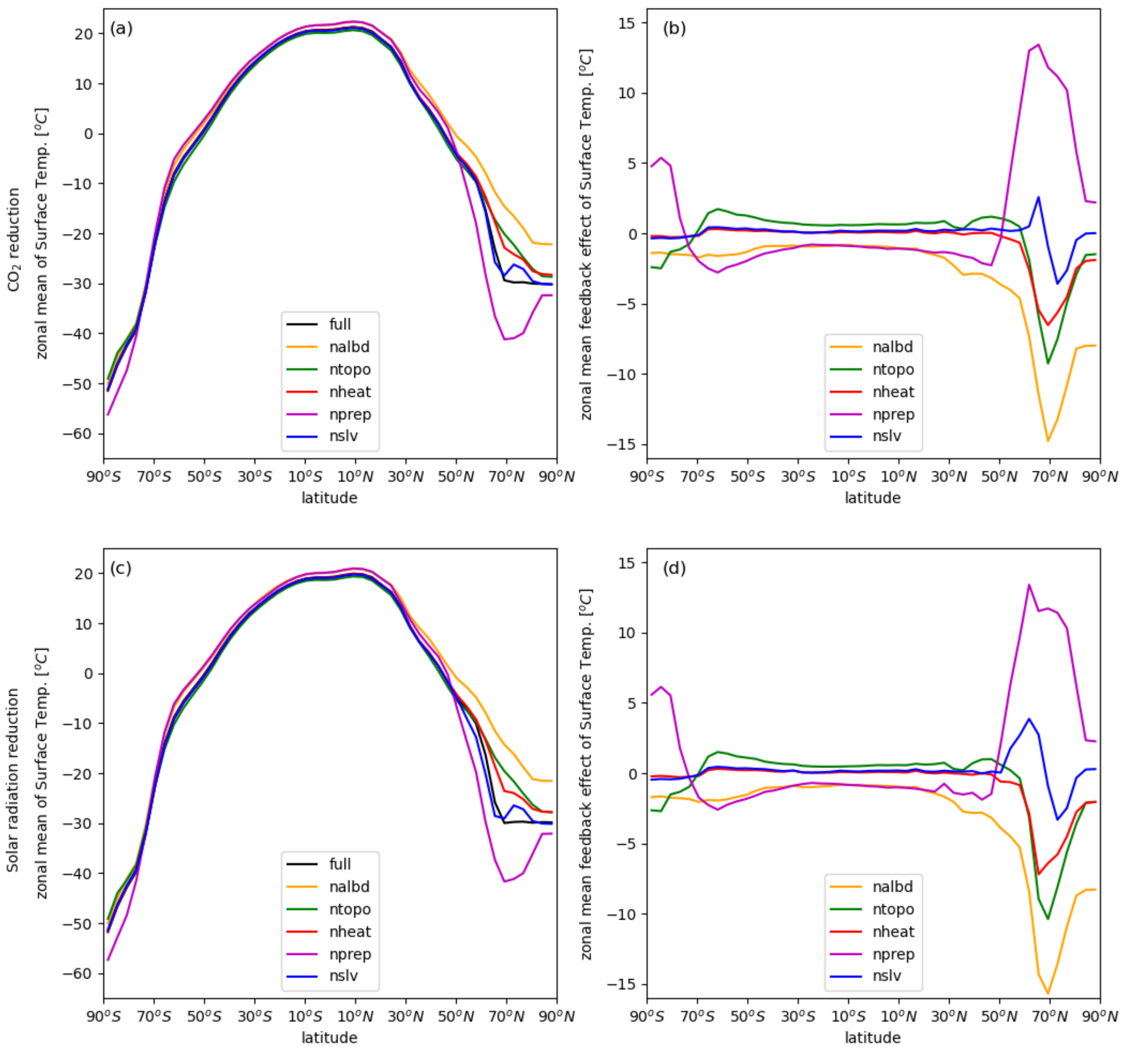

Fig 5.6 Same as Fig 5.4 but for surface temperature (unit: °C).

5.4 Analysis of the feedback processes

5.4.1 Albedo feedback

The GREB-ISM applied a new albedo scheme different from the original GREB. For the original GREB, the albedo change is based on the difference between surface temperature and frozen temperature (Fig 5.7a). However, in the GREB-ISM, the albedo is a function of ice thickness (Fig

5.7b). Since snow albedo is usually larger than sea ice, parameterization of ice thickness differs in land and ocean grid. It is worth to note that we did not systematically evaluate the difference caused by the albedo scheme change. Willeit and Ganopolski (2018) pointed out that the Northern Hemisphere ice sheets over the last glacial cycle is very sensitive to the representation of snow albedo in the modelling by conducting a series of sensitivity experiments. So, the impact of albedo scheme changes is an interesting subject that warrants further investigation.

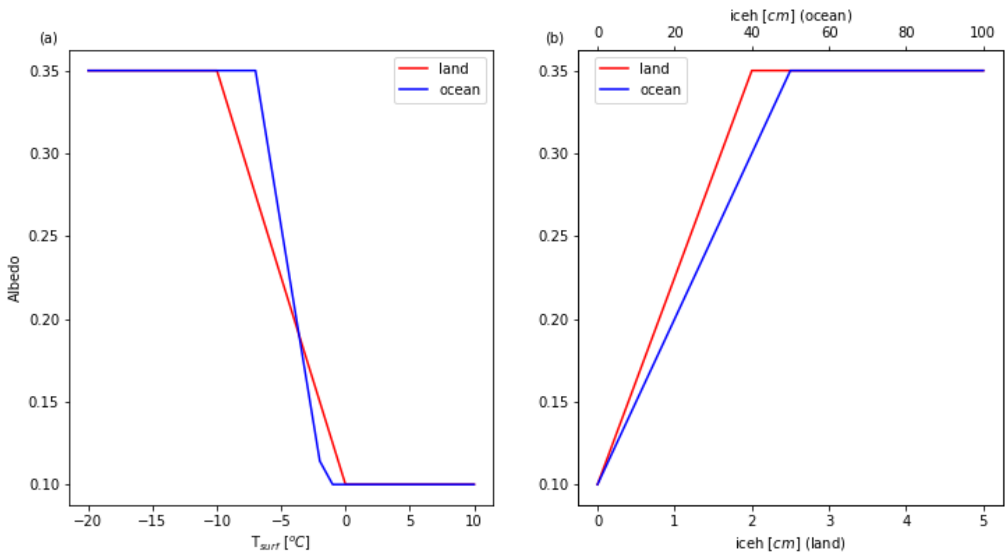

Fig 5.7 The parameterization of the surface albedo in (a) the original GREB and (b) the GREB-ISM.

High surface albedo is an essential feature of snow-covered area. As a result, adjacent surface temperature drops due to less shortwave radiation abortion. The process of albedo feedback is quite clear. The initial surface cooling caused by solar radiation and CO_2 reduction favors ice sheet formation, which in turn further increases the surface albedo in most of Northern Hemisphere land more than 5% (Fig 5.8a, c). The brighter ice surface leads to more than 10 W m^{-2} annual surface solar radiation reduction in the whole Northern Hemisphere land, facilitating the initial surface cooling from the external forcing (Fig 5.8b, d). So, albedo feedback is a positive feedback. The process here is same as the classical albedo feedback described in previous literatures (Fyke et al., 2018; Willeit and Ganopolski, 2018).

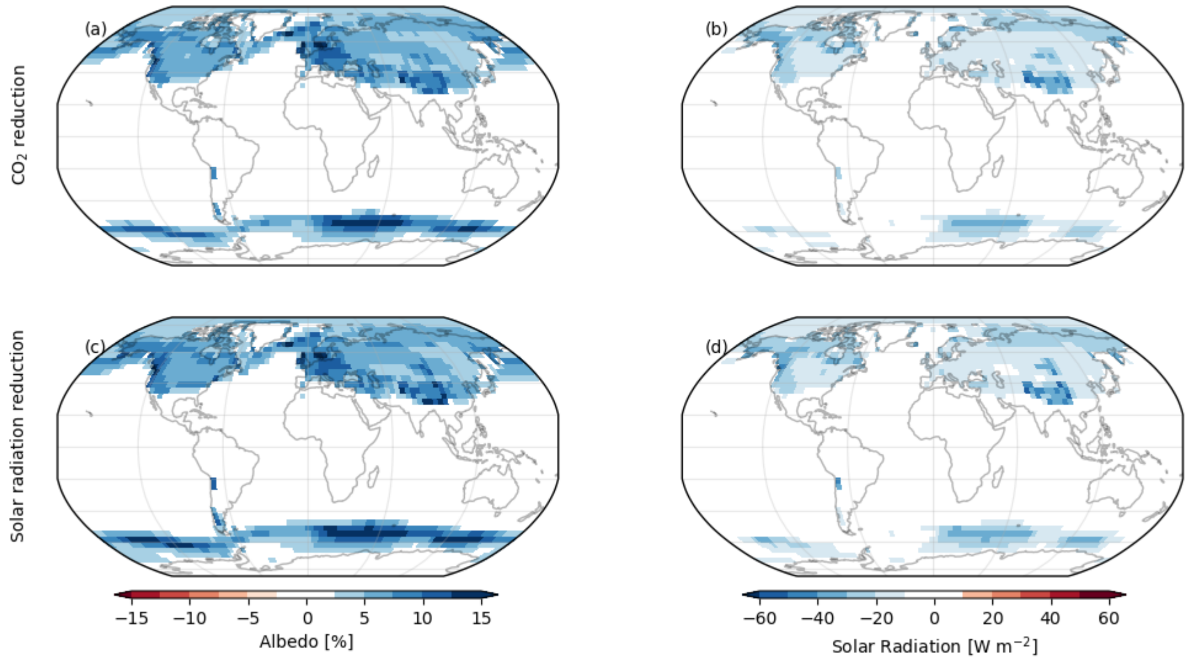

Fig 5.8 Albedo feedback effect on surface albedo (a, c; unit: %) and solar radiation (b, d; unit: W m^{-2}). The feedback effect on the variable is defined as the variable response in the FULL experiment minus the NALBD experiment.

As a result, the albedo feedback provides a global surface cooling impact because it alters the net incoming shortwave radiation directly (Fig 5.9a, d). The global cooling at the tropics is modest, ranging between 0.5 and 1.0 °C. However, at high latitudes, the cooling exceeds 2 °C, and even exceeds 4 °C in the Northern Hemisphere land zone. At ice sheet development zones, the highest temperature cooling, which is more than 16 °C, is recorded. Nevertheless, rather than a direct albedo feedback effect, the large surface temperature reduction near the ice sheet development zone is due to surface elevation lifting. As for the scattered hotspots in the map, it is related to the sea level change, which we will discuss later. The air potential temperature change shows a similar pattern but with less cooling in ice development zone (Fig 5.9b, e). In the NALBD experiment, there are just a few ice sheets formed in the scenario run. As a result, the ice thickness anomalies due to the albedo feedback is by more than 3000 meters (Fig 5.9c, f).

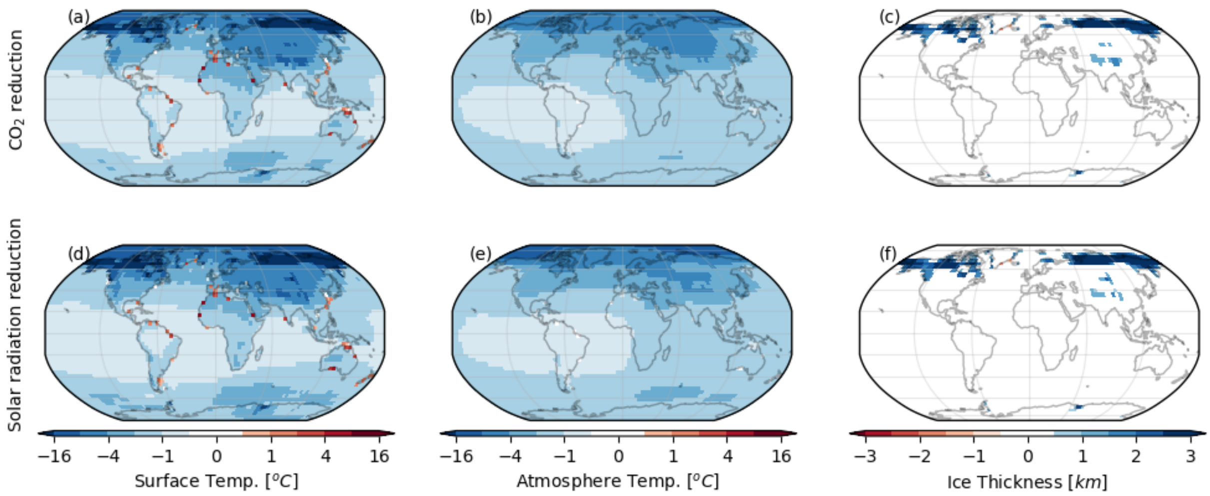

Fig 5.9 Albedo feedback effect on surface temperature (a, d; unit: °C), air temperature (b, e; unit: °C), and ice thickness (c, f; unit: km). The feedback effect on the variable is defined as the variable response in the FULL experiment minus the NALBD experiment.

5.4.2 Topography feedback

A large ice sheet plays a role similar to that of a great mountain on the surface, leading to a significant topography effect. In the GREB-ISM, the surface air temperature decreases with height according to the lapse rate, triggering lower surface air temperature. Consequently, the surface temperature will also decrease as less sensible heat from air to surface. This feedback is widely discussed and also called as “elevation-surface mass balance feedback” (Abe-Ouchi et al., 2007; Edwards et al., 2014; Fyke et al., 2018), which is a critical positive feedback during deglaciation period (Abe-Ouchi et al., 2013; Kapsch et al., 2021). Another important impact from topography feedback is the air transportation change. In the early study, air transportation was frequently associated with ice sheet growth via circulation changes caused by the topography change (Felzer et al., 1996; Herrington and Poulsen, 2012). Instead, in the GREB, the elevated topography limits the local diffusion rate and thus prevents the exchange of heat and water vapour. We simply call this process as ice sheet blocking effect in the later text.

In our sensitivity experiment, following a significant cooling caused by CO_2 and solar radiation decrease, the large ice sheets start growing, eventually raising the surface height to thousands of metres (Fig 5.10a, c). This raised surface enlarges the air-surface temperature gradient, invoking sensible heat more than 30 W m^{-2} from surface to air (Fig 5.10b, d), which further cools down the surface temperature while warming up the air column. Therefore, for the local surface temperature, the initial surface cooling tendency due to the external forcing is enhanced by the topography feedback. On the other hand, more sensible heat flux from the surface to air column leads to the warming of the air potential temperature post the elevation lifting (Fig 5.11b, e). The air potential temperature warming propagates over the surrounding region, resulting in neighbouring sensible heat positive anomalies.

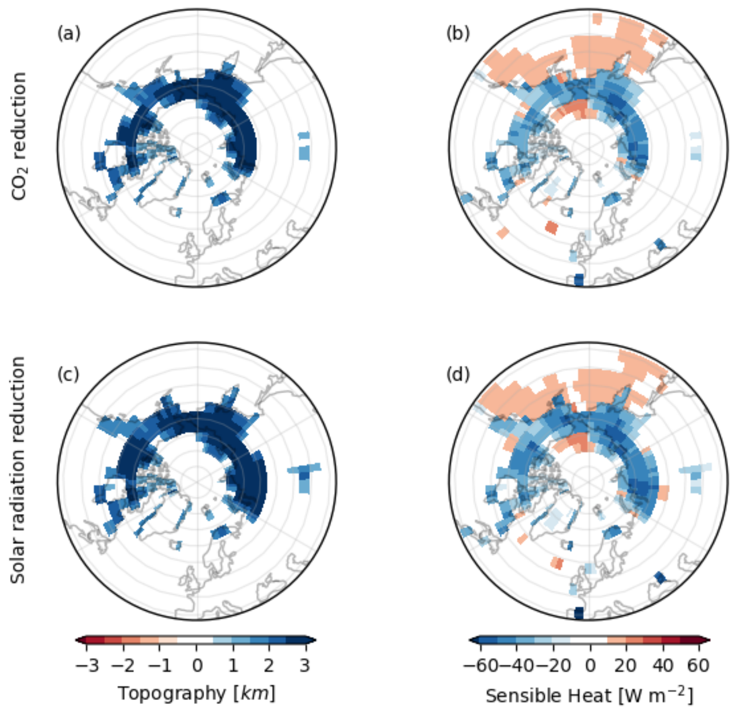

Fig 5.10 Topography feedback effect on surface elevation (a, c; unit: km) and sensible heat (b, d; unit: W m^{-2}). The feedback effect on the variable is defined as the variable response in the FULL experiment minus the NTOPO experiment.

As a result, we can observe that the topography feedback effect amplifies the forced surface cooling impact mostly at high latitudes, where massive ice sheets form (Fig 8a, d, c, f). The cooling effect at ice sheet development zones can be more than 8 ^{o}C. The construction of an "ice sheet wall" around the North Pole inhibits heat and water vapour from being transported between various latitudes (ice sheet blocking effect), resulting in polar cooling and low latitude warming (Fig 8b, e, c, f). The warming impact of topography feedback on low latitude air is the greatest of all feedbacks. It results in a more than 2 °C increase in the air potential temperature from western North America to eastern Russia. Besides temperature, topography feedback also has an influence on the change in ice thickness, but not as much as albedo feedback (Fig 5.11c, f).

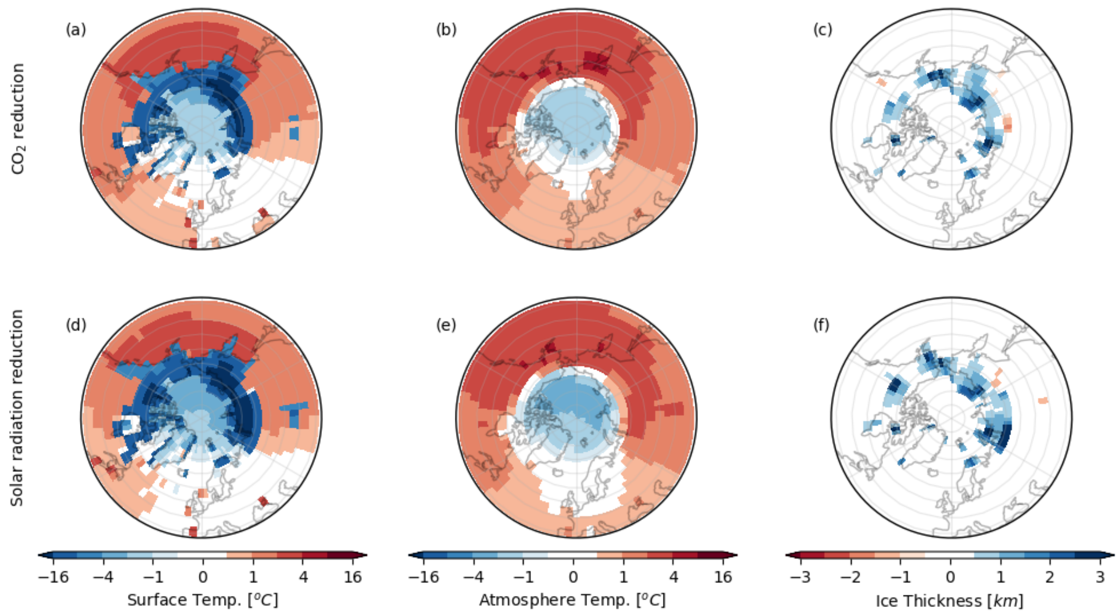

Fig 5.11 Same as Fig 5.9 but with NTOPO experiment.

5.4.3 Ice latent heat feedback

For the ice-covered regions, the ice latent heat feedback is one of direct interactions between the surface temperature and ice thickness. For instance, to melt 1 m ice requires 3.03×10^8 J energy in the GREB-ISM, which is roughly equivalent to 0.6 °C land surface temperature increase. So, including ice latent heat feedback introduces an extra temperature cooling during the melting season.

Considering a Site (90oE, 70oN; Fig 5.12), in the FULL experiment, compared with NHEAT experiment, during the spring, a portion of the surface energy flux is consumed by ice melting (Fig 5.12c, f), resulting in a decrease of the surface temperature (Fig 5.12a, d). This cooling impact reduces the number of positive degree days in the following months (Fig 5.12a, d), which causes a longer ice cover period (Fig 5.12b, e). As a result, more surface shortwave radiation is reflected during the warm season (Fig 5.12c, f), further reducing the temperature (Fig 5.12a, d). After multiple repetitions, it ends up with a permanent ice cover zone.

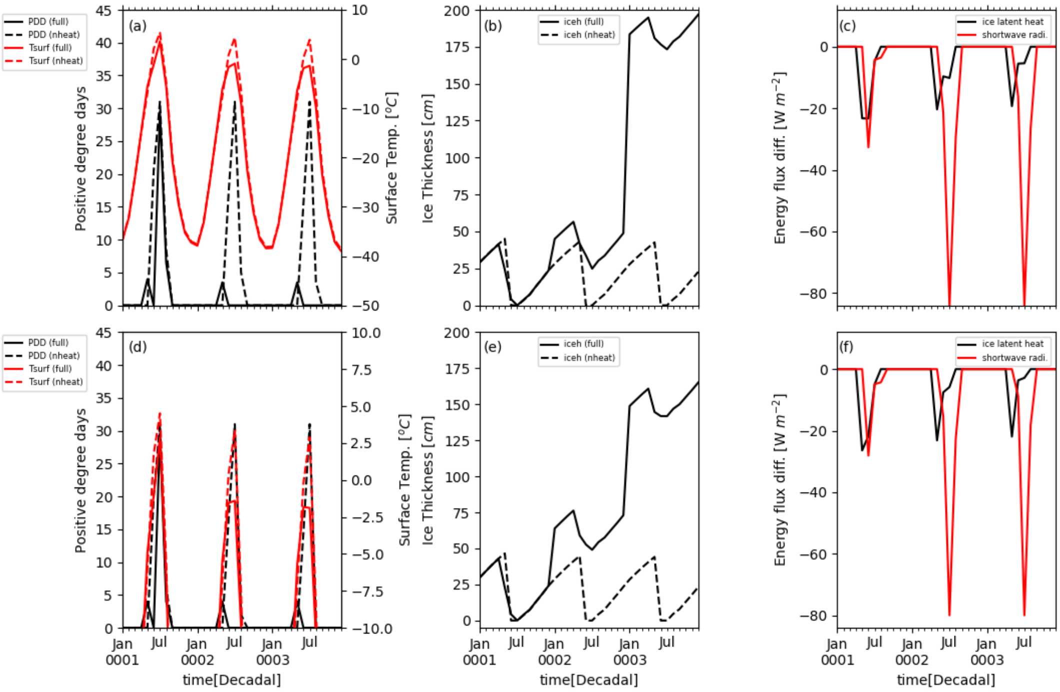

Fig 5.12 (a, d) Surface temperature and positive degree days (PDD), as well as (b, e) ice thickness throughout the first three decades of the FULL and NHEAT experiments under (upper) CO2 and (lower) solar radiation reduction scenarios. (c, f) Ice latent heat and shortwave radiation difference between FULL and NHEAT experiments in the first three decades under (upper) CO_2 and (lower) solar radiation radiation decrease scenarios.

For spatial map, the effect of ice latent heat feedback mainly works on seasonal ice cover zone, especially for the short melting season region, where the decreasing melting season length eventually causes irreversible ice accumulation like Site (90°E, 70°N; Fig 5.12). As a result, the ice latent heat feedback favors a series of large ice sheets building at seasonal ice cover areas with more than 3000 meters (Fig 5.13c, f). Corresponding to the creation of those ice sheets, the surface elevation raising and ice sheet blocking effect result in around 8 °C cooling at the ice sheet development zone and 1

°C cooling at the Arctic, while roughly 1 °C warming at the North Pacific (Fig 5.13a, d). Meanwhile, the pattern of air potential temperature anomalies is analogous to the topography feedback effect, but at lower latitudes with half the warming (Fig 5.13b, e).

The ice latent heat, as seen in the process, mostly increases the area where the ice sheet is able to develop rather than directly contributing to the temperature anomalies at equilibrium. The major surface temperature cooling at equilibrium mostly comes from topography and albedo feedback.

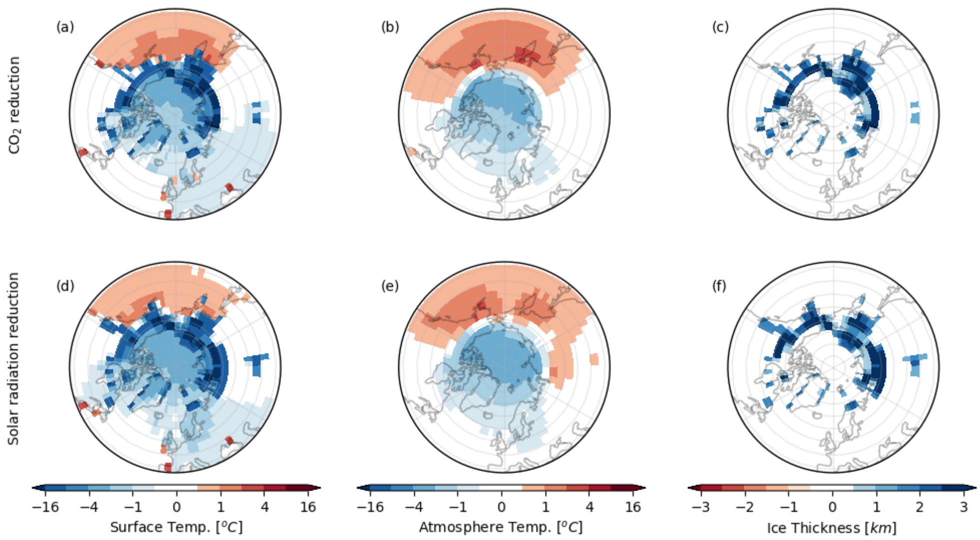

Fig 5.13 Same as 5.9 but with the NHEAT experiment.

5.4.4 Precipitation feedback

Snowfall rate is an essential source of ice mass. When the surface and air temperatures drop below the freezing point in the GREB-ISM, precipitation turns to snow. Most of previous studies linked the precipitation feedback with topography change (Fyke et al., 2018; Hakuba et al., 2012; Löfverström and Liakka, 2016; Medley and Thomas, 2019). In the GREB-ISM, the precipitation is estimated based on the local or zonal mean atmospheric water capacity, so it is indirectly connected with surface temperature and also topography.

To illustrate the difference between ice growth processes in the FULL and NPREP experiments, we compare the growth of ice in a box in both experiments (165-175°E, 65-75°N). In the FULL experiment, the external forcing together with albedo feedback leads to the initial surface cooling. The strong temperature decrease produces a quick decline in snowfall of around 22 mm during January at the end of 1 kyr (Fig 5.14a). Considering the climatology of snowfall rate here is 42.9 mm, the initial temperature decrease causes more 50% snowfall drop. Therefore, the ice thickness increase in FULL experiment is slower than that in the NPREP experiment. As ice sheet grows, the increase in ice thickness causes surface elevation raising, resulting in air column decrease and surface temperature dropping, both of which lead to extra 1-2 mm snowfall reduction in January. As a result, when compared to the NPREP experiment, in which the snowfall rate remains as the control run, the FULL experiment results in a thinner ice sheet at the end. In another word, the precipitation feedback is a negative feedback that limits the ice sheet development under cooling environment.

We want to underline the crucial role of albedo feedback in enhancing early cooling, as external forcing alone cannot sustain the creation of large ice sheets, as demonstrated by the NALBD experiment (Fig 5.14a, c). Actually, compared to the impact of early surface cooling, the change in snowfall owing to ice sheet growth is not very considerable. Because of the above process, surface mass balance in north Eurasia and North America displays a strong negative anomaly due to precipitation feedback (Fig 5.14b, d). The negative anomalies range from near zero around the North Pole to roughly -0.8 to -0.4 m a^{-1} at the lower latitudes, eliminating the ice growth at those areas. A positive circle appears at the boundary of negative anomalies, representing substantial ice melting at the large ice sheet boundary in the NPREP experiment. In summary, the precipitation feedback is a negative feedback which slows down the ice sheet growth during the evolution.

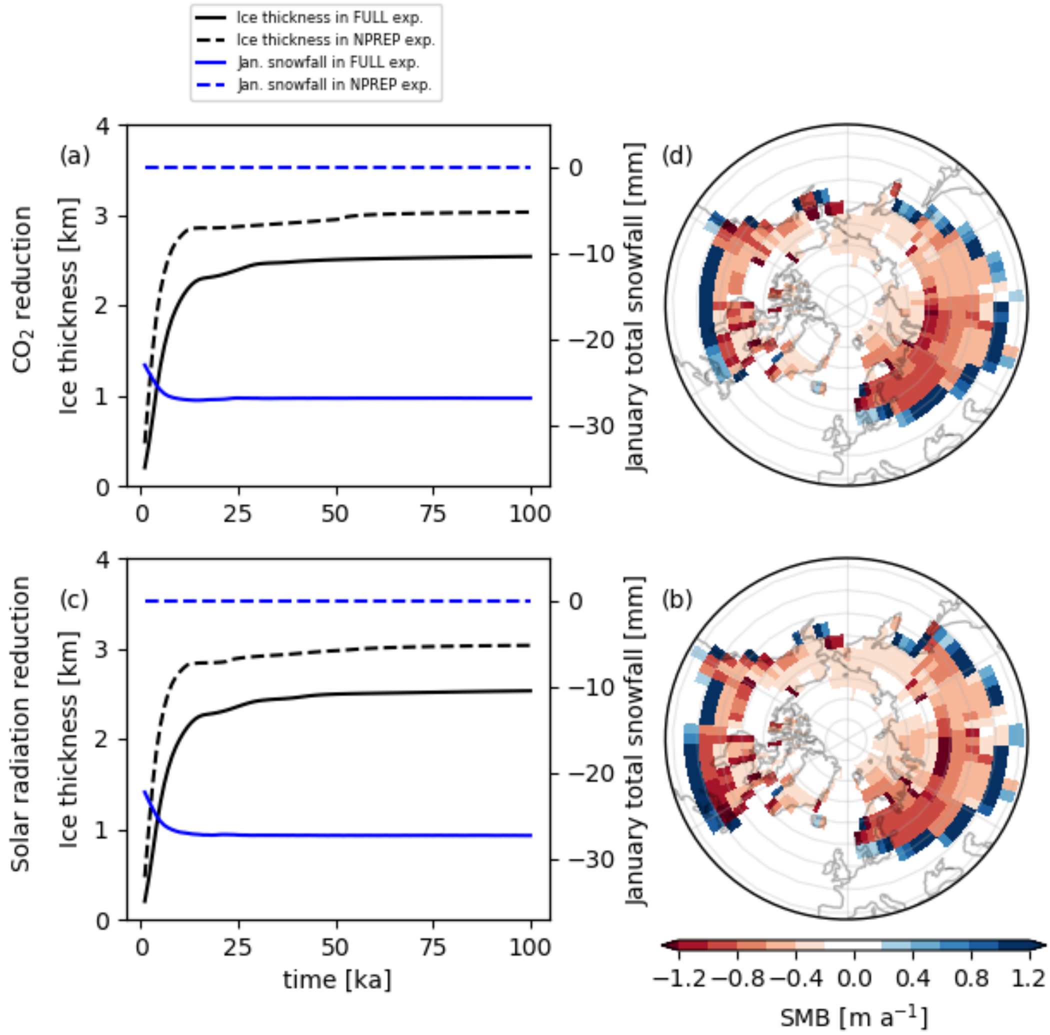

Fig 5.14 (a, c) Response of ice thickness (black) and total snowfall in January (blue) in FULL (solid line) and NPREP (dash line) experiment under (a) CO_2 and (c) solar radiation reduction scenarios at a high latitude box (165-175°E, 65-75°N). The response of variable defined as the scenario run equilibrium minus the control run equilibrium. (b, d) The precipitation feedback effect on surface mass balance (unit: km) under (b) CO_2 and (d) solar radiation reduction scenarios. The feedback effect of variable is defined as using variable response in FULL experiment minus the NPREP experiment.

The Fig 5.15 depicts the precipitation feedback effect on ice thickness, surface and air temperature. The result shows that precipitation feedback effectively eliminates ice sheet growth and extension owing to forcing (Fig. 5.15c, f), as well as surface temperature cooling (Fig 5.15a, d). The majority of Northern Hemisphere land to the north of 55°N has positive surface temperature anomalies of more than 16 °C (Fig 5.15a, d). The positive anomalies are surrounded by negative anomalies at low latitudes, which is linked to a surface elevation drop owing to a 3 km ice thickness reduction (Fig 5.15c, f). As massive ice sheets in NPREP experiment vanish in the FULL experiment, the ice sheet blocking effect results in polar warming of 2 °C and low latitude land cooling of around 4 °C in air potential temperatures (Fig 5.15a, d, b, e).

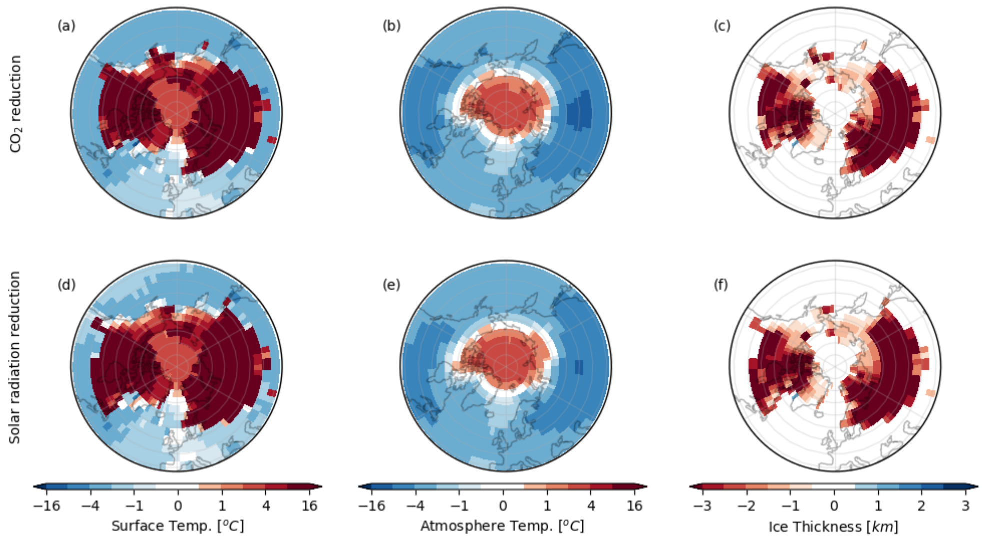

Fig 5.15 Same as Fig 5.9 but with NPREP experiment.

5.4.5 sea level feedback

Different from the previous Antarctica studies (Gomez et al., 2020; Maris et al., 2015; Tigchelaar et al., 2019), in this section, we will focus on the global impact of sea level feedback. The interaction between the sea level and ice sheet is quite complex. In the GREB-ISM, the sea level change is calculated using the total grounded ice sheet volume change from a reference stage, divided by the total ocean area. The massive ice sheets store a large amount of fresh water, consequently leading to a sea level drop. As a result, some shallow ocean grids in the model gets lifted above the sea level and is converted into land grids. Land has a different heat capacity and surface evaporation than the ocean grid, which causes the change of surface energy balance. And also, large ice sheets are easier to form on solid land than on ocean grids. So, the displacement of the land and sea also influences the ice sheet formation and retreat.

In CO_2 reduction and solar radiation reduction experiments, the sea level lowers by 120 and 141 metres, respectively. As a result of the sea level drop, all ocean grids with bedrock less than 100 m (Fig 5.16a) become land grids (Fig 5.16b, c). In the case of tropic grids, the conversion leads to a change in the surface energy balance. Take a site (140ºE, 10ºS; Fig 5.17) as an example, where the sea-land conversion occurred between 3 and 4 kyr, following the sea-to-land transition, surface humidity decreased significantly (Fig 5.17a, c). As a result, the surface energy loss due to surface latent heat reduces by roughly 20 W m^{-2} (Fig 5.17b, d), causing a 1 ºC increase in surface temperature (Fig 5.17a, c). Of course, sensible heat and net surface longwave radiation begin to compensate for the warming caused by surface latent heat, until a new surface energy balance has achieved (Fig 5.17b, d). This process finally leads to scattered shoreline grids at low latitudes with significant temperature warming (Fig 5.18a, d).

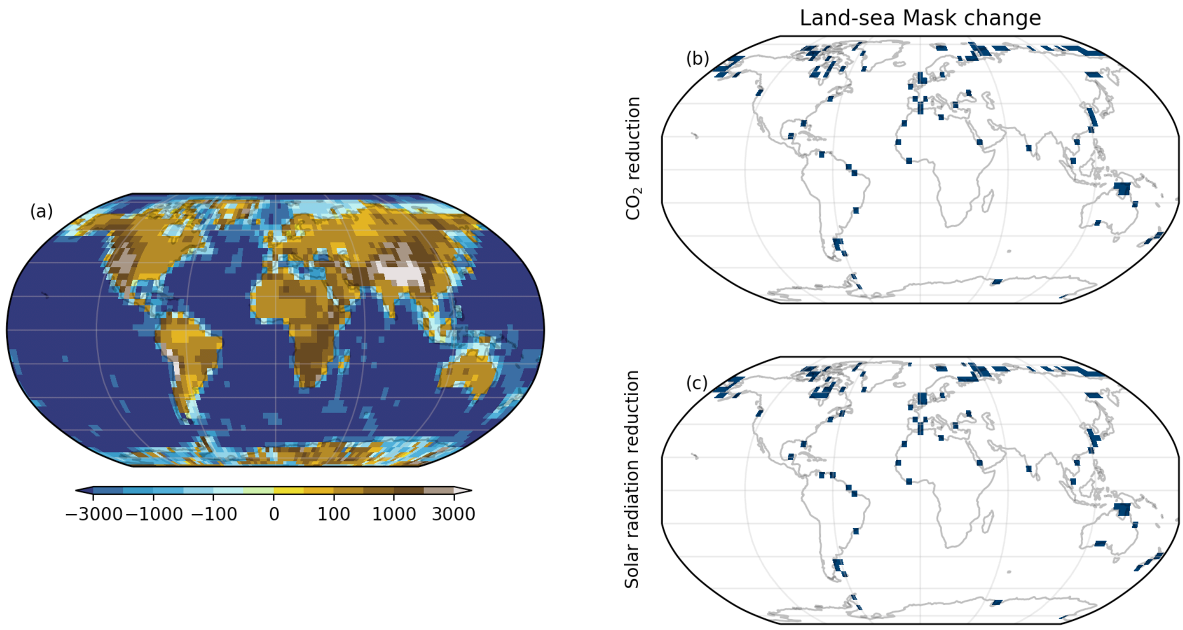

Fig 5.16 (a) Initial bed rock (unit: m) in the GREB-ISM. (b, c) Land-sea mask change (blue represents from ocean to land grid) between FULL and NSLV experiment under (b) CO_2 reduction and (c) solar radiation reduction scenarios.

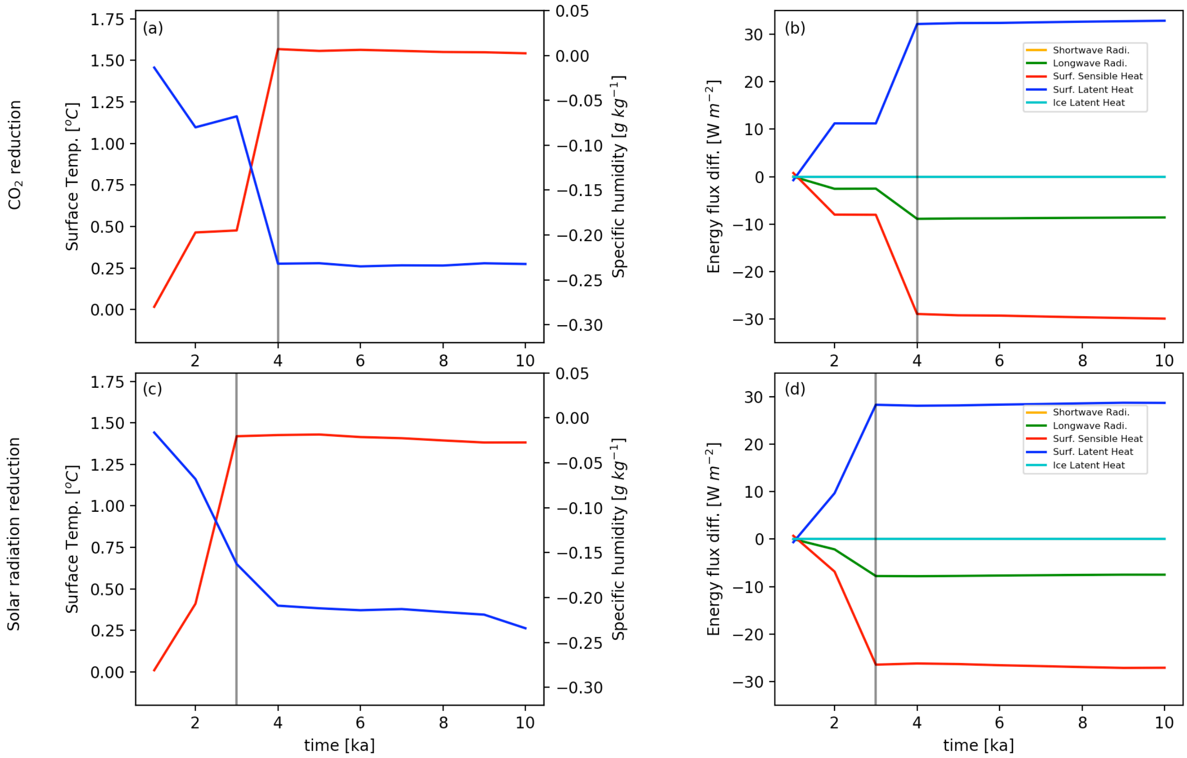

Fig 5.17 (a, c) Sea level feedback effect on the time evolution of surface temperature (red; unit: ºC) and specific humidity (blue; unit: g kg^{-1}), as well as (b, d) surface energy flux terms (unit: W m^{-2}) at a tropical site (140ºE, 10ºS). The feedback effect of variable is defined as using variable response in FULL experiment minus the NSLV experiment. The gray line represents the time point sea-land transition occurs.

On the other hand, at a series of shallow ocean grids on the Russian side of the Arctic, the sea level drop induces massive large ice sheets (Fig 5.18c, f), which also results in a significant local surface temperature cooling of more than 4 ºC. As discussed in other sections, the large ice sheets surrounded Arctic warm up the local and lower latitude air potential temperature (Fig 5.18c, f), as well as corresponding surface temperature in North Pacific (Fig 5.18a, d).

Another interesting feature for sea level feedback is that it has distinct influence in two different scenarios. In both scenarios, the experiment without sea level change generates large ice sheets in central Siberia, but in solar radiation experiment, the ice sheet tends to extend much southward. The reason for this phenomenon is not fully understood yet. We guess the different external forcing impact on different season may play roles in this ice sheet growth.

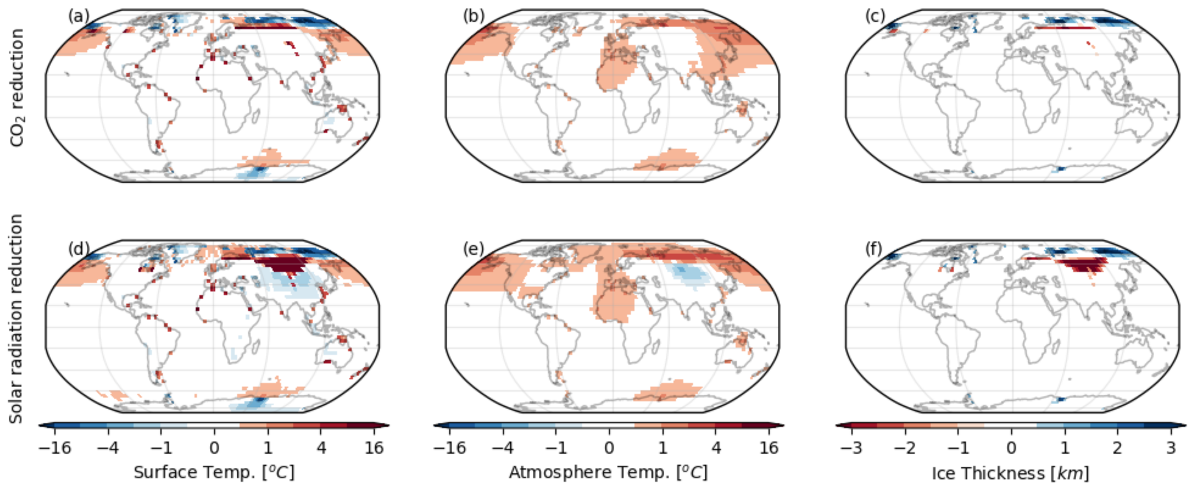

Fig 5.18 Same as Fig 5.9 but with NSLV experiment

5.5 Summary and discussion

In this chapter, we explore the climate-ice sheet interaction by a series of sensitivity experiments in CO_2 and solar radiation reduction scenarios. The results are summarised as following:

Compared with the original GREB, including ice sheets in the GREB-ISM leads to several major changes in model response to the external forcing. First, under the given forcing, the coupled Earth system takes a longer model time to reach its equilibrium. Second, where large ice sheets grow at high latitudes and altitudes, the surface temperature response to external forcing is greatly amplified due to surface elevation and albedo change. Meanwhile, the large topography created by ice sheet growth can prevent heat and water vapor from being transported between latitudes, cooling the high latitudes and warming the low latitudes. Furthermore, the sea level drop owing to the global ice volume growth renders shallow coastline grids shift from sea to land, resulting in a strong surface temperature response.

The climate impact of 5 different climate-ice sheet feedbacks is evaluated in the experiments. For ice sheet formation, the albedo feedback is the most significant positive feedback. Massive ice sheets in the North Hemisphere are difficult to build without cooling from albedo feedback. Similarly, the ice latent heat and topography feedbacks are also positive feedback for the ice sheet growth. The ice latent heat feedback cools down seasonal ice cover areas and causes many of them to become permanent ice sheet, while topography feedback cools the ice surface and thus supress the ice ablation during the ice sheet lifting. Both effects lead to further ice growth and eventually, the formation of gigantic ice sheets around the Arctic. On the other hand, precipitation feedback – the most important negative feedback - suppresses the growth of the ice sheet in the cold and mountainous areas via snowfall decrease. Besides those, sea level feedback shows distinct difference between two scenarios, which tends to impact the coastline grid by sea-to-land transition and shift ice sheet forming position at high latitude.

In terms of surface temperature cooling, all feedbacks cause more or less global effect. The albedo feedback is the major positive feedback, leading to an overall global surface temperature decrease with a maximum cooling near the Arctic. Meanwhile, both the topography and ice latent heat feedbacks contribute to the growth of large ice sheets surrounding the North Pole. Those ice sheets significantly cool down the land around the Arctic due to surface lifting, whereas slightly warms up the low latitudes by mitigating the atmospheric transport between different latitudes. By contrast, the precipitation feedback eliminates the ice accumulation when ice sheet grows, which results in an opposite pattern to that of topography and ice latent heat feedback, i.e., high latitudes warming and low latitudes cooling. As for the sea level feedback, besides the surface temperature anomalies due to the ice thickness change, the sea level drop converts a series of shoreline ocean grids into land grids, raising the surface temperature because of surface latent heat loss.

Synthesizing the all feedback effect, a brief process of ice sheet and climate interaction in the GREB-ISM can be described as following: In response to CO_2 and solar radiation forcing, the initial temperature cooling at a seasonally ice-covered grid point causes longer snowing season, leading to more ice accumulation before melting season. This extra ice accumulation, on the one hand, takes more ice latent heat from surface during melting season, and on the other hand, extends the ice cover period to summer and reflect more shortwave radiation. Both effects enhance the initial local cooling, even though the snowfall decreases, slowing ice sheet growth and corresponding cooling. As the snowing season becomes longer and longer, a permanent ice sheet starts to form and surface elevation lifts. Then, air temperature at ice surface decreases based on lapse rate, further cooling down the surface temperature. After above processes, a large ice sheet forms at a land grid. The vast ice sheets that encircle the Arctic act as a significant barrier to air transport, reducing heat and water vapour mixing between various latitudes and resulting in cooling at the North Pole while warming elsewhere. As a result of massive ice sheets formation, sea level significantly drops, causing many shoreline hotspots due to less heat loss of surface latent heat and northward shift of large ice sheets on Siberia.

Many previous researches have already pointed out that the albedo and topography feedback are two critical feedbacks in ice-age cycle, and albedo feedback is usually more important than topography feedback (Abe-Ouchi et al., 2007; Felzer et al., 1996). However, the climate-ice sheet feedbacks have a strong nonlinear interaction. For example, the ice latent heat feedback also includes the change in surface albedo. To better evaluate the physical process, we not only included more feedbacks in our discussion, but also discussed the nonlinear interaction between different feedbacks.

However, we also need to cover a number of unsolved issues in the future. the seasonality change was not covered in this chapter. The seasonal variations of the surface temperature are generally fairly large due to seasonal ice cover. Nonetheless, the creation of an ice sheet renders the region permanently ice-covered. We skipped over the issue of what causes seasonality to shift and what feedbacks are associated with it.

Similarly, another question is the cause of the ice sheet inertia effect. In the above section, we have discussed two different inertial effect on climate and ice sheet interaction. One is the seasonal inertial effect due to ice latent heat feedback. This inertial effect amplifies the effect of the ice latent heat feedback by causing a nonlinear interaction between various feedbacks. Another one is the long-time scale inertial effect (more than 10 kyr). The ice sheets are a climate component with a long-term variation. As we discussed, it delays the climate response to the external forcing. However, the most important feedback for this inertial effect is still unclear and needs to be further explored.

In addition, our simulation does not count the effect from atmospheric and oceanic general circulation change, which are also recognized as important factors in climate-ice sheet interaction (Felzer et al., 1996; Larour et al., 2012). Furthermore, the real situation in paleoclimate is much complex. We isolated the greenhouse gas and solar insolation forcing in our experiment. But in the real world, the combination of those two forcing is probably causing additional nonlinearity during climate evolution, such as hysteresis of equilibrium states (Abe-Ouchi et al., 2013). Last but not least, GREB-ISM v1.0 still has bias on Southern Hemisphere ice sheet. From our simulation, the Antarctica ice sheet does not have a strong response. Here, even though Antarctica ice sheet is likely to be quite stable, we could not exclude the impact from model bias. The further model development and data analysis is required to solve all above issues.

Chapter 6 Summary and discussion

In this project, we introduced a newly developed global ice sheet model coupled to the GREB model, defining the new model GREB-ISM. The ice sheet is simulated on the global grid fully interacting with the climate simulation on all grid points. The ice sheet mass balance is driven by accumulation of snow, melting by surface heat fluxes and changes due to ice transport. The ice transport follows the shallow ice approximation for grounded ice and shallow shelf approximation for ice shelves. Sea ice-climate interactions are also included.

The GREB-ISM climate simulation interacts with ice sheets through surface temperature, precipitation, albedo, land-sea mask, topography and sea level. To allow for these interactions, the original GREB model was changed by: improving the precipitation simulation of land, including a prognostic sea ice thickness scheme, coupling the surface albedo to the ice thickness, allowing variable land topography as function of ice thickness, introducing global sea level variation and associated changes in land-sea masks and improving the meridional turbulent, atmospheric heat transport. Thus, the new GREB-ISM is a fully coupled atmosphere, ocean, land and ice sheet model.

We next used a number of benchmark experiments to verify the ISM. The ISM is tested using the EISMINT I/II standard experiments, which show that it performs similarly to other ice sheet models. The model's ability to simulate real ice sheets was then assessed by performing dynamic equilibrium of ice sheets today and a transition experiment during the past 200 kyr. Following that, we put the coupled GREB-ISM to the test by replicating current surface temperature, precipitation, sea level, and ice sheets climatology, as well as modelling the climate and ice sheet response to idealised solar forcing. The results indicate the coupled GREB-ISM is capable of simulating key aspects of modern climatology as well as evolution during paleoclimate forcing.

The current version GREB-ISM is a useful tool to explore climate-ice sheet global interaction in ice age cycle. By carrying a series of sensitivity experiments, we explored the process of different climate-ice sheet feedback and also quantified their importance. Including ice sheets in the Earth system tends to increase the climate response time. Meanwhile, ice sheets enhance the initial cooling driven by the external forcing at high latitude and altitude in the Northern Hemisphere and also slightly warm the other latitudes by blocking air transportation. As for individual feedbacks, albedo feedback is the most important positive feedback, contributing the creation of massive ice sheets and temperature decrease, while precipitation feedback is the most pronounced negative feedback, preventing the gigantic ice sheets buildup and associated surface cooling. Moreover, the topography and ice latent heat feedback are both positive feedbacks for ice sheet growth and relevant temperature change, while sea level feedback tends to shift the ice sheet position as well as warming shoreline grids by sea level drop.

The new GREB-ISM model offers us some new perspective to understand paleoclimate change. First, a globally fully coupled model enables us to explore the interaction between the two hemispheres. Most previous studies only simulate north or south hemisphere ice sheet and take the other as prescribed boundary condition (Ganopolski et al., 2010; Tigchelaar et al., 2019). Second, the model is very cheap and it has a high potential to do a fully coupled transition simulation for glacial cycles and sensitivity test. The previous studies pointed out that the ice sheet in paleoclimate has multiple stable equilibria (Abe-Ouchi et al., 2013). Therefore, the simulation of transition is necessary for ice-age cycle processes. For instance, only in transition experiments can we see the ice sheet inertia effect that the longer forcing period leads to stronger ice thickness response (e.g., Fig 4.11).

To test the capability of the GREB-ISM to simulate million years ice-age cycle, we run a series of paleoclimate simulations for 3 million years. In practice, the 3 million years experiment took around 42 days. The simulation is driven by the solar radiation varied based on orbital forcing parameters in last 3 million years under CO_2 concentration of 190, 230 and 280 ppm, respectively. The Fig 6.1 is the global sea level and annual mean temperature variation during the last one million years simulation. The result shows although the sea level simulation has some bias, the GREB-ISM is able to stably simulate the paleoclimate evolution driven by solar radiation and CO_2 concentration forcing. When comparing all three experiments under different CO_2 levels, we can find that CO_2 concentration increase not only rises sea level and warms up climate, but also eliminate the variability of the sea level and surface temperature. Those experiments indicate that it is feasible to simulate million years climate change with the GREB-ISM.

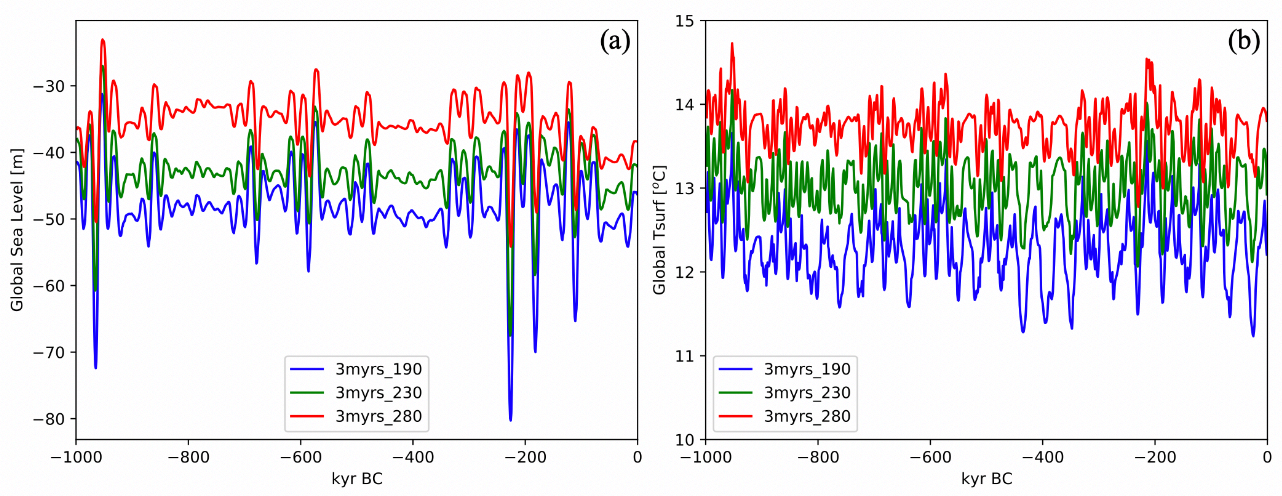

Fig 6.1 Time evolution of the global sea level (a) and mean surface temperature (b) during the last one million years in a three-million-years simulation under last three-million-years orbital forcing and constant CO_2 concentration levels. The “3myrs_190”, “3myrs_230” and “3myrs_280” represent the given CO_2 concentration forcing of 190, 230 and 280 ppm respectively.

In summary, we presented a new model that is suited for the simulations of global-scale climate variability on time scales of 100 kyr and longer. Given the coarse resolution of the model, it may be less suitable for shorter time scale studies. The model is computationally efficient, calculating 100,000 model years global simulations per day on a desktop computer, allowing the simulation of the whole Quaternary period (2.6 Myrs) within one month. For simulations of climate and ice sheet variability over the Quaternary period the GREB-ISM model is, as presented here, a good starting point. Further development may include other relevant climate processes, such as the carbon cycle, deep ocean reservoirs or the ability of the atmosphere and ocean circulation to respond to changes in topography and the climate state, as well as glacial isostatic adjustment. Such further developments are possible within the framework of the GREB-ISM model and will be addressed in future studies.

Code availability

The GREB-ISM v1.0 source code, the model input data as well as a simple user manual are available on Zenodo: https://zenodo.org/badge/latestdoi/372993505.

Reference

Abe-Ouchi, A., Segawa, T. and Saito, F.: Climatic conditions for modelling the Northern Hemisphere ice sheets throughout the ice age cycle, Clim. Past, 3(3), 423–438, doi:10.5194/cp-3-423-2007, 2007.

Abe-Ouchi, A., Saito, F., Kawamura, K., Raymo, M. E., Okuno, J., Takahashi, K. and Blatter, H.: Insolation-driven 100,000-year glacial cycles and hysteresis of ice-sheet volume, Nature, 500(7461), 190–193, doi:10.1038/nature12374, 2013.

Adler, R. F., Huffman, G. J., Chang, A., Ferraro, R., Xie, P. P., Janowiak, J., Rudolf, B., Schneider, U., Curtis, S., Bolvin, D., Gruber, A., Susskind, J., Arkin, P. and Nelkin, E.: The version-2 global precipitation climatology project (GPCP) monthly precipitation analysis (1979-present), J. Hydrometeorol., 4(6), 1147–1167, doi:10.1175/1525-7541(2003)004<1147:TVGPCP>2.0.CO;2, 2003.

Allen, D. J., Douglass, A. R., Rood, R. B. and Guthrie, P. D.: Application of a monotonic upstream-biased transport scheme to three- dimensional constituent transport calculations, Mon. Weather Rev., 119(10), 2456–2464, doi:10.1175/1520-0493(1991)119<2456:AOAMUB>2.0.CO;2, 1991.

Anonymous: Mass-balance terms, J. Glaciol., 8(52), 3–7 [online] Available from: https://www.igsoc.org/journal/8/52/igs_journal_vol08_issue052_pg3-7.pdf (Accessed 23 June 2019), 1969.

Bauska, T. K., Brook, E. J., Marcott, S. A., Baggenstos, D., Shackleton, S., Severinghaus, J. P. and Petrenko, V. V.: Controls on Millennial-Scale Atmospheric CO2 Variability During the Last Glacial Period, Geophys. Res. Lett., 45(15), 7731–7740, doi:10.1029/2018GL077881, 2018.

Behrangi, A., Gardner, A. S. and Wiese, D. N.: Comparative analysis of snowfall accumulation over Antarctica in light of Ice discharge and gravity observations from space, Environ. Res. Lett., 15(10), doi:10.1088/1748-9326/ab9926, 2020.

Bentley, M. J.: Volume of Antarctic Ice at the Last Glacial Maximum, and its impact on global sea level change, Quat. Sci. Rev., 18(14), 1569–1595, doi:10.1016/S0277-3791(98)00118-8, 1999.

Berends, C. J., De Boer, B. and Van De Wal, R. S. W.: Application of HadCM3@Bristolv1.0 simulations of paleoclimate as forcing for an ice-sheet model, ANICE2.1: Set-up and benchmark experiments, Geosci. Model Dev., 11(11), 4657–4675, doi:10.5194/gmd-11-4657-2018, 2018.

Bigg, G. R.: An Estimate of the Flux of Iceberg Calving from Greenland, Arctic, Antarct. Alp. Res., 31(2), 174–178, doi:10.1080/15230430.1999.12003294, 1999.

Bintanja, R. and Van De Wal, R. S. W.: North American ice-sheet dynamics and the onset of 100,000-year glacial cycles, Nature, 454(7206), 869–872, doi:10.1038/nature07158, 2008.

Van Breedam, J., Huybrechts, P. and Crucifix, M.: A Gaussian process emulator for simulating ice sheet-climate interactions on a multi-million-year timescale: CLISEMv1.0, Geosci. Model Dev., 14(10), 6373–6401, doi:10.5194/gmd-14-6373-2021, 2021.

Budyko, M. I.: The effect of solar radiation variations on the climate of the Earth, Tellus, 21(5), 611–619, doi:10.3402/tellusa.v21i5.10109, 1969.

Bueler, E. and Brown, J.: Shallow shelf approximation as a “sliding law” in a thermomechanically coupled ice sheet model, J. Geophys. Res. Solid Earth, 114(3), 1–21, doi:10.1029/2008JF001179, 2009.

Bueler, E., Brown, J. and Lingle, C.: Exact solutions to the thermomechanically coupled shallow-ice approximation: effective tools for verification, J. Glaciol., 53(182), 499–516, doi:10.3189/002214307783258396, 2007.

Bush, A.: Modelling of late Quaternary climate over Asia: a synthesis, Boreas, 33(2), 155–163, doi:10.1111/j.1502-3885.2004.tb01137.x, 2004.

Calov, R. and Ganopolski, A.: Multistability and hysteresis in the climate-cryosphere system under orbital forcing, Geophys. Res. Lett., 32(21), 1–4, doi:10.1029/2005GL024518, 2005.

Carpenter, R. L., Droegemeier, K. K., Woodward, P. R. and Hane, C. E.: Application of the Piecewise Parabolic Method (PPM) to meteorological modeling, Mon. Weather Rev., 118(3), 586–612, doi:10.1175/1520-0493(1990)118<0586:AOTPPM>2.0.CO;2, 1990.

Clark, P. U., Dyke, A. S., Shakun, J. D., Carlson, A. E., Clark, J., Wohlfarth, B., Mitrovica, J. X., Hostetler, S. W. and McCabe, A. M.: The Last Glacial Maximum, Science (80-.)., 325(5941), 710–714, doi:10.1126/science.1172873, 2009.

Colella, P. and Woodward, P. R.: The Piecewise Parabolic Method (PPM) for gas-dynamical simulations, J. Comput. Phys., 54(1), 174–201, doi:10.1016/0021-9991(84)90143-8, 1984.

Cornford, S. L., Seroussi, H., Asay-Davis, X. S., Hilmar Gudmundsson, G., Arthern, R., Borstad, C., Christmann, J., DIas Dos Santos, T., Feldmann, J., Goldberg, D., Hoffman, M. J., Humbert, A., Kleiner, T., Leguy, G., Lipscomb, W. H., Merino, N., Durand, G., Morlighem, M., Pollard, D., Rückamp, M., Rosie Williams, C. and Yu, H.: Results of the third Marine Ice Sheet Model Intercomparison Project (MISMIP+), Cryosphere, 14(7), 2283–2301, doi:10.5194/tc-14-2283-2020, 2020.

Cuzzone, J. K., Schlegel, N. J., Morlighem, M., Larour, E., Briner, J. P., Seroussi, H. and Caron, L.: The impact of model resolution on the simulated Holocene retreat of the southwestern Greenland ice sheet using the Ice Sheet System Model (ISSM), Cryosphere, 13(3), 879–893, doi:10.5194/tc-13-879-2019, 2019.

Deconto, R. M. and Pollard, D.: Rapid Cenozoic glaciation of Antarctica induced by declining atmosheric CO2, Nature, 421(2001), 245–249, 2003.

Dee, D. P., Uppala, S. M., Simmons, A. J., Berrisford, P., Poli, P., Kobayashi, S., Andrae, U., Balmaseda, M. A., Balsamo, G., Bauer, P., Bechtold, P., Beljaars, A. C. M., van de Berg, L., Bidlot, J., Bormann, N., Delsol, C., Dragani, R., Fuentes, M., Geer, A. J., Haimberger, L., Healy, S. B., Hersbach, H., Hólm, E. V., Isaksen, L., Kållberg, P., Köhler, M., Matricardi, M., Mcnally, A. P., Monge-Sanz, B. M., Morcrette, J. J., Park, B. K., Peubey, C., de Rosnay, P., Tavolato, C., Thépaut, J. N. and Vitart, F.: The ERA-Interim reanalysis: Configuration and performance of the data assimilation system, Q. J. R. Meteorol. Soc., 137(656), 553–597, doi:10.1002/qj.828, 2011.

Dommenget, D. and Flöter, J.: Conceptual understanding of climate change with a globally resolved energy balance model, Clim. Dyn., 37(11–12), 2143–2165, doi:10.1007/s00382-011-1026-0, 2011.

Dommenget, D. and Rezny, M.: A Caveat Note on Tuning in the Development of Coupled

Climate Models, J. Adv. Model. Earth Syst., 10(1), 78–97, doi:10.1002/2017MS000947, 2018.

Dommenget, D., Nice, K., Bayr, T., Kasang, D., Stassen, C. and Rezny, M.: The Monash Simple Climate Model Experiments: An interactive database of the mean climate, climate change and scenarios simulations, Geosci. Model Dev., (August), 1–45, doi:https://doi.org/10.5194/gmd-12-2155-2019, 2019.

Ebrahimi, S. and Marshall, S. J.: Surface energy balance sensitivity to meteorological variability on Haig Glacier, Canadian Rocky Mountains, Cryosphere, 10(6), 2799–2819, doi:10.5194/tc-10-2799-2016, 2016.

Edwards, T. L., Fettweis, X., Gagliardini, O., Gillet-Chaulet, F., Goelzer, H., Gregory, J. M., Hoffman, M., Huybrechts, P., Payne, A. J., Perego, M., Price, S., Quiquet, A. and Ritz, C.: Probabilistic parameterisation of the surface mass balance-elevation feedback in regional climate model simulations of the Greenland ice sheet, Cryosphere, 8(1), 181–194, doi:10.5194/tc-8-181-2014, 2014.

F. B. Hildebrand: Introduction to Numerical Analysis, Courier Corporation, North Chelmsford., 1966.

Fairbanks, G.: A 17,000-year glacio-eustatic sea level record: influence of glacial melting rates on the Younger Dryas event and deep-ocean circulation, Nature, 342, 637–642, 1989.

Felzer, B., Oglesby, R. J., Webb, T. and Hyman, D. E.: Sensitivity of a general circulation model to changes in northern hemisphere ice sheets, J. Geophys. Res. Atmos., 101(14), 19077–19092, doi:10.1029/96jd01219, 1996.

Fyke, J., Sergienko, O., Löfverström, M., Price, S. and Lenaerts, J. T. M.: An Overview of Interactions and Feedbacks Between Ice Sheets and the Earth System, Rev. Geophys., 56(2), 361–408, doi:10.1029/2018RG000600, 2018.

Fyke, J. G., Weaver, A. J., Pollard, D., Eby, M., Carter, L. and MacKintosh, A.: A new coupled ice sheet/climate model: Description and sensitivity to model physics under Eemian, Last Glacial Maximum, late Holocene and modern climate conditions, Geosci. Model Dev., 4(1), 117–136, doi:10.5194/gmd-4-117-2011, 2011.

Ganopolski, A. and Brovkin, V.: Simulation of climate, ice sheets and CO2 evolution during the last four glacial cycles with an Earth system model of intermediate complexity, Clim. Past, 13(12), 1695–1716, doi:10.5194/cp-13-1695-2017, 2017.

Ganopolski, A., Calov, R. and Claussen, M.: Simulation of the last glacial cycle with a coupled climate ice-sheet model of intermediate complexity, Clim. Past, 6(2), 229–244, doi:10.5194/cp-6-229-2010, 2010.

Gardner, A. S. and Sharp, M. J.: A review of snow and ice albedo and the development of a new physically based broadband albedo parameterization, J. Geophys. Res. Earth Surf., 115(1), 1–15, doi:10.1029/2009JF001444, 2010.

Gates, W. L.: Modeling the Ice-Age Climate, Science (80-.)., 191(4232), 1138–1144, doi:10.1126/science.191.4232.1138, 1976.

Glen, J. W.: Rate of flow of polycrystalline ice, Nature, 172(4381), 721–722, doi:10.1038/172721a0, 1953.

Glen, J. W.: The Stability of Ice-Dammed Lakes and other Water-Filled Holes in Glaciers, J. Glaciol., 2(15), 316–318, doi:10.3189/s0022143000025132, 1954.

Glen, J. W.: The creep of polycrystalline ice, Proc. R. Soc. London. Ser. A. Math. Phys. Sci., 228(1175), 519–538, doi:10.1098/rspa.1955.0066, 1955.

Gomez, N., Weber, M. E., Clark, P. U., Mitrovica, J. X. and Han, H. K.: Antarctic ice dynamics amplified by Northern Hemisphere sea-level forcing, Nature, 587(7835), 600–604, doi:10.1038/s41586-020-2916-2, 2020.

Goosse, H., Kay, J. E., Armour, K. C., Bodas-Salcedo, A., Chepfer, H., Docquier, D., Jonko, A., Kushner, P. J., Lecomte, O., Massonnet, F., Park, H. S., Pithan, F., Svensson, G. and Vancoppenolle, M.: Quantifying climate feedbacks in polar regions, Nat. Commun., 9(1), doi:10.1038/s41467-018-04173-0, 2018.

Greve, R.: Application of a polythermal three-dimensional ice sheet model to the Greenland Ice Sheet: Response to steady-state and transient climate scenarios, J. Clim., 10(5), 901–918, doi:10.1175/1520-0442(1997)010<0901:AOAPTD>2.0.CO;2, 1997.

Greve, R. and Blatter, H.: Dynamics of Ice Sheets and Glaciers, Springer, Berlin., 2009.

Hakuba, M. Z., Folini, D., Wild, M. and Schr, C.: Impact of Greenland's topographic height on precipitation and snow accumulation in idealized simulations, J. Geophys. Res. Atmos., 117(9), 1–15, doi:10.1029/2011JD017052, 2012.

Han, H. K., Gomez, N., Pollard, D. and DeConto, R.: Modeling Northern Hemispheric Ice Sheet Dynamics, Sea Level Change, and Solid Earth Deformation Through the Last Glacial Cycle, J. Geophys. Res. Earth Surf., 126(4), 1–15, doi:10.1029/2020JF006040, 2021.

Herrington, A. R. and Poulsen, C. J.: Terminating the last interglacial: The role of ice sheet-climate feedbacks in a GCM asynchronously coupled to an ice sheet model, J. Clim., 25(6), 1871–1882, doi:10.1175/JCLI-D-11-00218.1, 2012.

Hock, R.: Temperature index melt modelling in mountain areas, J. Hydrol., 282, 104--115 [online] Available from: https://www.sciencedirect.com/science/article/pii/S0022169403002579 (Accessed 23 June 2019), 2003.

Hock, R.: Glacier melt: A review of processes and their modelling, Prog. Phys. Geogr., 29(3), 362–391, doi:10.1191/0309133305pp453ra, 2005.

Hogg, A. M. C.: Glacial cycles and carbon dioxide: A conceptual model, Geophys. Res. Lett., 35(1), 1–5, doi:10.1029/2007GL032071, 2008.

Hutter, K.: Theoretical glaciology: material science of ice and the mechanics of glaciers and ice sheets., 1983.

Huybers, P.: Combined obliquity and precession pacing of late Pleistocene deglaciations, Nature, 480(7376), 229–232, doi:10.1038/nature10626, 2011.

Huybrechts, P.: Sea-level changes at the LGM from ice-dynamic reconstructions of the Greenland and Antarctic ice sheets during the glacial cycles, Quat. Sci. Rev., 21(1–3), 203–231, doi:10.1016/S0277-3791(01)00082-8, 2002.

Huybrechts, P., Payne, T., Abe-Ouchi, A., Calov, R., Fabre, A., Fastook, J. L., Greve, R., Hindmarsh, R. C. A., Hoydal, O., Jóhannesson, T., MacAyeal, D. R., Marsiat, I., Ritz, C., Verbitsky, M. Y., Waddington, E. D. and Warner, R.: The EISMINT benchmarks for testing ice-sheet models, Ann. Glaciol., 23, 1–12, doi:10.3189/s0260305500013197, 1996.

Imbrie, J.: Astronomical theory of the Pleistocene ice ages: A brief historical review, Icarus, 50(2–3), 408–422, doi:10.1016/0019-1035(82)90132-4, 1982.

Imbrie, J., Hays, J. D., Martinson, D. G., Mclntyre, A., Mix, A. C., Morley, J. J., Pisias, N. G., Prell and, W. L. and Shackleton, N. J.: The orbital theory of Pleistocene climate: support from a revised chronology of the marine d18O record, Milankovitch Clim., (January), 269–305, 1984.

Irvine, P. J., Gregoire, L. J., Lunt, D. J. and Valdes, P. J.: An efficient method to generate a perturbed parameter ensemble of a fully coupled AOGCM without flux-adjustment, Geosci. Model Dev., doi:10.5194/gmd-6-1447-2013, 2013.

Johnsen, S., Clausen, H. B., Dansgaard, W., Gundestrup, N. S., Hammer, C. U., Andersen, U., Andersen, K. K., Hvidberg, C. S., Steffensen, P., White, J., Jouzel, J. and Fisher, D.: core and the problem of possible Eemian climatic instability, J. Geophys. Res., 102(97), 26,397-26,410, 1997.

Joughin, I.: Measures greenland annual ice sheet velocity mosaics from sar and landsat, version 1, NASA Natl. Snow Ice Data Cent. Distrib. Act. Arch. Center, Boulder, Color. USA, 2017.

Joughin, I., Smith, B. E., Howat, I. M., Scambos, T. and Moon, T.: Greenland flow variability from ice-sheet-wide velocity mapping, J. Glaciol., 56(197), 415–430, doi:10.3189/002214310792447734, 2010.

Kageyama, M., Albani, S., Braconnot, P., Harrison, S. P., Hopcroft, P. O., Ivanovic, R. F., Lambert, F., Marti, O., Richard Peltier, W., Peterschmitt, J. Y., Roche, D. M., Tarasov, L., Zhang, X., Brady, E. C., Haywood, A. M., Legrande, A. N., Lunt, D. J., Mahowald, N. M., Mikolajewicz, U., Nisancioglu, K. H., Otto-Bliesner, B. L., Renssen, H., Tomas, R. A., Zhang, Q., Abe-Ouchi, A., Bartlein, P. J., Cao, J., Li, Q., Lohmann, G., Ohgaito, R., Shi, X., Volodin, E., Yoshida, K., Zhang, X. and Zheng, W.: The PMIP4 contribution to CMIP6 - Part 4: Scientific objectives and experimental design of the PMIP4-CMIP6 Last Glacial Maximum experiments and PMIP4 sensitivity experiments, Geosci. Model Dev., 10(11), 4035–4055, doi:10.5194/gmd-10-4035-2017, 2017.

Kageyama, M., Braconnot, P., Harrison, S. P., Haywood, A. M., Jungclaus, J. H., Otto-Bliesner, B. L., Peterschmitt, J., Abe-Ouchi, A., Albani, S., Bartlein, P. J., Brierley, C., Crucifix, M., Dolan, A., Fernandez-Donado, L., Fischer, H., Hopcroft, P. O., Ivanovic, R. F., Lambert, F., Lunt, D. J., Mahowald, N. M., Peltier, W. R., Phipps, S. J., Roche, D. M., Schmidt, G. A., Tarasov, L., Valdes, P. J., Zhang, Q. and Zhou, T.: The PMIP4 contribution to CMIP6 – Part 1: Overview and over-arching analysis plan, Geosci. Model Dev., 11(3), 1033–1057, doi:10.5194/gmd-11-1033-2018, 2018.

Kageyama, M., Harrison, S. P., Kapsch, M. L., Lofverstrom, M., Lora, J. M., Mikolajewicz, U., Sherriff-Tadano, S., Vadsaria, T., Abe-Ouchi, A., Bouttes, N., Chandan, D., Gregoire, L. J., Ivanovic, R. F., Izumi, K., Legrande, A. N., Lhardy, F., Lohmann, G., Morozova, P. A., Ohgaito, R., Paul, A., Richard Peltier, W., Poulsen, C. J., Quiquet, A., Roche, D. M., Shi, X., Tierney, J. E., Valdes, P. J., Volodin, E. and Zhu, J.: The PMIP4 Last Glacial Maximum experiments: Preliminary results and comparison with the PMIP3 simulations, Clim. Past, 17(3), 1065–1089, doi:10.5194/cp-17-1065-2021, 2021.

Kalnay, E., Collins, W., Deaven, D., Gandin, L., Iredell, M., Jenne, R. and Joseph, D.: The NCEP/NCAR 40-year reanalysis project, Bull. Am. Meteorol. Soc., 77(3), 437–472, doi:https://doi.org/10.1175/1520-0477(1996)077<0437:TNYRP>2.0.CO;2, 1996.

Kanamitsu, M., Ebisuzaki, W., Woollen, J., Yang, S. K., Hnilo, J. J., Fiorino, M. and Potter, G. L.: NCEP-DOE AMIP-II reanalysis (R-2), Bull. Am. Meteorol. Soc., 83(11), 1631–1644, doi:10.1175/bams-83-11-1631, 2002.

Kapsch, M. L., Mikolajewicz, U., Ziemen, F. A., Rodehacke, C. B. and Schannwell, C.: Analysis of the surface mass balance for deglacial climate simulations, Cryosphere, 15(2), 1131–1156, doi:10.5194/tc-15-1131-2021, 2021.

Lambeck, K., Rouby, H., Purcell, A., Sun, Y. and Sambridge, M.: Sea level and global ice volumes from the Last Glacial Maximum to the Holocene, Proc. Natl. Acad. Sci. U. S. A., 111(43), 15296–15303, doi:10.1073/pnas.1411762111, 2014.

Larour, E., Seroussi, H., Morlighem, M. and Rignot, E.: Continental scale, high order, high spatial resolution, ice sheet modeling using the Ice Sheet System Model (ISSM), J. Geophys. Res. Earth Surf., 117(1), doi:10.1029/2011JF002140, 2012.

Leguy, G. R., Lipscomb, W. H. and Asay-Davis, X. S.: Marine ice sheet experiments with the

Community Ice Sheet Model, Cryosphere, 15(7), 3229–3253, doi:10.5194/tc-15-3229-2021, 2021.

Levermann, A., Albrecht, T., Winkelmann, R., Martin, M. A., Haseloff, M. and Joughin, I.: Kinematic first-order calving law implies potential for abrupt ice-shelf retreat, Cryosphere, 6(2), 273–286, doi:10.5194/tc-6-273-2012, 2012.

Lin, S. J. and Rood, R. B.: Multidimensional flux-form semi-Lagrangian transport schemes, Mon. Weather Rev., 124(9), 2046–2070, doi:10.1175/1520-0493(1996)124<2046:MFFSLT>2.0.CO;2, 1996.

Lin, S. J. and Rood, R. B.: An explicit flux-form semi-Lagrangian shallow-water model on the sphere, Q. J. R. Meteorol. Soc., 123(544), 2477–2498, doi:10.1002/qj.49712354416, 1997.

Lin, S. J., Chao, W. C., Sud, Y. C. and Walker, G. K.: A class of the van Leer-type transport schemes and its application to the moisture transport in a general circulation model, Mon. Weather Rev., 122(7), 1575–1593, doi:10.1175/1520-0493(1994)122<1575:acotvl>2.0.co;2, 1994.

Liu, Y., Moore, J. C., Cheng, X., Gladstone, R. M., Bassis, J. N., Liu, H., Wen, J. and Hui, F.: Ocean-driven thinning enhances iceberg calving and retreat of Antarctic ice shelves, Proc. Natl. Acad. Sci. U. S. A., 112(11), 3263–3268, doi:10.1073/pnas.1415137112, 2015.

Löfverström, M. and Liakka, J.: On the limited ice intrusion in Alaska at the LGM, Geophys. Res. Lett., 43(20), 11,030-11,038, doi:10.1002/2016GL071012, 2016.

Lorbacher, K., Dommenget, D., Niiler, P. P. and Köhl, A.: Ocean mixed layer depth: A subsurface proxy of ocean-atmosphere variability, J. Geophys. Res. Ocean., 111(7), 1–22, doi:10.1029/2003JC002157, 2006.

Macayeal, D. R.: Large-scale ice flow over a viscous basal sediment: theory and application to ice stream B, Antarctica, J. Geophys. Res., 94(134), 4071–4087, doi:10.1029/jb094ib04p04071, 1989.

Manabe, S. and Broccoli, A. J.: The Influence of Continental Ice Sheets on the Climate of an Ice Age, J. Geophys. Res., 90(D1), 2167– 2190, doi:https://doi.org/10.1029/JD090iD01p02167, 1985.

Maris, M. N. A., van Wessem, J. M., van de Berg, W. J., de Boer, B. and Oerlemans, J.: A model study of the effect of climate and sea-level change on the evolution of the Antarctic Ice Sheet from the Last Glacial Maximum to 2100, Clim. Dyn., 45(3–4), 837–851, doi:10.1007/s00382-014-2317-z, 2015.

Marshall, S. J. and Miller, K.: Seasonal and interannual variability of melt-season albedo at Haig Glacier, Canadian Rocky Mountains, Cryosphere, 14(10), 3249–3267, doi:10.5194/tc-14-3249-2020, 2020.

Martin, M. A., Winkelmann, R., Haseloff, M., Albrecht, T., Bueler, E., Khroulev, C. and Levermann, A.: The Potsdam Parallel Ice Sheet Model (PISM-PIK) - Part 2: Dynamic equilibrium simulation of the Antarctic ice sheet, Cryosphere, 5(3), 727–740, doi:10.5194/tc-5-727-2011, 2011.

Medley, B. and Thomas, E. R.: Increased snowfall over the Antarctic Ice Sheet mitigated twentieth-century sea-level rise, Nat. Clim. Chang., 9(1), 34–39, doi:10.1038/s41558-018-0356-x, 2019.

Milankovitch, M.: Kanon der Erdbestrahlung und seine Anwendung auf das Eiszeitenproblem, Belgrade., 1941.

Mix, A. C., Bard, E. and Schneider, R.: Environmental processes of the ice age: Land, oceans, glaciers (EPILOG), Quat. Sci. Rev., 20(4), 627–657, doi:10.1016/S0277-3791(00)00145-1, 2001.

Morland, L. W.: Thermomechanical Balances of Ice Sheet Flows, Geophys. Astrophys. Fluid Dyn., 29, 237–266, doi:10.1080/03091928408248191, 1984.

Morlighem, M., Williams, C. N., Rignot, E., An, L., Arndt, J. E., Bamber, J. L., Catania, G., Chauché, N., Dowdeswell, J. A., Dorschel, B., Fenty, I., Hogan, K., Howat, I., Hubbard, A., Jakobsson, M., Jordan, T. M., Kjeldsen, K. K., Millan, R., Mayer, L., Mouginot, J., Noël, B. P. Y., O'Cofaigh, C., Palmer, S., Rysgaard, S., Seroussi, H., Siegert, M. J., Slabon, P., Straneo, F., van den Broeke, M. R., Weinrebe, W., Wood, M. and Zinglersen, K. B.: BedMachine v3: Complete Bed Topography and Ocean Bathymetry Mapping of Greenland From Multibeam Echo Sounding Combined With Mass Conservation, Geophys. Res. Lett., 44(21), 11,051-11,061, doi:10.1002/2017GL074954, 2017.

Morlighem, M., Rignot, E., Binder, T., Blankenship, D., Drews, R., Eagles, G., Eisen, O., Ferraccioli, F., Forsberg, R., Fretwell, P., Goel, V., Greenbaum, J. S., Gudmundsson, H., Guo, J., Helm, V., Hofstede, C., Howat, I., Humbert, A., Jokat, W., Karlsson, N. B., Lee, W. S., Matsuoka, K., Millan, R., Mouginot, J., Paden, J., Pattyn, F., Roberts, J., Rosier, S., Ruppel, A., Seroussi, H., Smith, E. C., Steinhage, D., Sun, B., Broeke, M. R. va. den, Ommen, T. D. va., Wessem, M. van and Young, D. A.: Deep glacial troughs and stabilizing ridges unveiled beneath the margins of the Antarctic ice sheet, Nat. Geosci., 13(2), 132–137, doi:10.1038/s41561-019-0510-8, 2020.

Mouginot, J., Scheuch, B. and Rignot, E.: Mapping of ice motion in antarctica using synthetic-aperture radar data, Remote Sens., 4(9), 2753–2767, doi:10.3390/rs4092753, 2012.

Nicholl, J. A. L., Hodell, D. A., Naafs, B. D. A., Hillaire-Marcel, C., Channell, J. E. T. and Romero, O. E.: A Laurentide outburst flooding event during the last interglacial period, Nat. Geosci., 5(12), 901–904, doi:10.1038/ngeo1622, 2012.

Nicholls, R. J. Z., Meinshausen, M., Lewis, J., Gieseke, R., Dommenget, D., Dorheim, K., Fan5, C. S., Fuglestvedt, J. S., Gasser, T., Goluke, U., Goodwin, P., Hartin, C., P. Hope, A., Kriegler, E., J. Leach, N., Marchegiani, D., A. McBride, L., Quilcaille, Y., Rogelj, J., J. Salawitch, R., Samset, B. H., Sandstad, M., N. Shiklomanov, A., B. Skeie, R., J. Smith, C., Smith, S., Tanaka, K., Tsutsui, J. and Xie, Z.: Reduced Complexity Model Intercomparison Project Phase 1: Introduction and evaluation of global-mean temperature response, Geosci. Model Dev., 13(11), 5175–5190, doi:10.5194/gmd-13-5175-2020, 2020.

Niu, L., Lohmann, G., Hinck, S., Gowan, E. J. and Krebs-Kanzow, U.: The sensitivity of Northern Hemisphere ice sheets to atmospheric forcing during the last glacial cycle using PMIP3 models, J. Glaciol., 65(252), 645–661, doi:10.1017/jog.2019.42, 2019.

Nowicki, S. M. J., Payne, A., Larour, E., Seroussi, H., Goelzer, H., Lipscomb, W., Gregory, J., Abe-Ouchi, A. and Shepherd, A.: Ice Sheet Model Intercomparison Project (ISMIP6) contribution to CMIP6, Geosci. Model Dev., 9(12), 4521–4545, doi:10.5194/gmd-9-4521-2016, 2016.

Otto-Bliesner, B. L., Braconnot, P., Harrison, S. P., Lunt, D. J., Abe-Ouchi, A., Albani, S., Bartlein, P. J., Capron, E., Carlson, A. E., Dutton, A., Fischer, H., Goelzer, H., Govin, A., Haywood, A., Joos, F., LeGrande, A. N., Lipscomb, W. H., Lohmann, G., Mahowald, N., Nehrbass-Ahles, C., Pausata, F. S. R., Peterschmitt, J.-Y., Phipps, S. J., Renssen, H. and Zhang, Q.: The PMIP4 contribution to CMIP6 – Part 2: Two interglacials, scientific objective and experimental design for Holocene and Last Interglacial simulations, Geosci. Model Dev., 10(11), 3979–4003, doi:10.5194/gmd-10-3979-2017, 2017.

Overpeck, J. T., Otto-Bliesner, B. L., Miller, G. H., Muhs, D. R., Alley, R. B. and Kiehl, J. T.: Paleoclimatic evidence for future ice-sheet instability and rapid sea-level rise, Science (80-.)., 311(5768), 1747–1750, doi:10.1126/science.1115159, 2006.

Parry, M. L., Change, C., Watson, R. T., Zinyowera, M. C., Moss, R. H., Burke, M. B. and Lobell, D. B.: Sr-Nd-Pb Isotope Evidence for, Science, 333(July), 620–623, 2011.

Patel, A., Goswami, A., Dharpure, J. K., Thamban, M., Sharma, P., Kulkarni, A. V. and Oulkar, S.: Estimation of mass and energy balance of glaciers using a distributed energy balance model over the Chandra river basin (Western Himalaya), Hydrol. Process., 35(2), 1–22, doi:10.1002/hyp.14058, 2021.

Pattyn, F.: A new three-dimensional higher-order thermomechanical ice sheet model: Basic sensitivity, ice stream development, and ice flow across subglacial lakes, J. Geophys. Res., 108(B8), 1–15, doi:10.1029/2002jb002329, 2003.

Pattyn, F., Schoof, C., Perichon, L., Hindmarsh, R. C. A., Bueler, E., De Fleurian, B., Durand, G., Gagliardini, O., Gladstone, R., Goldberg, D., Gudmundsson, G. H., Huybrechts, P., Lee, V., Nick, F. M., Payne, A. J., Pollard, D., Rybak, O., Saito, F. and Vieli, A.: Results of the marine ice sheet model intercomparison project, MISMIP, Cryosphere, 6(3), 573–588, doi:10.5194/tc-6-573-2012, 2012.

Pattyn, F., Perichon, L., Durand, G., Favier, L., Gagliardini, O., Hindmarsh, R. C. A., Zwinger, T., Albrecht, T., Cornford, S., Docquier, D., Fürst, J. J., Goldberg, D., Gudmundsson, G. H., Humbert, A., Hütten, M., Huybrechts, P., Jouvet, G., Kleiner, T., Larour, E., Martin, D., Morlighem, M., Payne, A. J., Pollard, D., Rückamp, M., Rybak, O., Seroussi, H., Thoma, M. and Wilkens, N.: Grounding-line migration in plan-view marine ice-sheet models: Results of the ice2sea MISMIP3d intercomparison, J. Glaciol., 59(215), 410–422, doi:10.3189/2013JoG12J129, 2013.

Payne, A. J., Huybrechts, P., Abe-Ouchi, A., Calov, R., Fastook, J. L., Greve, R., Marshall, S. J., Marsiat, I., Ritz, C., Tarasov, L. and Thomassen, M. P. A.: Results from the EISMINT model intercomparison: The effects of thermomechanical coupling, J. Glaciol., 46(153), 227–238, doi:10.3189/172756500781832891, 2000.

Petit, J. R., Jouzel, J., Raynaud, D., Barkov, N. I., Barnola, J.-M., Basile, I., Bender, M., Chappellaz, J., Davis, M., Delaygue, G., Delmotte, M., Kotlyakov, V. M., Legrand, M., Lipenkov, V. Y., Lorius, C., PÉpin, L., Ritz, C., Saltzman, E. and Stievenard, M.: Climate and atmospheric history of the past 420,000 years from the Vostok ice core, Antarctica, Nature, 399(6735), 429–436, doi:10.1038/20859, 1999.

Pollard, D.: A retrospective look at coupled ice sheet-climate modeling, Clim. Change, 100(1), 173–194, doi:10.1007/s10584-010-9830-9, 2010.

Pollard, D. and Deconto, R. M.: Description of a hybrid ice sheet-shelf model, and application to Antarctica, Geosci. Model Dev., 5(5), 1273–1295, doi:10.5194/gmd-5-1273-2012, 2012.

Pollard, D. and DeConto, R. M.: Modelling West Antarctic ice sheet growth and collapse through the past five million years, Nature, 458(7236), 329–332, doi:10.1038/nature07809, 2009.

Pollard, D., Kump, L. R. and Zachos, J. C.: Interactions between carbon dioxide, climate, weathering, and the Antarctic ice sheet in the earliest Oligocene, Glob. Planet. Change, 111, 258–267, doi:10.1016/j.gloplacha.2013.09.012, 2013.

Pollard, D., DeConto, R. M. and Alley, R. B.: Potential Antarctic Ice Sheet retreat driven by hydrofracturing and ice cliff failure, Earth Planet. Sci. Lett., 412, 112–121, doi:10.1016/j.epsl.2014.12.035, 2015.

Rayner, N. A., Parker, D. E., Horton, E. B., Folland, C. K., Alexander, L. V., Rowell, D. P., Kent, E. C. and Kaplan, A.: Global analyses of sea surface temperature, sea ice, and night marine air temperature since the late nineteenth century, J. Geophys. Res. Atmos., 108(14), 4407, doi:10.1029/2002jd002670, 2003.

Rignot, E., Mouginot, J. and Scheuchl, B.: Ice flow of the antarctic ice sheet, Science (80-.)., 333(6048), 1427–1430, doi:10.1126/science.1208336, 2011.

Rignot, E., Mouginot, J. and Scheuchl, B.: MEaSUREs InSAR-based Antarctica ice velocity map, version 2, Boulder, Color. USA. NASA Natl. Snow Ice Data Cent. Distrib. Act. Arch. Center. doi https//doi. org/10.5067/D7GK8F5J8M8R, 2017.

Risebrobakken, B., Dokken, T., Otterå, O. H., Jansen, E., Gao, Y. and Drange, H.: Inception of the Northern European ice sheet due to contrasting ocean and insolation forcing, Quat. Res., 67(1), 128–135, doi:10.1016/j.yqres.2006.07.007, 2007.

Robinson, D., David, A., Estilow, T. and Program, N. C.: NOAA Climate Date Record (CDR) of Northern Hemisphere (NH) Snow Cover Extent (SCE), Version 1., NOAA Natl. Clim. Data Cent., 137–142, doi:10.7289/V5N014G9, 2012.

Roche, D. M., Dumas, C., Bügelmayer, M., Charbit, S. and Ritz, C.: Adding a dynamical cryosphere to iLOVECLIM (version 1.0): Coupling with the GRISLI ice-sheet model, Geosci. Model Dev., 7(4), 1377–1394, doi:10.5194/gmd-7-1377-2014, 2014.

Rood, R. B.: Numerical advection algorithms and their role in atmospheric transport and chemistry models, Rev. Geophys., 25(1), 71–100, doi:10.1029/RG025i001p00071, 1987.

Rossow, W. B. and Schiffer, R. A.: ISCCP cloud data products, Bull. - Am. Meteorol. Soc., 72(1), 2–20, doi:10.1175/1520-0477(1991)072<0002:ICDP>2.0.CO;2, 1991.

Ryan, J. C., Smith, L. C., Van As, D., Cooley, S. W., Cooper, M. G., Pitcher, L. H. and Hubbard, A.: Greenland Ice Sheet surface melt amplified by snowline migration and bare ice exposure, Sci. Adv., 5(3), 1–11, doi:10.1126/sciadv.aav3738, 2019.

Schneider, E. K.: Flux correction and the simulation of changing climate, Ann. Geophys., 14, 336–341, doi:10.1007/s00585-996-0336-8, 1996.

Schoof, C.: Ice sheet grounding line dynamics: Steady states, stability, and hysteresis, J. Geophys. Res. Earth Surf., 112(3), 1–19, doi:10.1029/2006JF000664, 2007a.

Schoof, C.: Marine ice-sheet dynamics. Part 1. The case of rapid sliding, J. Fluid Mech., 573, 27–55, doi:10.1017/S0022112006003570, 2007b.

Shackelton, N. J.: The 100,000-year ice-age cycle identified and found to lag temperature, carbon dioxide, and orbital eccentricity, Science (80-.)., 289(5486), 1897–1902, doi:10.1126/science.289.5486.1897, 2000.

Shi, X., Yang, H., Danek, C. and Lohmann, G.: AWI AWI-ESM1.1LR model output prepared for CMIP6 PMIP, , doi:10.22033/ESGF/CMIP6.9302, 2020.

Short, D. A., Mengel, J. G., Crowley, T. J., Hyde, W. T. and North, G. R.: Filtering of Milankovitch Cycles by Earth's Geography, Quat. Res., 35(2), 157–173, doi:10.1016/0033-5894(91)90064-c, 1991.

Stassen, C., Dommenget, D. and Loveday, N.: A hydrological cycle model for the Globally Resolved Energy Balance (GREB) model v1.0, Geosci. Model Dev., 12(1), 425–440, doi:10.5194/gmd-12-425-2019, 2019.

Suarez, M. J. and Takacs, L. L.: Technical report series on global modeling and data assimilation. Volume 5: Documentation of the ARIES/GEOS dynamical core, version 2., 1995.

Sundquist, E. T. (Eric T. ., Broecker, W. S., American Geophysical Union. and Chapman Conference on Natural Variations in Carbon Dioxide and the Carbon Cycle (1984 : Tarpon Springs, F. .: The Carbon cycle and atmospheric CO_2 : natural variations, Archean to present, American Geophysical Union., 1985.

Tabor, C. R., Poulsen, C. J. and Pollard, D.: How obliquity cycles powered early Pleistocene global ice-volume variability, Geophys. Res. Lett., 42(6), 1871–1879, doi:10.1002/2015GL063322, 2015.

Tigchelaar, M., Timmermann, A., Friedrich, T., Heinemann, M. and Pollard, D.: Nonlinear response of the Antarctic Ice Sheet to late Quaternary sea level and climate forcing, Cryosphere, 13(10), 2615–2631, doi:10.5194/tc-13-2615-2019, 2019.

Velichko, A. A., Kononov, Y. M. and Faustova, M. A.: The last glaciation of earth: Size and volume of ice-sheets, Quat. Int., 41–42(96), 43–51, doi:10.1016/s1040-6182(96)00035-3, 1997.

Webb, T., Anderson, K. H., Bartlein, P. J. and Webb, R. S.: Late Quaternary climate change in eastern North America: A comparison of pollen-derived estimates with climate model results, Quat. Sci. Rev., 17(6–7), 587–606, doi:10.1016/S0277-3791(98)00013-4, 1998.

Willeit, M. and Ganopolski, A.: The importance of snow albedo for ice sheet evolution over the last glacial cycle, Clim. Past, 14(5), 697–707, doi:10.5194/cp-14-697-2018, 2018.

Willeit, M., Ganopolski, A., Calov, R. and Brovkin, V.: Mid-Pleistocene transition in glacial cycles explained by declining CO2 and regolith removal, Sci. Adv., 5(4), 1–9, doi:10.1126/sciadv.aav7337, 2019.

Winkelmann, R., Martin, M. A., Haseloff, M., Albrecht, T., Bueler, E., Khroulev, C. and Levermann, A.: The Potsdam Parallel Ice Sheet Model (PISM-PIK) - Part 1: Model description, Cryosphere, 5(3), 715–726, doi:10.5194/tc-5-715-2011, 2011.

Wunsch, C.: Quantitative estimate of the Milankovitch-forced contribution to observed Quaternary climate change, Quat. Sci. Rev., 23(9–10), 1001–1012, doi:10.1016/j.quascirev.2004.02.014, 2004.

Zeitz, M., Reese, R., Beckmann, J., Krebs-Kanzow, U. and Winkelmann, R.: Impact of the melt-albedo feedback on the future evolution of the Greenland Ice Sheet with PISM-dEBM-simple, Cryosph. Discuss., (March), 1–32, doi:10.5194/tc-2021-91, 2021.

Zhang, X., Lohmann, G., Knorr, G. and Purcell, C.: Abrupt glacial climate shifts controlled by ice sheet changes, Nature, 512(7514), 290–294, doi:10.1038/nature13592, 2014.

Symbols and Parameters List

variable name	symbol	dimensions	value/unit
ice sheet softness parameter	A	t	Pa m^{-3}
softness parameter in isotherm case	A_0	constant	1.96×10^{3} Pa m^{-3} (T'>-10°C) 3.99×10^{-13} Pa m^{-3} (T'<-10°C)
ocean area	A_{ocean}	t	m^2
ablation rate	a	x, y, t	m s^{-1}
bed rock elevation	b	x, y, t	m
specific heat capacity for ice	C_p	constant	2009 J kg^{-1} K^{-1}
slide law coefficient for basal velocity	C_{sl}	constant	$6\times10^{4}yr^{-1}$
regression coefficient for ice temperature	c_i for i from 0 to 3	x, y, t	K
precipitation parameter for relative humidity	c_{rq}	constant	$Pa^{-1}s$
sensible heat bulk coefficient	ct_{sense}	constant	22.5 $W\ m^{-2}\ K^{-1}$
precipitation parameter for vertical velocity	c_{ω}	constant	$Pa^{-1}s$
precipitation parameter for standard deviation of vertical velocity	$c_{\omega SD}$	constant	$Pa^{-2}s^{2}$
enhance factor for SIA	E	constant	3
net longwave radiation for T_{atmos}	$Fa_{thermal}$	x, y, t	W m^{-2}
surface flux correction	$F_{correct}$	x, y, t	W m^{-2}
ice latent heat flux	F_{ice}	x, y, t	W m^{-2}
latent heat flux	F_{latent}	x, y, t	W m^{-2}
total heat flux for melting all ice	$Fmax_{melt}$	x, y, t	W m^{-2}
net heat flux without ice latent heat	F_{net}	x, y, t	W m^{-2}

land-sea heat difference	F_{ocean}	x, y, t	W m^{-2}
ocean heat flux correction	$Fo_{correct}$	x, y, t	W m^{-2}
sensible heat flux between ocean and surface	Fo_{sense}	x, y, t	W m^{-2}
sensible heat flux between air and surface	F_{sense}	x, y, t	W m^{-2}
solar radiation	F_{solar}	x, y, t	W m^{-2}
surface net heat flux without ice	F_{surf}	x, y, t	W m^{-2}
net longwave radiation for T_{surf}	$F_{thermal}$	x, y, t	W m^{-2}
geothermal heat flux	G	constant	4.2×10^{-2} W m^{-2}
ice thickness	H	x, y, t	m
ice thickness reference for 0 sea level	H_{ref}	x, y, t	m
latent heat flux of fusion	L_m	constant	3.335×10^5 J kg^{-1}
precipitation	p	x, y, t	m s^{-1}
precipitation correction	$p_{correct}$	x, y, t	kg kg^{-1} s^{-1}
activate energy	Q	constant	1.39×10^5 $(T' > -10^oC)$ 6.4×10^4 $(T' < -10^oC)$
latent heat flux in air	Q_{latent}	x, y, t	W m^{-2}
air specific humidity	q_{air}	x, y, t	kg kg^{-1}
zonal specific humidity mean	q_{zonal}	x, y, t	kg kg^{-1}
universal gas constant	R	constant	8.314 J mol^{-1} K^{-1}
snowfall rate	r	x, y, t	unitless
Earth radius	r_e	constant	$6.37 \times 10^6 m$
relative humidity	rq	x,y,t	unitless
Mean lifetime of water vapour	r_{precip}	constant	$kg\ kg^{-1}\ s^{-1}$
ice accumulation rate (snowfall)	s	x, y, t	m s^{-1}
sea level	slv	t	m
ice strata temperature	T	x, y, z, t	K

homologous temperature corrected by pressure melting point	T'	x, y, z, t	K
air temperature	T_{atmos}	x, y, t	K
ice melting temperature	T_m	x, y, z, t	K
ocean temperature	T_{ocean}	x, y, t	K
estimated temperature without ice latent heat	T_{se}	x, y	K
sea water frozen temperature	T_{sm}	constant	$271.45K$
surface temperature	T_{surf}	x, y, t	K
ice vertical velocity	w	x, y, z, t	m s^{-1}
wind velocity at 850hPa	$\vec{u}$	x, y	m s^{-1}
ice flow horizontal velocity (strata)	$\vec{V}$	x, y, z, t	m s^{-1}
ice flow horizontal velocity (base)	$\vec{V}_b$	x, y, t	m s^{-1}
ice flow horizontal velocity (vertical mean)	$\vec{V}_m$	x, y, t	m s^{-1}
surface velocity zonal component for ice shelf	V_x	x, y, t	m s^{-1}
surface velocity meridian component for ice shelf	V_y	x, y, t	m s^{-1}
ice flow horizontal velocity (vertical mean)	$\vec{V}_m$	x, y, t	m s^{-1}
altitude above sea level	z	z	m
ice sheet bottom layer	z_b	x, y, t	m
surface topography	z_{topo}	x, y, t	m
surface albedo	α_{surf}	x, y, t	unitless
Clausius–Clapeyron gradient	β	constant	$8.7\times 10^{-4} K\ m^{-1}$
lapse rate	Γ	constant	-0.006 $K\ m^{-1}$
heat capacity of atmosphere layer	γ_{atmos}	x, y, t	J K^{-1} m^{-2}
heat capacity of ocean layer	γ_{ocean}	x, y, t	J K^{-1} m^{-2}
heat capacity of surface layer	γ_{surf}	x, y, t	J K^{-1} m^{-2}
humidity tendency due to precipitation	Δq_{precip}	x, y, t	kg kg^{-1} s^{-1}

humidity tendency due to correction	$\Delta q_{correct}$	x, y, t	kg kg^{-1} s^{-1}
humidity tendency due to evaporation	Δq_{eva}	x, y, t	kg kg^{-1} s^{-1}
humidity tendency due to precipitation	Δq_{precip}	x, y, t	kg kg^{-1} s^{-1}
sea ice mass balance	ΔH_{seaice}	x, y, t	$m\ s^{-1}$
ocean temperature tendency due to entertainment	$\Delta To_{entrain}$	x, y, t	K
model time step (GREB)	Δt	constant	12 hrs
ice viscosity	η	t	Pa s
ice viscosity for ice shelf	η_{SSA}	constant	2×10^{14} Pa s
ice sheet diffusion coefficient	κ	constant	2.1 W $(\mathrm{K\ m})^{-1}$
air diffusion rate	κ_a	constant	4×10^{6} m^2 s^{-1}
sea ice diffusion rate	κ_{si}	constant	0.25 m^2 month^{-1}
longitude	λ	x	degree
ice sheet model vertical coordinate	ξ	z	1
ice density	ρ_i	constant	910 kg m^{-3}
ocean density	ρ_o	constant	991 kg m^{-3}
stress tensor	σ	x, y, t	N m^{-2}
stress tensor component at a-b direction	σ_{ab}	x, y, t	N m^{-2}
effective stress	σ_e	t	N m^{-2}
latitude	ϕ	y	degree
climate mean of air vertical velocity	ω_{mean}	x, y	$Pa\ s^{-1}$
standard deviation of air vertical velocity	ω_{SD}	x, y	$Pa^2\ s^{-2}$